The completion of this thesis
was supported by the
Randy Seeling Award
given, in his memory, to another
outstanding graduate student
of the Geology Department,
University of Minnesota, Duluth.

STRATIGRAPHY AND ALTERATION OF THE FOOTWALL VOLCANIC ROCKS BENEATH THE ARCHEAN MATTABI MASSIVE SULFIDE DEPOSIT, STURGEON LAKE, ONTARIO

A Thesis Submitted to the Faculty of the Graduate School of the University of Minnesota

by

DAVID ALAN GROVES

In Partial Fufillment of the Requirements For the Degree of Master of Science

March 1984

ABSTRACT

Subaqueous mafic lava flows and breccias, mafic debris-flow and felsic pyroclastic-flow deposits, and felsic lavas form a 2 km thick succession beneath the Archean Mattabi massive sulfide deposit in northwestern Ontario. The lowermost 500 m is composed of massive amygdaloidal mafic flows, flow breccias, and heterolithic debris flows. Thin (<50m) amygdaloidal felsic lava flows and felsic block and ash deposits overlie the basal mafic flow sequence. This felsic horizon thickens both eastward and westward away from the Mattabi deposit and suggests the former existence of localized felsic vents on a broad shield volcano.

Rocks interpreted to be mafic debris-flow and felsic pyroclastic-flow deposits lie above the felsic horizon and represent a change in eruptive style from lava extrusion to phreatomagmatic volcanism. The change is believed to be a result of a shallowing upward sequence and/or an increasing water/magma ratio. The mafic debris-flow deposits are massive to thick-bedded, poorly graded and composed of scoriaceous to amygdaloidal mafic clasts. Felsic pyroclastic-flow deposits include a) massive basal beds and overlying bedded ash tuff, b) well-bedded, graded lapilli tuff and c) massive pumice-rich beds. Felsic pyroclastic deposits intercalate and intermix with mafic debris flow deposits west of Mattabi and together these constitute the upper 500-600 m of the footwall succession. Massive pyroclastic beds truncate mafic debris-flow deposits and mark the culmination of explosive felsic volcanism prior to the ore-forming event. Massive pumiceous pyroclastic beds and quartz-porphyritic ash-flow tuff form the immediate mine footwall strata.

Alteration within the footwall strata has been divided into four major mineralogical assemblages: 1) least altered (typical greenschist facies assemblages with moderate carbonatization), 2) iron carbonate-chlorite, 3) sericite and 4) chloritoid. Least-altered assemblage rocks are largely amygdaloidal mafic lava flows and mafic debris-flow deposits which are situated 4 to 5 km west of the Mattabi deposit. Iron carbonate-chlorite alteration is confined largely to felsic pyroclastic rocks and lavas within the upper 600 m of the footwall strata; sericitization is also widespread within these rocks. Chloritoid is developed in both sericite and iron carbonate-chlorite assemblage rocks.

Mass balance computations indicate that constant volume has been maintained within all altered lithologies except iron carbonate-chlorite assemblages within felsic lavas; these rocks have undergone a 10 to 20% volume reduction. Iron carbonate-chlorite assemblage rocks display elemental gains of Fe, Mn and CO_2, and losses of Si. Sericitization produces marked K and Rb gains at the expense of Na. Comparisons of iron carbonate-chlorite and sericite-assemblage rocks to similar chloritoid-bearing equivalents reveal no consistent elemental trends.

It is envisioned that heated connate seawater/rock interactions within mafic lava flows and breccias produced a large reservoir of metal-rich hydrothermal solutions. Synvolcanic faulting allowed the rapid discharge of fluids from the reservoir. Diffuse, semiconformable alteration zones were developed in overlying felsic pyroclastic rocks and lavas as the solutions migrated upward to the seafloor surface. Focused discharge of fluids at several locations resulted in large-scale precipitation of iron sulfides on the seafloor.

ACKNOWLEDGEMENTS

Dr. J. M. Franklin of the Geological Survey of Canada and my advisor, Dr. R. L. Morton, deserve recognition for their efforts in initiating and developing this thesis project. Both have contributed in many ways to the production of this work.

Dr J. C. Green and Dr. R. W. Ojakangas reviewed several hyphen-deficient drafts of the thesis, and the manuscript benefited from their suggestions. Those who also had a hand in the development of this thesis included: Wally Gibb and his staff at Mattabi Mines Ltd., Steve Green at the Geological Survey of Canada, Ian Pirie and Corporation Falconbridge Copper, and Dr. Penelope Morton of the University of Minnesota-Duluth. Funding for the project was provided by the Geological Survey of Canada and Mattabi Mines Limited.

TABLE OF CONTENTS

ALTERATION AND METAMORPHISM (Continued)

LIST OF ILLUSTRATIONS

INTRODUCTION

The Mattabi massive sulfide deposit is a 13 million ton Zn-Cu-Pb-Ag-Au stratiform ore body which is located within Archean volcanic strata of the Wabigoon greenstone belt in northwestern Ontario (Franklin et al., 1977). The deposit , originally discovered with airborne and ground geophysical methods in 1969, is currently operated by Mattabi Mines Ltd., a joint venture operation between Mattagami Lake Mines Ltd. and Abitibi Price Paper Company. Open pit mining operations have recently ceased (1981), and construction of a 1500 ft (460 m) vertical shaft to mine the remaining deep portion of the deposit is currently underway. The Lyon Lake, Creek Zone, and F-Zone deposits, smaller massive sulfide lenses within the immediate Mattabi area, are also currently being mined and managed by Mattabi personnel.

PURPOSE OF STUDY

The Mattabi deposit is one of several massive sulfide deposits situated in the volcanic succession of the South Sturgeon Lake area. Extensive exploration for these deposit types has delineated several major felsic/mafic boundaries within the sequence, yet a thick succession of predominantly mafic lithologies in the footwall at Mattabi has been left undifferentiated. Although the homogeneity of these footwall rocks does not make them particularly suitable for key marker horizons in exploration, the rocks are nevertheless important in the overall volcanological model for the area.

It is the marked physical and chemical variability within the heretofore undifferentiated footwall unit at Mattabi that is the focus of this thesis research. The objectives of this study are:

1. to define the volcanic stratigraphy beneath the Mattabi deposit, including correlation of lateral facies equivalents;
2. to develop a model for the volcanic environment and modes of emplacement for different deposit types;
3. to delimit distinct hydrothermal alteration assemblages within the footwall stratigraphy, examine least altered - most altered samples within separate lithologies, and construct a plausible alteration model.

LOCATION, ACCESS, AND PHYSIOGRAPHY

The Mattabi deposit is located near the southern end of Sturgeon Lake in northwestern Ontario (Fig. 1). The mine is approximately 350 km NNE of Duluth, Minnesota and 200 km NW of Thunder Bay, Ontario. Access is obtained from TransCanada Highway 17 at Ignace, Ontario by proceeding north on Highway 599 for 80 km and then east on the mine access road another 16 kilometers.

The topography in the immediate mine area is typified by gently rolling hills, prominent bedrock ridges, and swampy perimeters around shallow lakes. The mine complex is located on one of the higher ridges in the area. Most of the immediate mine area is still forested, although extensive clearcut tracts are present several kilometers east of Mattabi.

Bedrock exposures, except along the ridges, are sparse as much of the area is covered by sandy glacial till and sporadic boulder fields. At best, outcrop exposure approaches 10% of the total ground

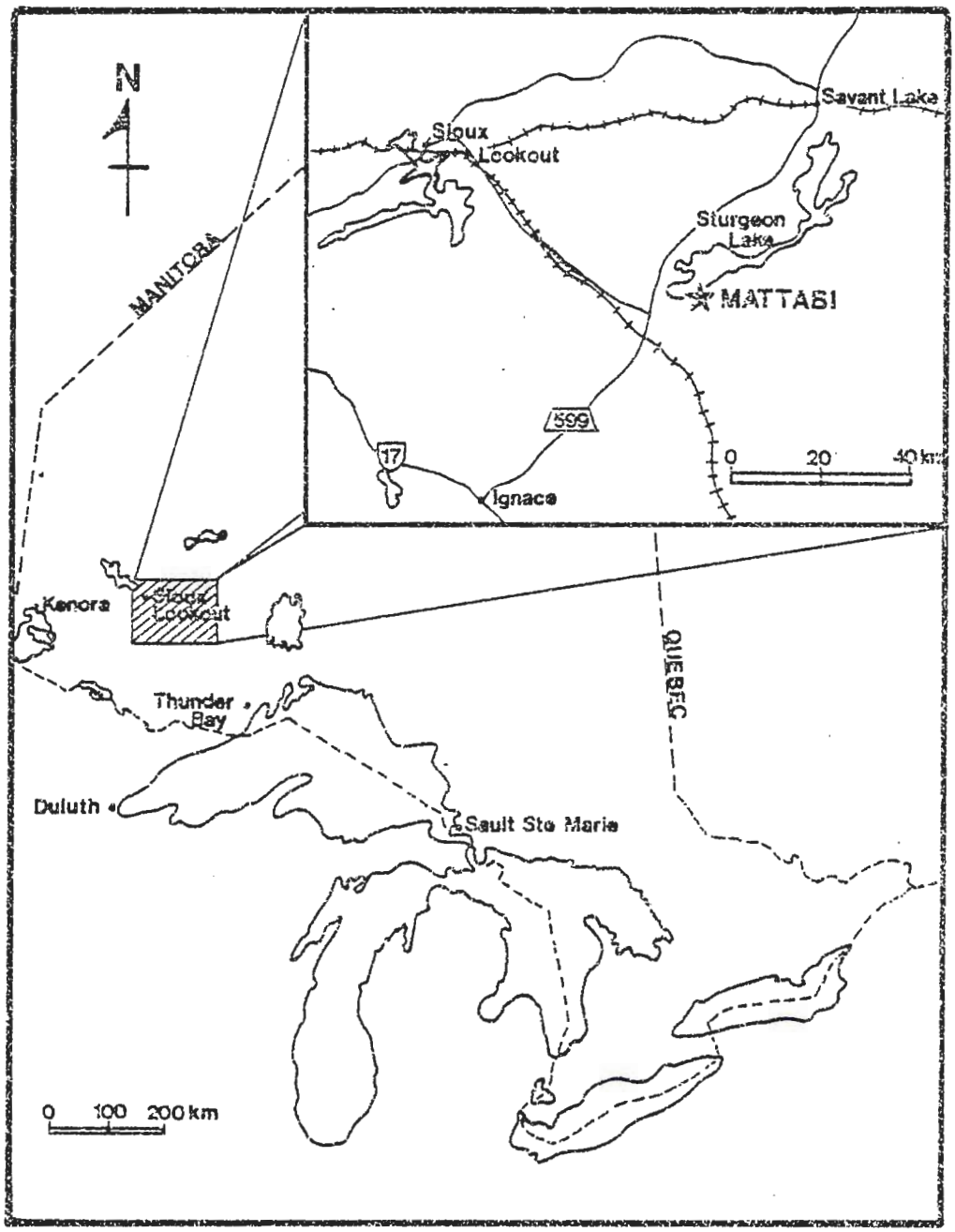

Figure 1. Location of the Mattabi massive sulfide deposit, Ontario, Canada.

area. The majority of the outcrops are glaciated elliptical mounds covered with a thick moss carpet. Outcrop stripping and overburden trenching have increased the exposures within the clearcut tracts.

METHODS OF STUDY

Field work was conducted during the months of June and July in 1982. Geologic mapping was confined to a roughly 12 km^2 area south of the Mattabi mine horizon. Data were compiled on existing 1:4800 (1 cm = 48 m) scale base maps provided by Mattabi Mines Ltd., and air photo bases (scale 1"=800') were also used in the clearcut areas east of Mattabi and in the immediate mine complex. Rock samples were obtained from each outcrop, and additional samples were taken at gradational contacts and altered exposures. Mapping of areas devoid of outcrop was facilitated by the logging of exploratory drill holes. Ten diamond drill holes were logged and sampled (see Plate 1).

One hundred and seventy-five thin sections were examined for primary textures, fragment types, and mineralogy. Estimates of modal mineralogy have been compiled and tabulated in Appendix A.

The Geological Survey of Canada performed whole rock major-oxide and trace element analyses on 103 samples from the study area. The analytical methods, statistical precision, and sample results are described and tabulated in Appendix B. Volatile-free normative mineral compositions for each of the analyzed samples are listed in Appendix C.

Specific gravities for each of the samples submitted for whole-rock analysis were determined on a modified beam balance. An aluminum standard with a specific gravity of 2.71 (approximately the same as

sample densities) was used to check the apparatus' accuracy. These data have been compiled with the major oxide lists in Appendix B.

X-ray diffraction was performed on selected sample powders for the determination of chlorite and carbonate species. 16 samples were analyzed, and these results are listed in Appendix C.

PREVIOUS WORK

The discovery of the Mattabi deposit by Mattagami Lake Mines Ltd. in 1969 sparked extensive exploration in the Sturgeon Lake area that has continued to date. Numerous mining firms utilizing diamond drilling and detailed grid mapping have provided improved stratigraphic control. Much of the work, however, has been confined to major felsic/mafic boundaries at the top of individual volcanic cycles.

Prior to Trowell's (1974) work in the Savant Lake-Sturgeon Lake area in the late 60's and early 70's, geologic interest and mapping had been confined largely to several small gold mines that operated in the mid 30's (Horwood, 1937). Trowell's compilation of the regional geology in the Sturgeon Lake area provided a working base for much of the later exploration and detailed mapping. He has more recently co-written a synthesis of the Savant Lake-Crow Lake metavolcanic-metasedimentary belt that includes the South Sturgeon Lake area (Trowell et al., 1980).

Franklin et al. (1975) did a detailed study of the hydrothermal alteration associated with the Mattabi ore-forming event. Continued work (Franklin, 1976; Franklin et al., 1977; Poulsen and Franklin,

1981) has included examination of the footwall lapilli tuff unit beneath Mattabi as an original base metal source rock, compilation of mining company data and individual mapping efforts, and the study of porphyry and shear-zone associated mineralization within the Beidelman Bay intrusion. Ongoing research (Campbell et al., 1981; Franklin, unpubl. data) has provided REE data for the Beidelman Bay Intrusion and felsic extrusives beneath Mattabi as well as radiometric ages for the aforementioned rock units.

Several recent studies have focused on the geologic setting of several other massive sulfide ore bodies in the Sturgeon Lake area. Severin (1982) gives a comprehensive overview of the Sturgeon Lake Mine, a small, high-grade ore body east of Mattabi discovered by Falconbridge Nickel Mines Ltd. in 1970. He argues strongly that the Sturgeon Lake Mine is situated on the Mattabi stratigraphic horizon and not the higher Lyon Lake-Creek Zone horizon as previously thought. The geology of the Lyon Lake deposit has been described by Harvey and Hinzer (1981).

Unpublished theses on the geology and geochemistry of the Sturgeon Lake area include Covello (1971), Kasarda (1973), Friske (1974), and Staargaard (1981). Covello's work is one of the earliest efforts dealing with the immediate stratigraphy at Mattabi; his mapping outlined several major felsic horizons in the lower cycles of volcanism at Sturgeon Lake.

REGIONAL GEOLOGY

The Mattabi massive sulfide deposit is situated within the Savant Lake-Sturgeon Lake segment of the Wabigoon greenstone belt, an Archean

volcanic - sedimentary sequence bounded to the north and south by the Quetico and English River gneiss belts respectively (Fig. 2). Within the South Sturgeon Lake area, several mafic to felsic successions of volcanic rocks are in turn overlain by a thin accumulation of laharic and turbiditic sedimentary rocks. The total thickness of volcanic and sedimentary strata is in excess of 9000 meters (Franklin et al., 1977).

Structurally, the Savant Lake-Sturgeon Lake region exhibits two attitudes of large-scale folding (Franklin et al., 1977) (Fig. 3). Large-amplitude fold axes trending E-W are warped by a more open N-S folding event. In the South Sturgeon Lake area, the strata dips steeply to the north and forms the southern limb of a syncline centered through Sturgeon Lake. However, Trowell et al. (1980) suggest that the volcanic lithologies of the northern synclinal limb are not correlative with the South Sturgeon Lake succession.

The Mattabi deposit is situated at the upper boundary of the lowest cycle of volcanism in the Sturgeon Lake area (Fig. 4). This 5 km thick succession of mafic flows, felsic lava flows, and mixed fragmental lithologies is bounded at the base (to the south) by the Bell Lake Complex, an extensive granitic terrain comprised of granite -granodiorite intrusions and tonalite gneiss (Franklin et al., 1977). South of the Mattabi deposit, the Beidelman Bay intrusion is situated approximately 500 m north of the gneissic basement. This dioritic to trondhjemitic sill-like body intrudes and cuts out a large portion of mafic flows which form the base of the volcanic succession (Fig. 4).

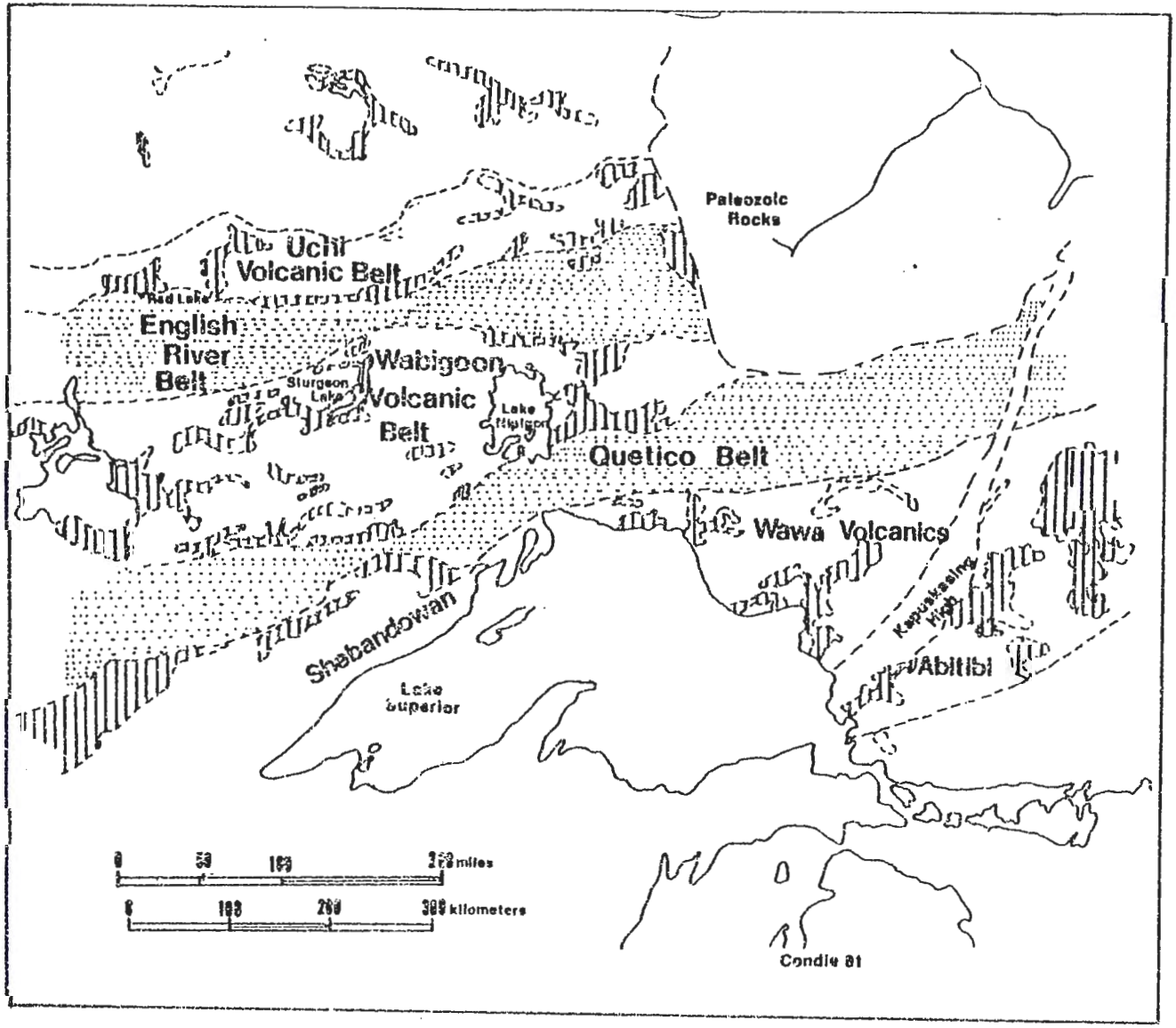

Figure 2. Geologic provinces of northwestern Ontario (after Condie, 1981).

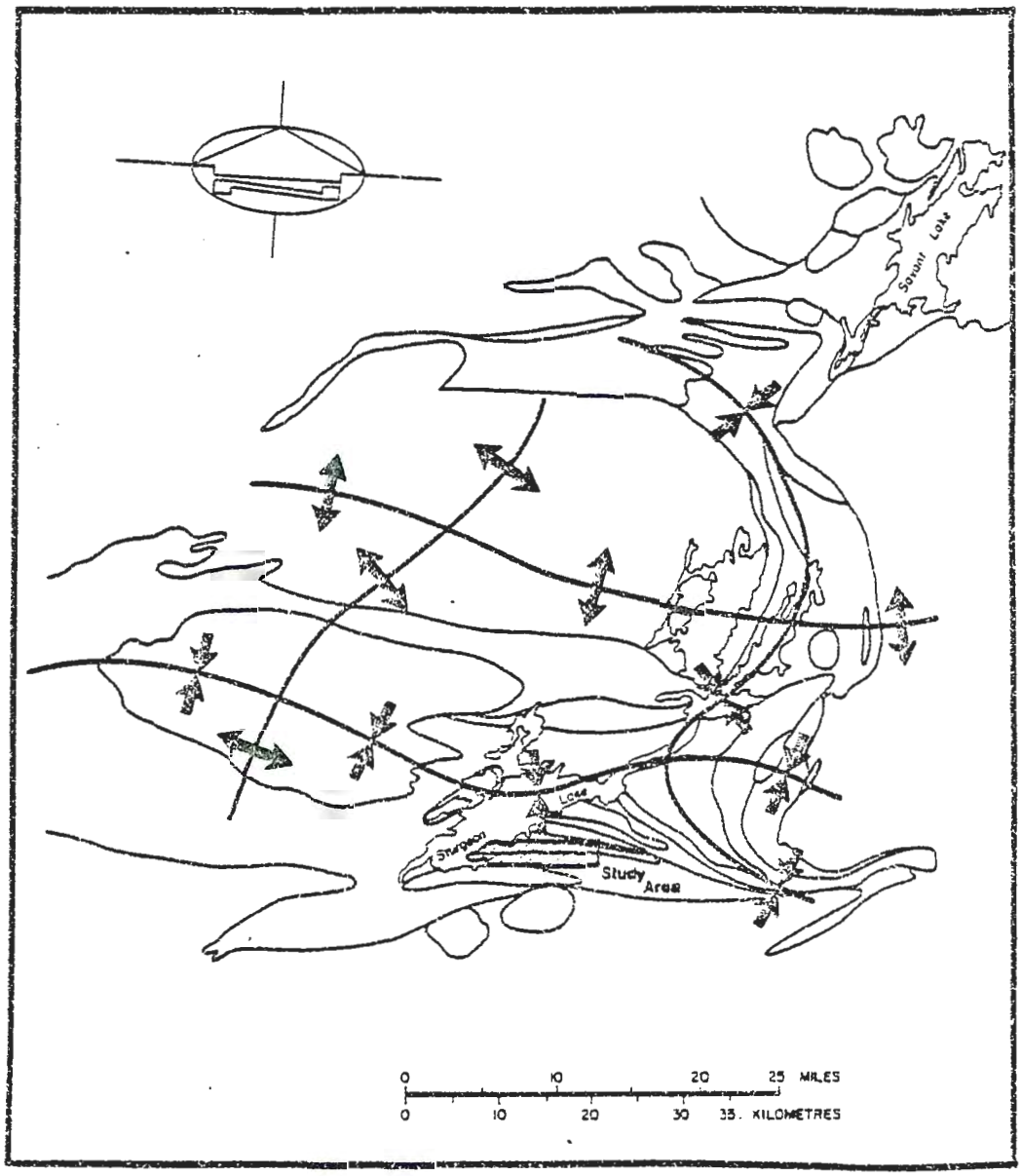

Figure 3. Major axial fold traces within the Savant-Sturgeon Lakes region. Lines other than lake perimeters are major rock contacts (see Trowell, 1974); boxed and ruled area represents approximate limits of study area. Figure from Franklin et al. (1977).

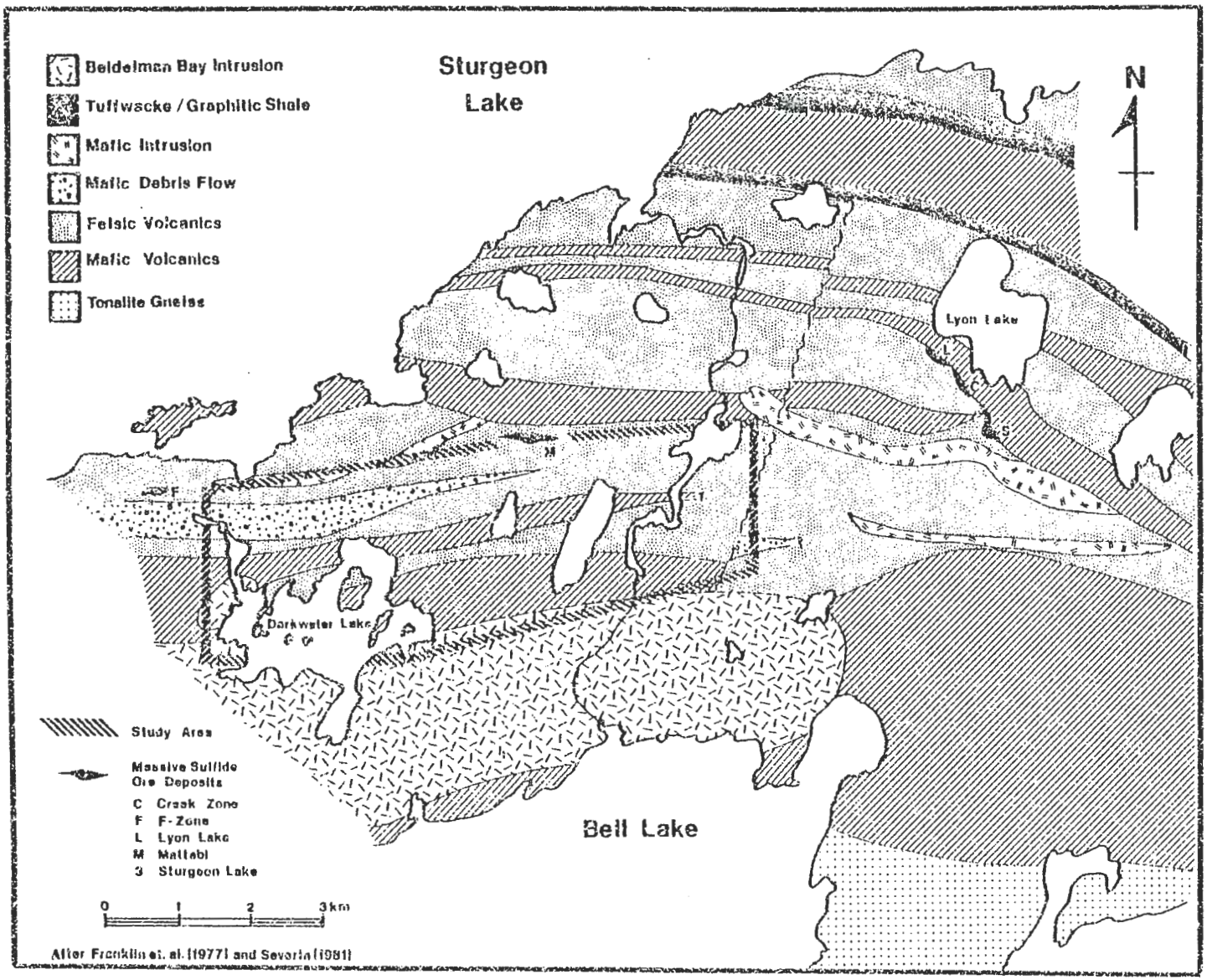

Figure 4. Geology of the South Sturgeon Lake area (from Franklin et. al., 1977; and Severin, 1982).

Radiometric dates and REE data (Franklin, unpubl. data; Campbell et al., 1981) from the intrusion and felsic extrusive rocks at the top of the cycle indicate that the sill is a cogenetic, subvolcanic feeder to the felsic extrusive units capping the Mattabi cycle. At the top of the section, pillowed mafic flows abruptly terminate the Mattabi volcanic cycle.

Rocks of the South Sturgeon Lake area have been subjected to regional greenschist facies metamorphism. Almandine-amphibolite assemblages are locally found at the base of the Mattabi cycle near the Beidelman Bay intrusion and the Bell Lake gneissic complex. Outside of the study area, metamorphic grades increase eastward across the South Sturgeon Lake area (Trowell, 1974).

LITHOLOGY AND STRATIGRAPHY

INTRODUCTION

The volcanic succession beneath the Mattabi deposit and within the study area has been subdivided into four major units on the basis of primary textures, fragment types, and composition. Proceeding stratigraphically upward from the southern limit of the study area to the immediate mine footwall, the major stratigraphic subdivisions are (Fig. 5):

1. mafic volcanic rocks.
2. felsic amygdaloidal lavas and pyroclastic deposits.
3. mafic debris flows.
4. felsic pyroclastic deposits which form the immediate mine footwall.

Present mineralogy within the footwall rocks reflects hydrothermal alteration associated with the formation of the Mattabi massive sulfide deposit (Franklin et al., 1975), as well as regional greenschist facies and localized amphibolite facies metamorphism (Trowell, 1974). The rocks within the study area are therefore metavolcanic in character; however, for simplicity, the prefix "meta-" has not been used in the remainder of this text.

The mafic rocks (lava flows and debris flows) consist largely of very fine-grained ($\leq$0.1 mm) felty to pilotaxitic intergrowths of plagioclase, chlorite, carbonate, epidote, actinolite, quartz, and iron oxides. Plagioclase microphenocrysts occur in most samples. Petrographically, the mafic flows, associated breccias and debris flows are basaltic in character.

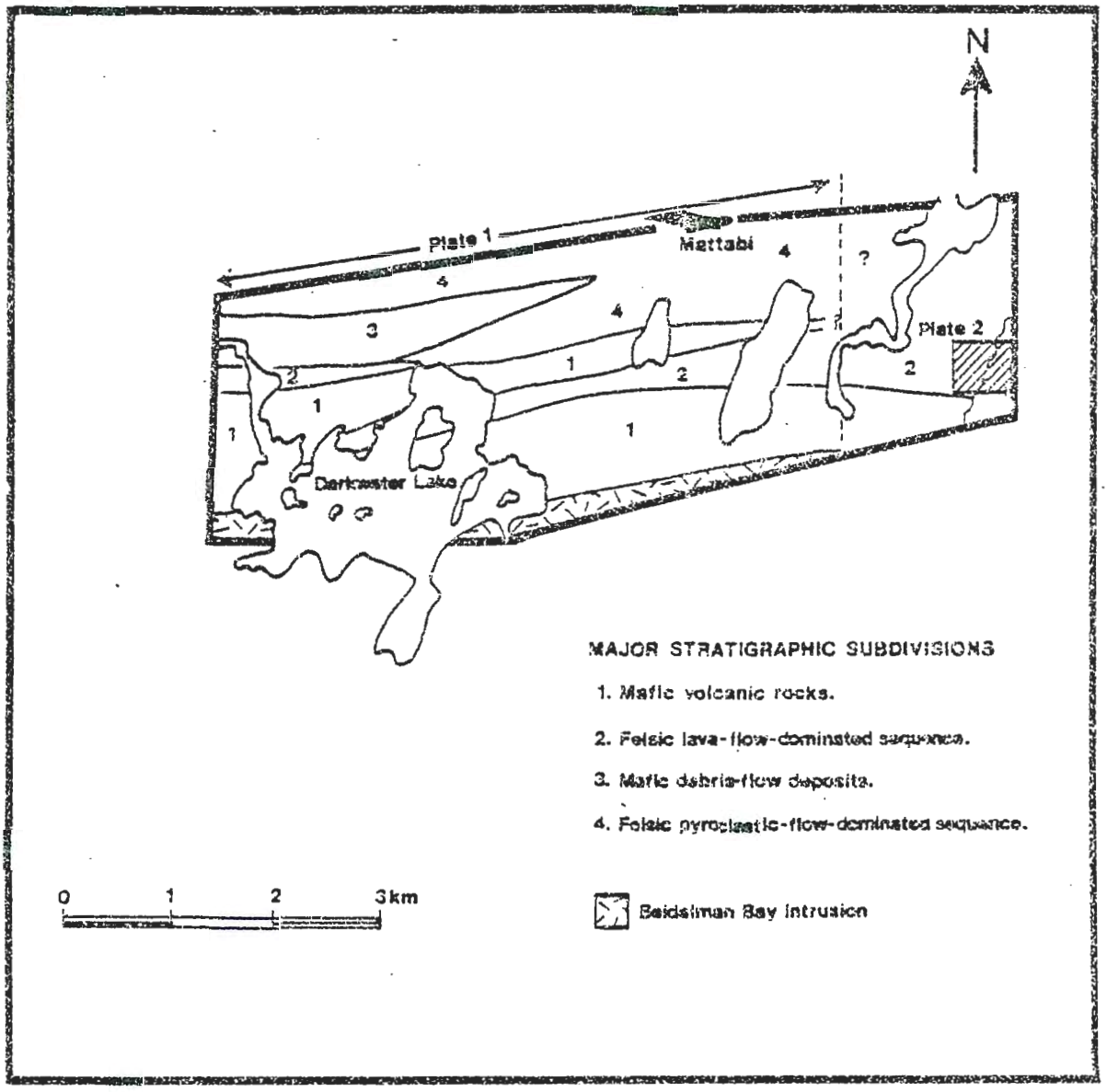

Figure 5. Distribution of major stratigraphic subdivisions within the study area. Diagram also shows the location of Plate 2 relative to Plate 1.

Felsic rocks, which include aphyric lava flows, associated hydroclastic margins of lava flows, and pyroclastic deposits, are composed of a fine-grained (0.1 mm) assemblage of quartz and feldspar with generally lesser amounts of sericite, chlorite, stilpnomelane, tourmaline, and iron oxides. Ash tuffs and matrices of coarse pyroclastic deposits commonly exhibit a more mafic character than the clasts due largely to abundant iron-bearing alteration minerals such as chlorite. The lava flows and fragmental margins are commonly amygdaloidal. Examination of relatively unaltered felsic lithologies indicates that the rocks are dacitic to rhyodacitic in character.

Mafic, intermediate, and felsic intrusive rocks are present within the study area, and they occur primarily as narrow dikes or subconcordant sills. Many display hydrothermally-altered mineral assemblages and are presumably feeder dikes to overlying flows.

The following unit descriptions are presented according to the order of the map legend on Plate 1. References to unit 1a, 2, etc. are according to map nomenclature, and Plate 1 should be consulted unless otherwise indicated. Modal mineral compositions for each unit are tabulated in Appendix A.

MAFIC VOLCANIC ROCKS (Units 1 and 2)

Mafic Lava Flows (Unit 1)

Mafic lava flows, autobrecciated flow tops, and flow-front breccias are situated north of the Beidelman Bay intrusion along the southern portion of the study area (Plate 1, unit 1). Total stratigraphic thickness (500 to 600 m) is markedly uniform across the length of the map area, and together with isolated mafic flows higher

in the section, they comprise roughly 30% of the Mattabi footwall strata within the study area.

Exposures of mafic flows are limited; most of the outcrops are situated on the islands or near the shore of Darkwater Lake (Plate 1). Exploratory diamond drill holes provide additional information north of Darkwater Lake and southeast of the Mattabi deposit near Tailings Lake.

Mafic flows are typically aphyric, amygdaloidal, and non-pillowed. They range in color from dark green to medium gray with gray varieties being more siliceous. Foliation is generally well-developed in the flows, but it is obscured with increasing carbonatization and silicification.

Most of the mafic flows are amygdaloidal and contain 1-5% quartz, carbonate, or chlorite - filled amygdules which range from 0.1 to 10 mm in diameter. Round to elongate quartz amygdules, which weather less rapidly than the surrounding chloritic groundmass, are readily visible on outcrop surfaces, whereas similar-size rounded, empty pits are believed to be the relics of carbonate-filled amygdules. More rarely pyrite fills part or all of the amygdules. Drill core samples of more markedly amygdaloidal flows situated north of Darkwater Lake (Plate 1) show 0.5-2 mm rounded quartz and carbonate - filled amygdules comprising upwards of 10% of the flows. Diamond drill holes also intersect a 30 meter thick sequence of amygdaloidal mafic flows southeast of the Mattabi pit and east of Tailings Lake at approximately the same stratigraphic level as the aforementioned

amygdaloidal flows. These flows contain abundant quartz, carbonate, and pyrite-filled amygdules (8-15%) that are inversely graded in size (from 2-5 mm to 5-20 mm) over 3 meter intervals, suggesting that the flows are quite thin. The larger amygdules display a quartz to carbonate to pyrite zonation into the interior of the filled vesicles.

At least one thin (<10 m) mafic flow is intercalated with mafic debris-flow deposits situated in the northwest corner of the study area (Plate 1, Unit 2). A small outcrop of this flow (#14) exhibits the only recognizable pillow structures within the footwall strata. Elongate, 20 to 30 cm wide pillows are outlined by 2-3 cm wide chloritic selvages which are in abrupt contact with mafic fragmental material (Fig. 6). Other isolated flows throughout the area are massive and sparsely amygdaloidal in character.

A distinctive porphyritic rock (Unit 1b) occurs at the contact with the Beidelman Bay intrusion on an island on Darkwater Lake (Plate 1). This rock exhibits unaltered 1-2mm plagioclase phenocrysts enclosed in a pilotaxitic groundmass composed mainly of 0.1 mm feldspar laths (Fig. 7). The feldspar-rich nature of the sample along with the presence of 8-10% anhedral quartz within the groundmass makes the rock texturally and mineralogically distinct from the more common amygdaloidal basaltic flows; its origin is uncertain.

Diamond drill holes intersect mafic flows on the western end of the map area (north of Darkwater Lake, unit 1d). The flows include several 5-15 meter thick autobrecciated flow tops which are composed of dark green, angular fragments 2 to 30 mm in diameter; many of the fragments display triangular or cuspate terminations. Brecciation

Figure 6. Isolated pillowed (?) flow within mafic debris - flow deposits; west end of study area (Plate 1).

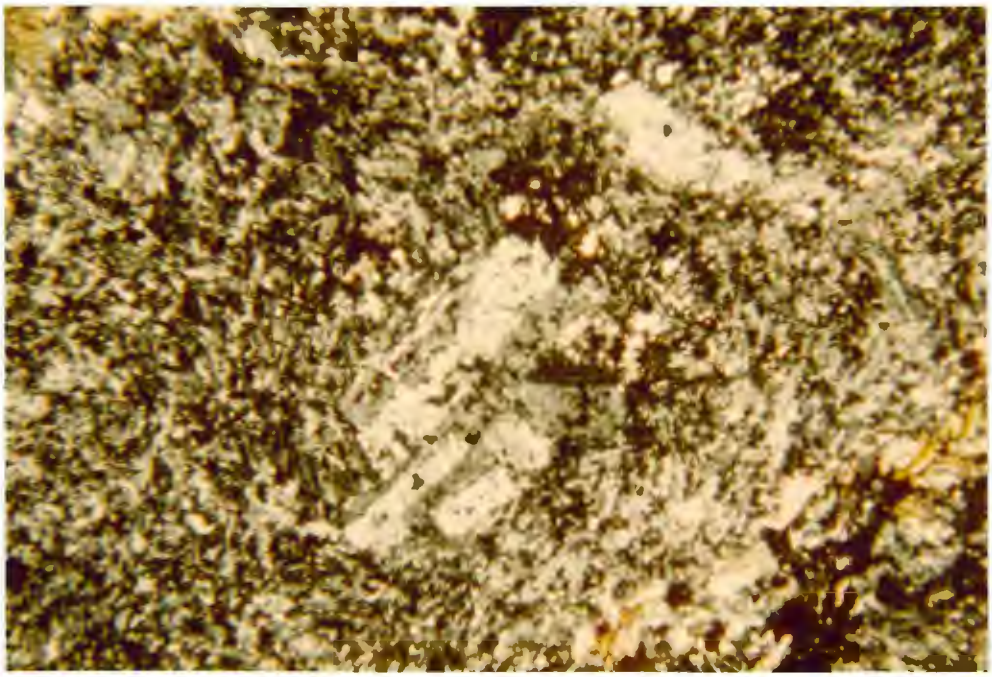

Figure 7. Photomicrograph of porphyritic mafic rock immediately north of the Beidelman Bay intrusion. Crossed polars, field of view: 2.5 x 4 mm.

intensifies outward from a massive flow interior with large, nearly in-situ fragments grading upward to a pronounced flow-oriented breccia which in turn typically terminates at a fine-grained granular top.

Mafic breccia is exposed in the southwestern portion of the map area (Plate 1) and is composed of green-gray, aphyric fragments (2-15 cm in diameter) and buff-colored fragments (2-8 cm in diameter) set in a green aphanitic matrix (Fig. 8). The former fragment type comprises roughly 50% of the deposit, the latter 5 to 10%. Grading or bedding is not evident. Several of the large buff-colored fragments are markedly vesicular, and vesicle interiors are lined with fine-grained crystalline quartz and carbonate which presumably gives the fragments their light color. The proximity of the breccia to an underlying mafic amygdaloidal flow, and the presence of angular aphyric mafic fragments mineralogically and texturally similar to the underlying flow suggest that the exposure represents flow-front rubble from one of the adjacent mafic flows.

In thin section mafic lava flows contain 0.2 to 0.5 mm plagioclase microphenocrysts which are commonly pseudomorphed by albite, carbonate, or sericite. Microphenocrysts comprise 4-10% of the flows, and they are set in a very fine-grained ($\leq$0.1 mm) groundmass composed of albite with lesser quantities of chlorite, epidote, and actinolite/hornblende. Magnetite and skeletal ilmenite grains (0.1-0.5 mm) constitute 1 to 4% of most samples (see Table 2, Appendix A).

Flow-top fragments consist of 0.5 mm albitic microphenocrysts and 0.1 to 1 mm anhedral carbonate grains set in a very fine-grained ($<<$0.1 mm) chlorite/actinolite mesostasis. The breccia matrix is

Figure 8. Mafic flow-front breccia north of Darkwater Lake.

composed of fine-grained (0.1mm) quartz, feldspar and carbonate.

Examination of thin sections from the flow-front breccia reveals that the dark green angular fragments are petrographically similar to the underlying lava flows, whereas the buff-colored, more rounded fragments are markedly amygdaloidal. These fragments contain 20 to 40% quartz and carbonate-filled amygdules (0.2 to 0.4 mm in diameter) which are enclosed in a matrix of 0.5-1 mm carbonate porphyroblasts, 0.2 mm epidote grains, and opaques. The breccia matrix encasing the fragments is composed of very fine-grained ($\leq$0.1 mm) quartz, chlorite, sericite, and carbonate.

Mafic Debris Flow Deposits (Unit 2)

The term mafic debris flow is hereby used to describe massive to poorly bedded, heterolithic basaltic breccias with less than 10% felsic clasts. In delineating this type of deposit from somewhat similar mafic flow-front or flow-top breccias, the following criteria have been used:

- flow-front breccias contain coarse angular fragments similar in composition to the underlying lava flows. These deposits are wedge - shaped and very limited in lateral extent (Dimroth et al., 1979), whereas debris flows form laterally extensive deposits of variable thicknesses.
- flow-top breccias are monolithic in nature and can be traced stratigraphically downward into a massive flow interior. The breccias display normal grading of fragment sizes outward from the flow interior. Debris flows lack

this vertical transition and are commonly composed of non-bedded or poorly bedded heterolithic clasts.

Mafic debris flows form a 3 km long wedge-shaped unit in the northwestern corner of the study area. The deposit reaches a maximum thickness of 350 meters on the western end and thins eastward before finally pinching out between felsic pyroclastic deposits (Plate 1).

Thin (less than 10 meters) debris-flow horizons also occur within the previously described mafic flow sequence. Clast types, sizes, and percentages of accessory felsic clasts within these deposits are similar to those in the major debris-flow unit. Many have been omitted from the geologic map because of their limited thickness.

Debris-flow deposits are also present in the southeast corner of the study area, east of the Bell River (Fig. 5, Plate 2). In this area mafic debris flows are intercalated with felsic tuff-breccia and felsic amygdaloidal lava flows. Lack of outcrop directly south of the Mattabi deposit makes correlation of these debris flows with those west of Mattabi difficult.

In outcrop the debris flows vary in appearance depending on clast/matrix color contrast and the intensity of alteration within clasts and matrix. Typically the debris flows consist of 40 to 90% buff to dark green, angular to subrounded mafic clasts which range from 5 to 20 mm in diameter (Figs 9,10). Buff-colored clasts (2-5cm, $\leq$10%) tend to be slightly larger than the dark green clasts, and they commonly give the deposit a crudely bedded appearance. Dark green aphyric mafic fragments averaging 1cm in size constitute the most

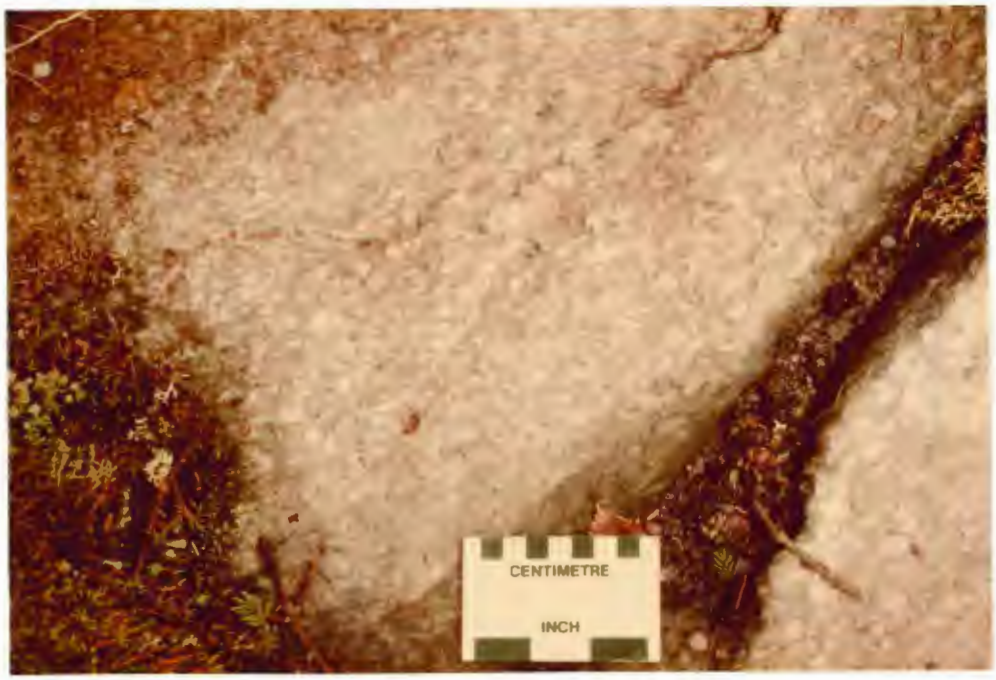

Figure 9. Mafic debris-flow deposit composed of scoriaceous to amygdaloidal mafic clasts.

Figure 10. Angular basaltic clasts within mafic debris-flow deposit. Knife is 8 cm long.

common fragment type within the flows, however they are generally difficult to distinguish from a matrix of similar composition.

Felsic clasts, which generally constitute less than 10% of the debris flow units, increase in abundance and size eastward as the unit becomes intercalated with felsic pyroclastic flows. Felsic clasts are pale to medium gray, siliceous, and commonly exhibit a "bleached" white rim which is 4-5 mm thick. Several outcrops display crudely layered, subrounded blocks 15-30 cm in size which are in marked contrast to smaller basaltic clasts and the chloritic matrix (Fig. 11).

Magnetite-rich clasts, which are similar in size and angularity to other mafic fragments within the deposit, are concentrated in irregular-shaped zones which are 1-3 m wide and restricted to several outcrops (#s 30, 37, Plate 1). The dark gray to black, strongly magnetic clasts are set in a light gray-green, chlorite-rich matrix (Fig. 12). In most cases, the magnetite-rich clasts bear a close spatial relationship to narrow (1-4 m) subconcordant feldspar porphyry sills.

Thin section examination of debris-flow samples reveals several distinctive types of mafic clasts. Although similar in mineralogy, the clasts vary according to the relative abundance of amygdules, groundmass textures, and the presence or absence of feldspar microphenocrysts. The noted clast types are:

1. amygdaloidal/scoriaceous clasts with 20-50% amygdules, (Fig. 13).

Figure 11. Felsic lithic blocks forming crude stratification within mafic debris-flow deposits.

Figure 12. Magnetite-rich clasts within mafic debris-flow deposit. Note that magnetite (black) is often concentrated around rim of clasts.

2. fine-grained, sparsely amygdaloidal (<5%), chlorite/actinolite-rich clasts.
3. amygdaloidal (8-15 %), feldspar-rich, felty to pilotaxitic clasts (Fig. 14).

The amygdaloidal/scoriaceous clasts (Type 1) vary from 6-25 mm in diameter and are subangular to subrounded. Round to almond-shaped amygdules average 0.1-0.5 mm in size, range from 20-50% in abundance, and are filled by carbonate and quartz. The groundmass is composed of very fine-grained (<<0.1 mm) feldspar, carbonate and epidote with lesser amounts of chlorite, actinolite, stilpnomelane/biotite, and magnetite (Table 3, Appendix A). Occasionally the groundmass contains 0.7-1 mm albitic microphenocrysts which are glomeroporphyritic. These scoriaceous clasts are ubiquitous throughout the entire debris flow horizon (western end of study area, Fig. 5) and commonly account for greater than 50% of total clasts.

Very fine-grained chlorite/actinolite-rich clasts (Type 2) range in size from 4-10 mm and comprise from 15-40% of the clasts present. These clasts are markedly angular, but they can be difficult to distinguish from a matrix of similar composition. Amygdules, if present, are generally 0.1-0.2 mm in length and less than 5% of clast volume. Felty microlitic feldspars constitute 40-50% of the clasts and are set in a dark green chloritic groundmass. This clast type is present in most debris-flow samples.

Amygdaloidal, pilotaxitic mafic clasts (Type 3) are the least abundant of the three clast types; their occurrence is limited to a narrow stratigraphic horizon on the westernmost end of the map area.

These particular clasts are characterized by 0.2-1 mm amygdules averaging 8-15%, a feldspar-rich pilotaxitic groundmass, and 0.5-1 mm magnetite euhedra. Magnetite commonly accounts for 5-10% of clast composition. The groundmass is composed of very fine-grained (<<0.1 mm) chlorite, actinolite, epidote, carbonate and quartz with up to 2% glomeroporphyritic feldspar microphenocrysts which range from 0.2 to 0.5 mm in diameter.

In thin section magnetite-rich clasts are similar in size and vesicularity to the scoriaceous clasts described above. The clast groundmass, however, contains abundant magnetite euhedra ($\leq$0.1 mm, 10-35%) and dark epidote grains which give the clasts a dark gray to black color (Fig. 15). The percentage of magnetite in the groundmass varies from clast to clast and is commonly gradational across individual clasts. In general, magnetite content is a function of the clast's vesicularity, with highly amygdaloidal clasts containing more abundant magnetite. The similarity of these clasts to other less magnetite-rich clasts in other areas of the debris flow, and the proximity of porphyritic sills and dikes suggests that the magnetite is a product of localized contact metasomatism.

The debris-flow matrix is composed of microlitic feldspar, chlorite, actinolite, carbonate, epidote and opaques (Table 3, Appendix A). Magnetite euhedra are common (1-4%), and in several thin sections the grains are poikiloblastic. Albitic microphenocrysts, tabular in shape and 0.2-1 mm in length, typically occur in glomeroporphyritic clusters similar to those within clasts.

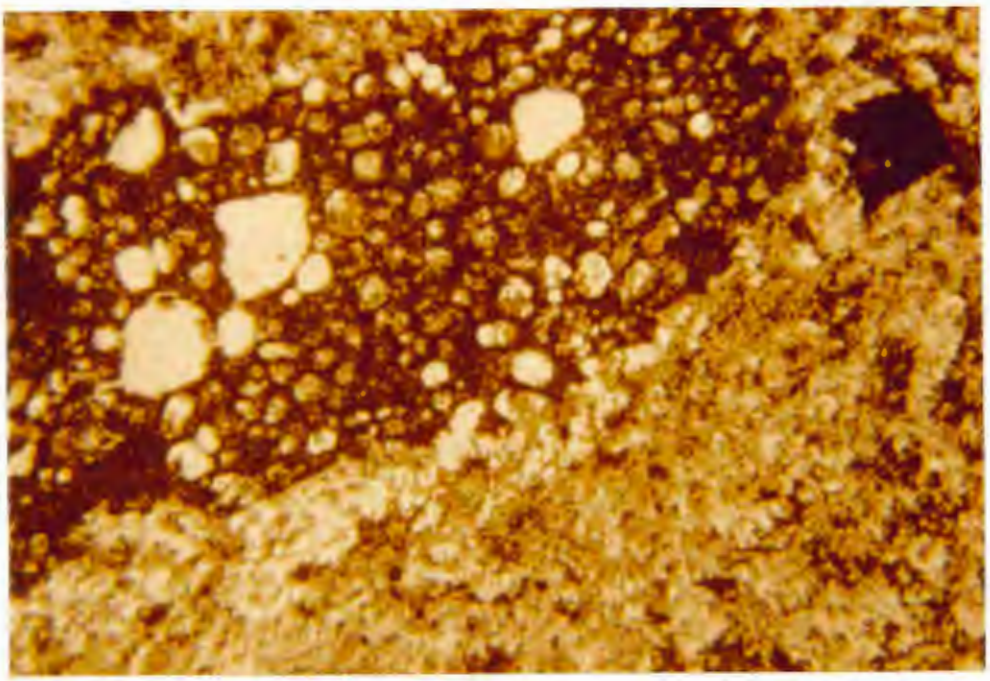

Figure 13. Photomicrograph of Type 1 mafic clast within mafic debris-flow deposits. Plane polarized light, field of view: 2 x 3 mm.

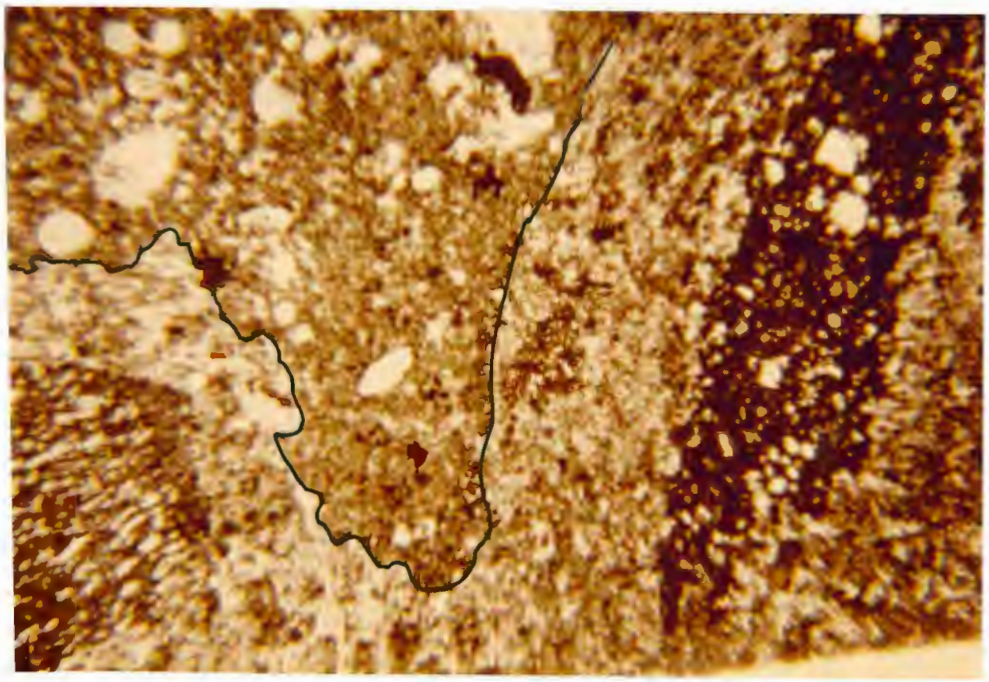

Figure 14. Photomicrograph of Type 3 mafic clast (outlined) which is flanked by two Type 1 clasts. Note larger amygdule size and subhedral magnetite grains. Plane polarized light, field of view: 5 x 7 mm.

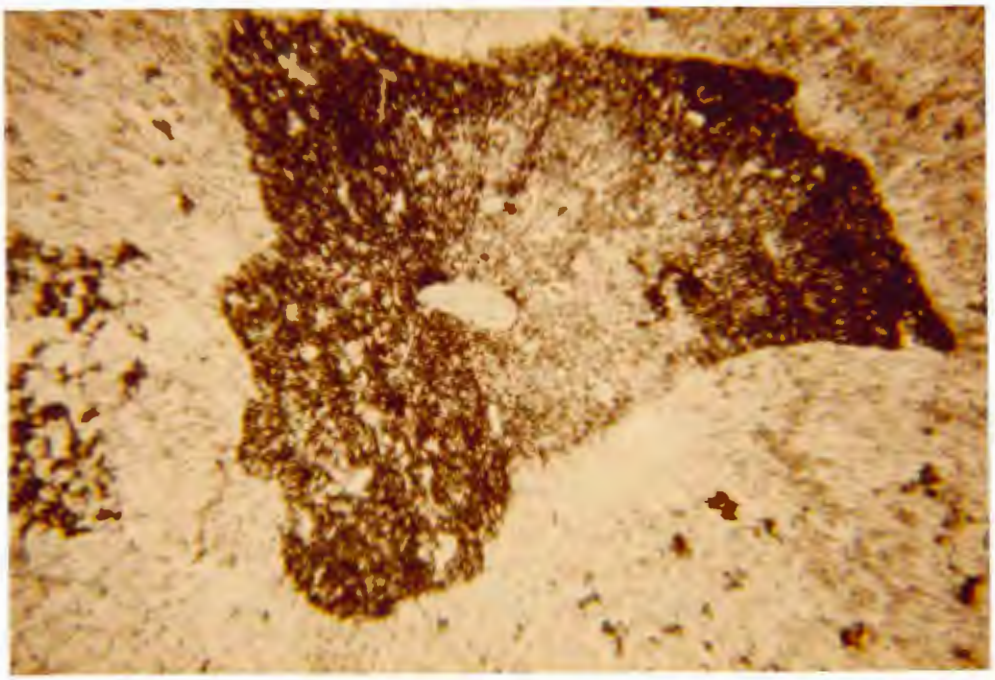

Figure 15. Photomicrograph of amygdaloidal, magnetite-rich clasts within mafic debris-flow deposits. Plane polarized light, field of view: 5 x 7 mm.

Hydrothermal-alteration minerals (ankerite, sericite, chloritoid, etc.) are not abundant within the major debris-flow horizon. Vesicle fillings within clasts are largely dolomite and/or calcite, and much of the clast mineralogy is typical of lower greenschist assemblages (albite, chlorite, epidote, actinolite, carbonate and quartz). The debris-flow matrix displays a similar mineralogy.

Felsic clasts within debris-flow deposits are easily recognizable in outcrop and this tends to suggest that the entire rock type is felsic; however, examination of samples in thin section reveals that 5-15 mm mafic clasts (of the types described above) are the predominant clast types. In thin section, felsic lithic clasts are composed of interlocking grains ($\leq$0.2 mm) of quartz and feldspar with lesser amounts of very fine-grained (<0.1 mm) sericite, chlorite, stilpnomelane, and opaques. Quartz-carbonate amygdules range from 0.2-0.5 mm in size and comprise less than 5% of total clast volume. Other felsic clasts are markedly amygdaloidal and therefore pumiceous in character; clast composition is similar to that of the lithic clasts, but quartz-carbonate amygdules approach 50% of clast volume. Some angular, fine-grained, sparsely amygdaloidal clasts show intense carbonate-sericite alteration obliterating much of the original mineral assemblage.

FELSIC PYROCLASTIC FLOW DEPOSITS (Units 3, 4 and 6)

Rocks interpreted to represent felsic pyroclastic flow deposits form two major stratigraphic horizons within the Mattabi footwall sequence. The deposits account for approximately 35% of the rocks in the study area (Plate 1).

The lower pyroclastic horizon (Plate 1) is poorly exposed; most outcrops are situated on the shores or immediate high ground surrounding Darkwater Lake. The pyroclastic rocks are approximately 250 to 300 meters thick and thin eastward where they are interlayered with felsic amygdaloidal lavas. To the west the unit is intercalated with mafic volcanic rocks. The deposit is composed of graded, lapilli-rich beds which are intercalated with fine grained (<2 mm) crystal-rich beds. Similar deposit types exposed near Tailings Lake (Plate 1) are inferred to be part of the same horizon, but the paucity of outcrop between the two areas makes correlation difficult.

The upper pyroclastic horizon forms the immediate footwall rock at the Mattabi deposit. The unit is approximately 600 meters thick and extends from east of the Mattabi deposit to the western extremity of the map area (Plate 1). The unit contains pyroclastic rocks similar to those within the lower horizon as well as quartz-porphyritic ash-flow and pumice-bearing deposits.

Based on field observations and preserved primary textures, the pyroclastic flow deposits (Unit 3, Plate 1) have been subdivided into several deposit types which are similar in character to documented subaqueous pyroclastic flow sequences (Fiske, 1963; Fiske and Matsuda, 1964; Morton and Nebel, 1983). The divisions include massive basal beds, bedded ash-tuff sequences, and graded lapilli-rich and pumice-bearing deposits. Quartz-porphyritic ash-flow (Unit 4) and felsic block-and-ash flow deposits (Unit 6) are also described in this section.

Massive Beds

Massive felsic pyroclastic beds, which range from 1 to 5 meters in thickness, are situated primarily within the upper 600 meters of the footwall strata in close proximity to the massive sulfide deposit. Massive beds are also present within the lower pyroclastic horizon, but their thickness or lateral extent is not known.

Massive beds are composed of buff to light gray, subrounded felsic lapilli and block-size fragments (20-60%) set in an altered iron carbonate, chlorite, and/or chloritoid-rich matrix. The fragments range from 2 to 30 cm in diameter and are poorly graded and sorted; bedding is recognized only by the intercalation of ash tuffs among the massive beds. Fragments are pitted on weathered surfaces and are commonly outlined by iron oxide. Most of the fragments are aphanitic, however occasional subrounded, less-altered quartz-porphyritic fragments are visible, and comprise less than 5% of fragment types.

Graded Lapilli-Rich Beds

West of Mattabi the aforementioned massive beds grade laterally into well sorted and graded lapilli-rich beds which are topped by fine-grained crystal-lithic tuffs. The lapilli-rich beds are 80-100 cm thick and contain subangular to subrounded felsic fragments which range from 5-50 mm in diameter and constitute from 35 to 75% of individual beds. Typical lapilli-rich beds display a basal "lag layer" (approximately 7 to 8 cm thick and composed of large 3-5 cm diameter fragments) which is overlain by well-graded lapilli that range from 10 to 25 mm in diameter. These beds are, in turn, overlain

by 25 to 50 cm thick successions of crystal-rich, lithic tuffs comprised of 2-4 mm feldspar crystals and lithic fragments. Close examination reveals that these tuffs are graded over 5-15 cm intervals. Together, the lower lapilli-rich bed and upper crystal-rich beds form a single cyclic unit approximately 1 to 2 meters thick which is repeated throughout outcrop exposures. Such grading may be analogous to distal subaqueous pyroclastic sequences described by Fiske and Matsuda (1964).

Further west on the same stratigraphic horizon, lapilli and ash-size deposits form well-bedded successions (Fig. 16). Lapilli-bearing beds are 50 to 110 cm thick, normally graded and composed of subangular to subrounded felsic fragments (5-50cm in diameter) within a chloritic matrix which contains smaller (5-10 mm diameter) mafic clasts. In thin section, the mafic clasts are similar to those described under Mafic Debris Flow Deposits. The presence of these mafic fragments suggests that the horizon represents a reworking and intermixing of felsic pyroclastic and mafic debris flow deposits.

Graded, lapilli-rich beds are also present within the lower horizon near Darkwater Lake. Here subangular to rounded pinkish siliceous lapilli (5-50 mm, 15-30 %) are normally graded and decrease in abundance over 2-meter intervals. The lapilli-tuff matrix is chlorite-rich and contains sparse 1 mm amphibole porphyroblasts. These beds are, in turn, topped by fine-grained (<2 mm) crystal-rich tuff beds varying from 30 to 150 cm in thickness.

Thin sections of samples from the lower horizon display tightly

packed, very fine-grained quartz and feldspar-rich felsic fragments which contain disseminated carbonate, biotite, chlorite, and trace opaques. The matrix contains abundant chlorite with euhedral hornblende porphyroblasts, 1 mm carbonate patches, and irregular quartz-feldspar domains comprising less than 20% of the total matrix.

Bedded Ash Tuff

Bedded ash tuff sequences overlie massive pyroclastic beds and graded, lapilli-rich deposits. Individual beds are 1-5 cm thick and form deposits that range from 5-100 cm in thickness. Felsic blocks and/or lapilli may be sparsely distributed throughout the lower portions of the bedded ash tuffs, especially where they overlie massive beds (Fig. 17). Massive beds are commonly overlain by 2-5 recognizable ash-tuff beds, whereas graded lapilli-rich beds are separated from each other by 30-70 cm successions composed of 4-10 recognizable ash-tuff beds.

In most areas the ash tuffs have undergone extensive alteration, and their present mineralogy is a function of alteration mineral assemblages within the footwall strata. These fine-grained rock types, therefore, contain abundant sericite, ankerite, chloritoid, and chlorite which replaces a very fine-grained quartz and feldspar-rich matrix. Broken 0.5-1 mm quartz phenocrysts are locally present in trace amounts.

Pumiceous Pyroclastic Deposits

Within the upper pyroclastic horizon and approximately 1 km west of Mattabi, a 200 meter thick sequence of pyroclastic deposits contains ragged, sometimes flattened fragments within an intensely

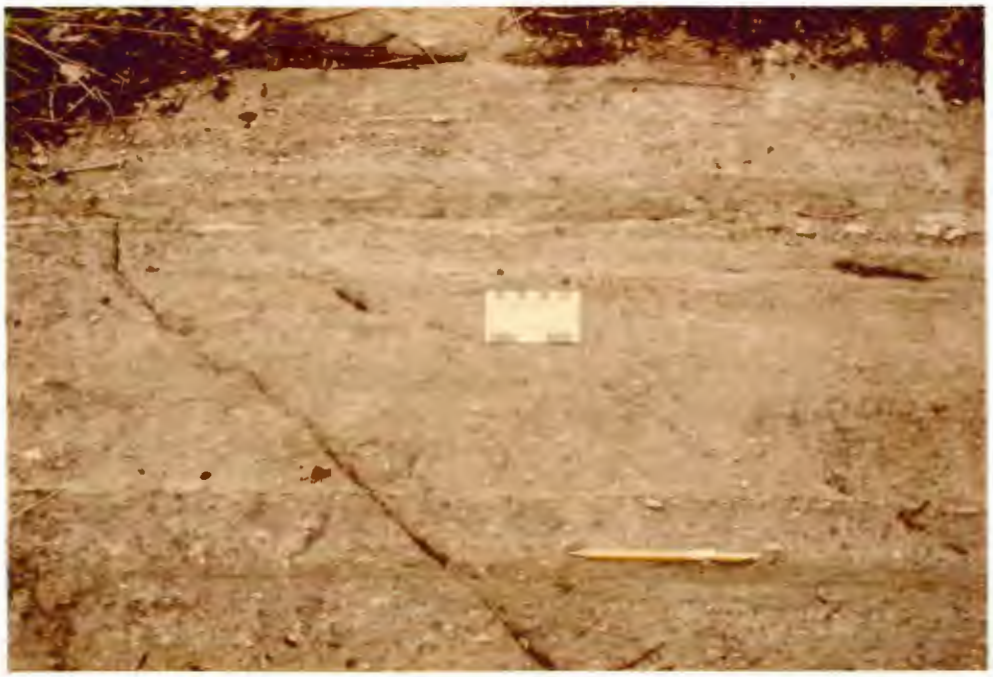

Figure 16. Thin-bedded lapilli and ash tuffs 4 km west of the Mattabi deposit. Lapilli beds exhibit normal grading (from pencil to top of scale card).

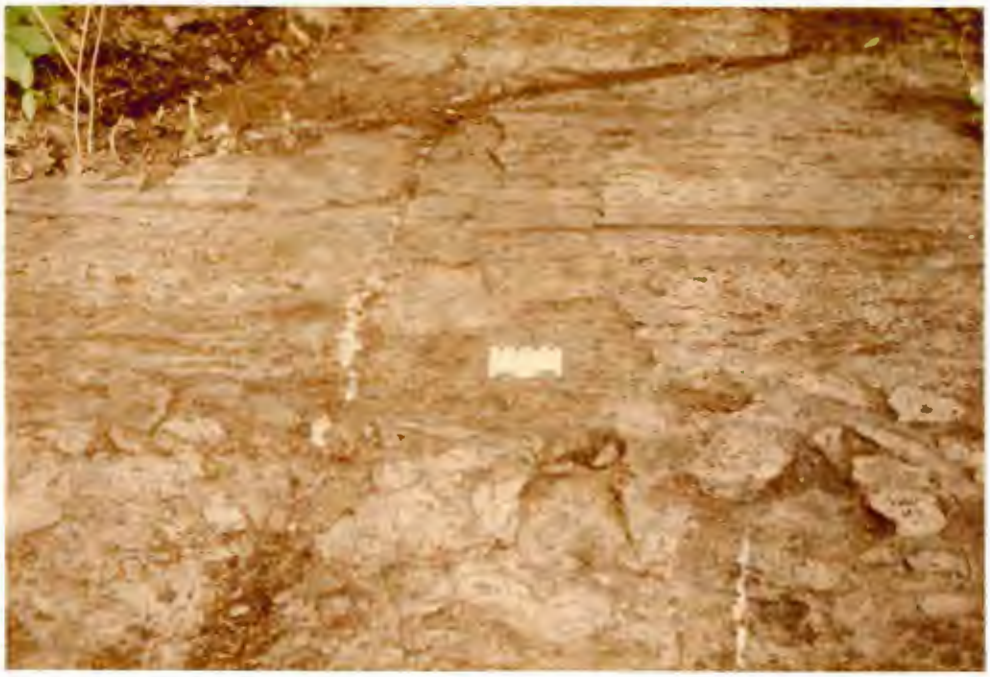

Figure 17. Bedded ash tuff overlying massive pyroclastic beds approximately 1 km WSW of the Mattabi deposit.

altered matrix. These 1-10 cm long fragments are commonly difficult to distinguish from the mottled, iron-stained matrix and, in outcrop, rarely appear to exceed 10% of the total rock. Similar-sized subangular, aphanitic, felsic lithic fragments, however, stand in relief and commonly show a greenish sericitic rim surrounding a bleached white core. These fragment types vary from 5 to 20% in abundance. Subrounded quartz-porphyritic blocks 15-20 cm in diameter are sparsely distributed throughout the horizon and comprise less than 2% of the deposit (Fig. 18).

Thin sections disclose that many of the fragments, both flattened and angular types, are highly amygdaloidal or pumiceous in texture. Amygdules 0.2-0.5 mm in size comprise 20-50% of the fragments and are composed of monocrystalline or polycrystalline quartz and feldspar. They are typically enclosed in a very fine-grained matrix of quartz and feldspar which has been partially or totally replaced by carbonate and/or sericite. Amygdules less than 0.2 mm in size, when set against a highly sericitized or carbonatized groundmass, give many pumiceous fragments a clastic appearance; i.e. the monocrystalline quartz and feldspar fillings appear as rounded, detrital-like grains.

In each of the aforementioned pyroclastic deposit types, fragments are set in a fine-grained matrix which exhibits considerable variation in mineralogy; its character is largely a function of alteration zoning around the Mattabi ore body. Massive pyroclastic beds directly beneath the ore body exhibit a well-foliated, sericitic groundmass, and light green sericitic rims (2-5 mm thick) outline

white to gray blocks. Dark green to black chloritoid grains (.2-1 mm) are also present. Further from the deposit, iron carbonate (ankerite) weathers easily and imparts a multicolored, blotchy nature to the pyroclastic beds. At even further distances from the deposit, pyroclastic beds commonly display a brownish-green chloritic ash matrix.

Quartz-Porphyritic Ash-Flow Deposits (Unit 4)

Two horizons within the upper pyroclastic sequence are quartz-porphyritic and appear as massive, buff to light gray-green flows or tuffs. One of the horizons is exposed in outcrop within the footwall study area. It is approximately 150 meters thick throughout its entire strike length. A similar quartz-porphyritic "rhyolite tuff" forms the immediate mine hanging wall and is well exposed along the eastern Mattabi pitwall.

In outcrop, the footwall unit is commonly a medium gray, markedly siliceous, quartz-porphyritic rock. Sparse, pale blue quartz phenocrysts 1-2 mm in size are readily visible. Greenish plagioclase phenocrysts are present in less foliated exposures; shearing obliterates the grains and highlights the resistant quartz phenocrysts. Close to the Mattabi orebody, this unit contains 5-10 mm massive pyritic fragments and disseminated 1mm pyrite euhedra.

Thin sections show 1 mm quartz phenocrysts set in a very fine-grained (< 0.1 mm) quartz and feldspar-rich groundmass (Fig. 19). The quartz grains are round to subangular, embayed, and some are broken. Alteration minerals, primarily sericite, overprint the groundmass and pseudomorph or totally mask 1 mm feldspar grains. Chlorite occurs as

Figure 18. Massive, pumiceous pyroclastic flow deposit. Flattened pumice fragments and two accessory quartz-porphyritic lithic blocks are visisble.

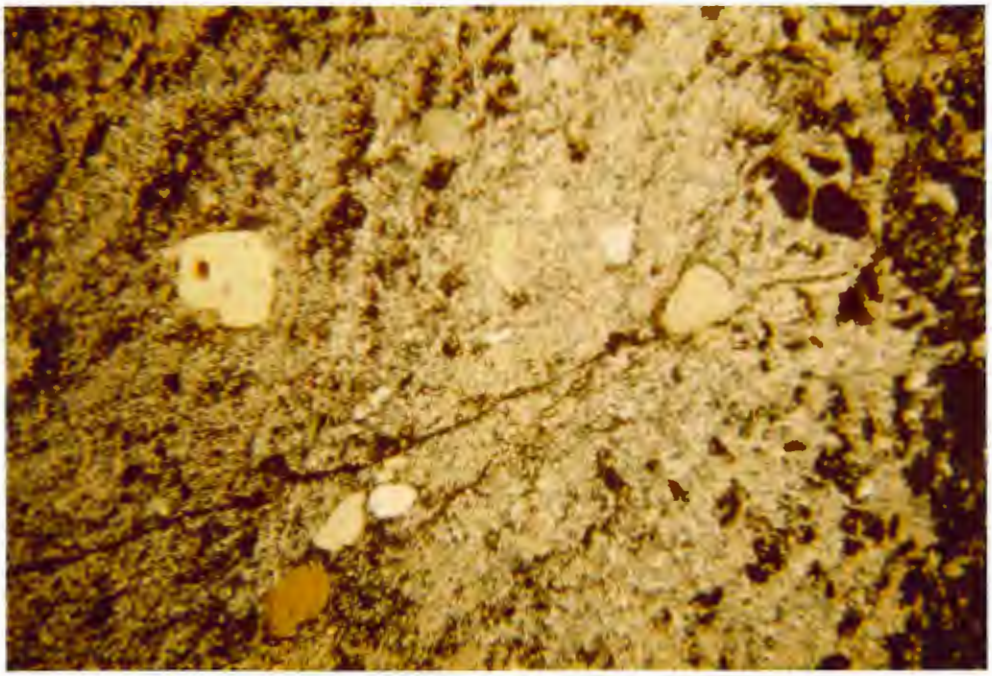

Figure 19. Photomicrograph of quartz-porphyritic ash-flow deposit. Note embayed and broken quartz phenocrysts. Crossed polars, field of view: 5 x 7 mm.

patchy domains or concentrations 0.2-2 mm in diameter, and 0.1 mm pyrite grains form diffuse circular concentrations 5-10 mm in size.

The abundance of broken quartz phenocrysts within a very fine-grained recrystallized groundmass suggests that the deposit is a product of an ash-rich pyroclastic eruption. Features that would be indicative of a felsic lava flow, such as amygdules or flow banding, are not evident. In addition, the deposit appears to be markedly uniform over a several-kilometer distance. For these reasons the unit has been labeled a quartz-porphyritic ash-flow deposit.

Felsic Block-and-Ash-Flow Deposit (Unit 6)

A felsic block-and-ash-flow deposit overlies a westward thickening horizon of amygdaloidal felsic lavas situated on the western end of the study area (Plate 1, Unit 6). The unit is roughly 100 meters thick and can be traced along strike for approximately 1 km; it comprises less than 5% of the total footwall strata.

In outcrop the block-and-ash-flow deposit is composed of large, angular to subangular felsic fragments which are poorly sorted and non-bedded (Fig. 20). Readily discernable fragment types include: a) angular white aphanitic fragments (2-20 cm), b) gray subangular to subrounded amygdaloidal fragments (8-30 cm) and c) alteration-outlined, possibly juvenile (pumiceous) fragments (2-8 cm). Overall fragment density varies from 20-50% within the deposit. Most of the fragments are readily contrasted by the mottled, altered matrix and stand in relief on weathered surfaces. Flattened, ragged juvenile(?) fragments are outlined by 5-10 mm iron oxide rims, whereas white siliceous fragments exhibit sharp fragment/matrix boundaries

(Fig. 21). The matrix shows abundant 1 cm iron-stained pits.

Easternmost exposures of the block-and-ash-flow deposit exhibit a considerably different weathered outcrop surface because of the difference in alteration. Fragment shapes and sizes are similar, but they display resistant rims and pitted interiors (Fig. 22). Black chloritoid porphyroblasts less than 1 mm in size are also visible within a green siliceous matrix.

Microscopic examination reinforces many of the field observations. Very fine-grained (<<.1 mm), angular quartz and feldspar-rich fragments exhibit either iron carbonate-chlorite or quartz-rich, granoblastic alteration rims. Fragment interiors are partially or completely obliterated by fine-grained carbonate. Chloritoid, where present, forms .5-1 mm anhedral porphyroblasts within the matrix.

The position of the block-and-ash flow within the footwall succession, i.e. its proximity to an underlying lava-flow horizon, suggests that this unit is genetically distinct from the previously described pyroclastic flows. A possible origin for the deposit is discussed in a following section.

FELSIC LAVA FLOWS (Unit 5)

Felsic lava flows comprise approximately 5% of the stratigraphic succession within the study area. The distribution of felsic lavas is limited to three primary locations: a) between mafic lava flows and debris flows north of Darkwater Lake, b) interbedded with felsic pyroclastic-flow deposits approximately 1 km due south of the Mattabi

Figure 20. Felsic block-and-ash-flow deposit north of Darkwater Lake.

Figure 21. Differential weathering of lithic and juvenile (?) fragments within block-and-ash deposit. Knife is 8 cm long.

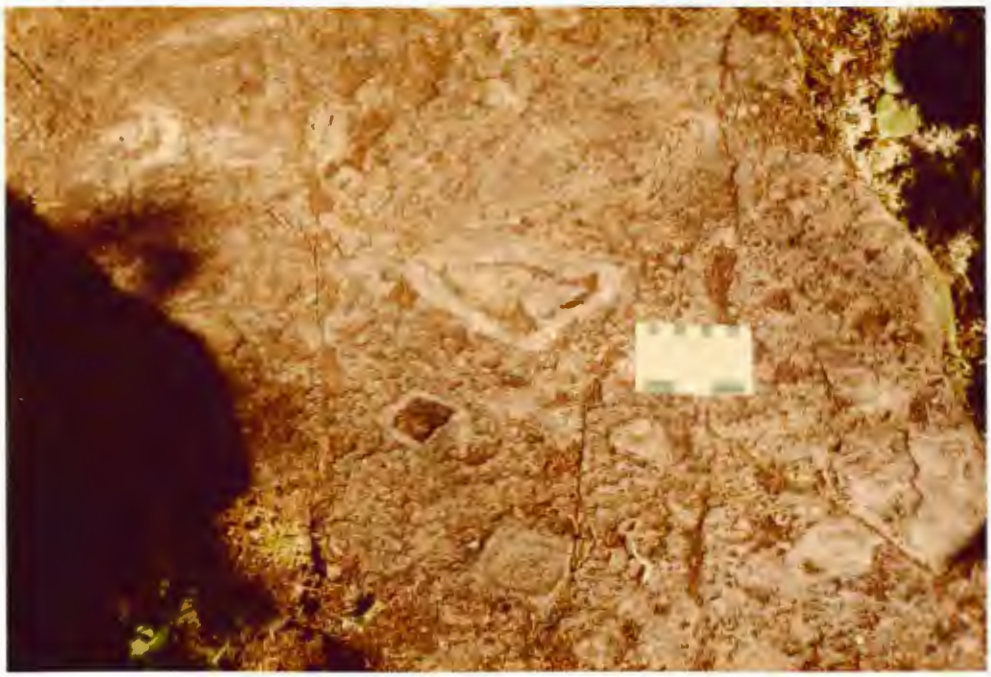

Figure 22. Carbonatized felsic block-and-ash deposit. Carbonate-rich fragment interiors weather out leaving "hollow core" fragments.

deposit and c) within a small, well-exposed area 2.5 km southeast of Mattabi (Plate 2).

Diamond drill holes have intersected an eastward-thinning horizon of altered felsic lavas immediately north of Darkwater Lake. The unit decreases in thickness from 100 meters to less than 30 meters over an 850 meter distance. Drill core samples of felsic lavas are composed of 5-8% plagioclase phenocrysts (1 mm) which are set in a buff to light gray, very fine-grained siliceous matrix. Chlorite veining increases with depth, and iron carbonate is present as diffuse 2-4 cm patches within irregular 1 to 3 meter zones.

Flows south of the Mattabi deposit are intercalated with pyroclastic deposits and heteroclithic debris flows. Outcrops on the shore of Tailings Lake (Plate 1) are light green to white in color, well-foliated and crosscut by 5 to 30 cm wide alteration veining (Fig. 23). The flows are in abrupt contact with 1 meter thick, poorly graded lapilli-tuff beds and 3-10 cm thick ash-tuff beds (Fig. 24).

In thin section relatively unaltered lava-flow samples are composed of 0.1 mm quartz and feldspar-rich mosaics with disseminated chlorite, sericite, stilpnomelane, carbonate and trace opaques. Quartz-filled, chlorite-rimmed amygdules, 0.2 to 0.5 mm in length, are present in trace amounts. Altered lava-flow samples exhibit complete obliteration of the quartz-feldspar mosaic by 0.1 mm anhedral carbonate and/or chlorite grains, and sericitic veining. Only larger, 0.2 mm quartz grains are locally preserved.

Figure 23. Altered felsic lava flow west of Tailings Lake. Flow is sheared and crosscut by carbonate-chlorite veining.

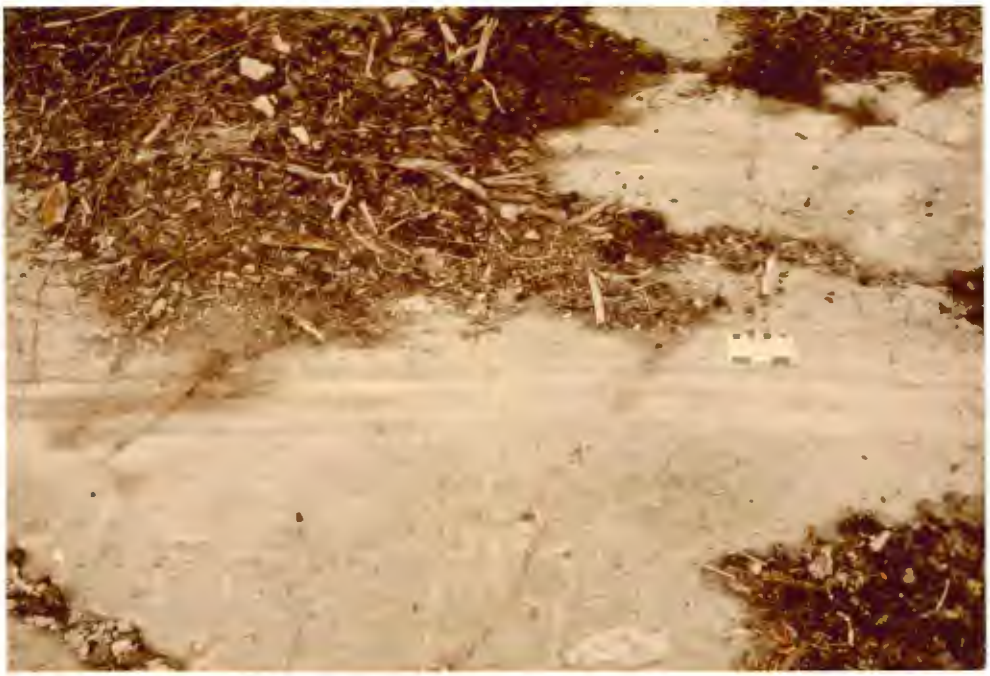

Figure 24. Normally graded, massive pyroclastic beds and overlying ash tuff. Succession immediately underlies lava flow in Figure 23.

Felsic Lava Flow/Tuff-Breccia Complex (Units 1 and 2, Plate 2)

A 400 m by 550 m area approximately 2.5 km southeast of Mattabi exhibits several amygdaloidal lava flows enveloped in felsic tuff-breccia (Plate 2). White to green massive lavas are outlined by 10 to 40 cm thick amygdaloidal margins (Fig. 25); resultant flow shapes are tongue or lobe-like in character and approximately 25 to 50 m thick. Surrounding the lava flows is an unsorted felsic tuff-breccia composed of 25-45% light gray, angular felsic blocks (3-20 cm in diameter) set in a similar-colored siliceous matrix.

The contact between the lava flows and the tuff-breccia is gradational over a 1 meter distance. Massive flow interiors with sparse amygdules are topped by a 0.5 meter thick faintly banded zone. The 1 to 3mm wide bands are composed of aligned amygdules and are separated from each other by massive non-amygdaloidal lava at 2-15 cm intervals. Chloritic veins 3 to 5 cm in width separate the banded portion of the flow from the outermost 40 cm thick amygdaloidal margin. This pitted, "popcorn-textured" margin contains rounded quartz- and chlorite-filled amygdules which are markedly drawn out around flow-folded portions of the margin (Fig. 26). The amygdules range from 5 to 20 mm in length and comprise 5-25% of the margin. At the outermost edge of the margin, markedly angular fragments (5-10 mm in diameter) increase in abundance (2-10%) into the overlying tuff-breccia. Here, the lava flow/tuff-breccia contact is a gradational, fragmental zone which is 5-10 cm in width.

The surrounding tuff-breccia contains 3-15% irregular-shaped chloritic fragments. The fragments are often drawn out into 25-30 cm

Figure 25. Amygdaloidal felsic lava-flow margin east of the Bell River. Hammer lies on felsic tuff-breccia; massive flow interior is visible in lower right corner of photo.

Figure 26. Stretched amygdules within flow margin pictured in Figure 25. Flow/tuff-breccia contact at top of photo. Pencil is 14 cm long.

Figur 27. Felsic tuff-breccia which envelopes lava flows east of the Bell River.

long ribbons and are bent around the more competent siliceous blocks (Fig. 27).

In thin section the massive flow interiors are composed of 0.1 mm quartz and feldspar mosaics with lesser amounts of disseminated chlorite, stilpnomelane, sericite and opaques. Subhedral tourmaline grains (0.1-0.2 mm in length) are also present in trace amounts. In several samples rare albite twinning is preserved in scattered, fine-grained dusty feldspar grains.

Thin sections from the flow margins display large (1-5 mm) amygdules with radial quartz growths rimmed by fine-grained chlorite. Sericitic veining envelopes the amygdules and replaces a very fine-grained quartz- and feldspar-rich groundmass. Angular felsic fragments (4 to 10 mm in diameter) are rimmed by 0.2 mm granoblastic quartz margins, and fragment interiors are composed of 0.1 mm subhedral chlorite and quartz grains.

The small, angular fragments at the outer edge of the flow margin (and grading into the tuff-breccia) are believed to be hyaloclastic material from a water-quenched lava skin. Larger fragments within the tuff-breccia are most likely products of dome/lava flow disintegration and subsequent avalanching down steep flow fronts. De Rosen-Spence et al. (1980), in comparing subaqueous felsic lava flows in the Rouyn-Noranda, Quebec area with analogous Pleistocene flows in Iceland, describe similar massive flow/breccia relationships. Their observations suggest that the Bell River area (Plate 2) represents a distal lava flow facies dominated by thin lava "tongues" or lobes enveloped in large amounts of felsic breccia.

INTERMEDIATE INTRUSION (Unit 7)

A subconcordant porphyritic intrusion is present along the northern boundary of the study area west of Mattabi (Plate 1). It intrudes and dilates a quartz-porphyritic ash-flow deposit and forms a lenticular body with a maximum thickness of 180 meters. The intrusion can be traced westward along strike for approximately 1 km before pinching out. Mapping by Franklin et al. (1977) indicates that the intrusion continues upward into the mafic hanging wall succession.

The intrusion is a buff to green, homogeneous, well- jointed rock with 2 mm plagioclase phenocrysts readily visible on weathered surfaces. Exposures are weakly to moderately magnetic.

In thin section the rock is composed primarily of 2-3 mm plagioclase phenocrysts which are pseudomorphed by chlorite, carbonate, and/or sericite. Anhedral quartz grains and magnetite grains (0.2-1 mm in diameter) are set in a very fine-grained granoblastic groundmass. Microlitic sphene grains commonly surround ragged subhedral magnetite grains, and several of the magnetite grains display lamellar ilmenite exsolution. Fine-grained carbonate replaces much of the quartzofeldspathic matrix.

QUARTZ-FELDSPAR PORPHYRY INTRUSION (Plate 2, Unit 4)

Mafic debris flows and felsic flow-breccias southeast of Mattabi (Plate 2) are intruded by a quartz- and feldspar-porphyritic rock. The intrusion is white to pink, and sparse 1 mm quartz phenocrysts are highlighted by 1-2mm wide, dark spidery veinlets which emanate outward from the phenocrysts.

In thin section the rock contains 1-2 mm diameter subhedral quartz phenocrysts and 2 mm plagioclase phenocrysts enclosed in a very fine-grained (<0.1 mm) granoblastic, quartzofeldspathic groundmass. The dark veinlets viewed in outcrop are composed of biotite and/or stilpnomelane. Tourmaline and magnetite (0.1 mm grains) are also present in trace amounts.

Intrusive contact relationships are not visible in the field. However, when compared to the altered, aphyric amygdaloidal lavas in the immediate area, the homogeneous, porphyritic, unaltered features of the rock suggest that it is an intrusion.

BEIDELMAN BAY INTRUSION (Unit 8)

The Beidelman Bay intrusion marks the southern boundary of the study area and has not been examined in detail. Trowell (1974) and Poulsen and Franklin (1981) have done detailed work on this differentiated (dioritic to trondhjemitic) intrusive body.

Within the study area the Beidelman Bay intrusion consists of: a) plagioclase-porphyritic andesite and b) trondhjemite. The porphyritic andesite is present along the northern intrusive contact near Darkwater Lake (Plate 1) and is intrusive into overlying mafic extrusive rocks. Trondhjemitic rocks crop out along the southern shores of Darkwater Lake and near the Bell River north of Bell Lake (Fig. 3, south of study area).

Porphyritic andesite exposures are typically dark gray-green and are well jointed. White to hematite-stained plagioclase phenocrysts (2-3 mm in diameter) are set in a dark aphanitic groundmass and range in abundance from 10 to 25%. The rock is commonly sheared; en echelon

Figure 28. Mafic xenoliths within porphyritic andesite intrusion west of Darkwater Lake.

tension gashes and 1 m wide shear zones are common. Outcrops in close contact to mafic flows exhibit 15-40 cm rounded mafic xenoliths set in a feldspar-rich groundmass (Fig. 28). Thin sections show that the dark aphanitic groundmass is composed largely of microcrystalline quartz and feldspar with lesser amounts of chlorite, actinolite, sericite, carbonate, magnetite and sphene. Epidote grains are present in plagioclase cores or as rounded 1 mm clusters.

Trondhjemitic rocks display blue-gray, rounded 2 mm quartz grains comprising 15-30% of the rock, whereas feldspar and minor biotite and chlorite form a slightly finer-grained groundmass. Thin sections exhibit 2 mm twinned plagioclase grains, anhedral quartz grains with undulose extinction and interstitial chlorite.

INTERPRETATION OF A PORTION OF THE UPPER FOOTWALL SUCCESSION

As shown in Figure 5 and Plate 1, the upper 600+ meters of footwall strata is composed largely of felsic pyroclastic and mafic debris-flow deposits which rest on a lower lava flow-dominated succession of rocks. The presence of these fragmental deposits in apparent juxtaposition with one another and the volume of massive to poorly-bedded mafic debris-flow material warrants discussion of a volcanological model. The abundance of outcrop north of Darkwater Lake provides a more complete section here than in other areas of the Mattabi footwall, and it is this complex stratigraphy which forms the foundation of the following argument.

The scoriaceous nature of much of the mafic debris, along with subordinate amounts of mafic hyaloclastite and pillowed lavas within the succession, indicates that this portion of the footwall section

has been emplaced predominantly by shallow water, mafic phreatomagmatic eruptions (Sheridan and Wohletz, 1983). Such hydrovolcanic eruptions (the interaction of magma and external water) is controlled primarily by water/magma ratios (Sheridan and Wohletz, 1981). Resultant eruptions produce either dry pyroclastic flows and surges (water/magma<1) or "wet" base surges, cypressoid ash clouds, mud hurricanes and/or lahars (water/magma>1). The subaqueous nature of the Mattabi footwall strata suggests that high water/magma ratios would have existed and that the majority of eruptions would have produced subaqueous mud hurricanes and/or debris flows (lahars).

Tuff cones are volcanic landforms commonly produced by hydrovolcanic eruptions (Sheridan and Wohletz, 1981). The deposit types present north of Darkwater Lake bear a close resemblance to documented tuff-cone successions (Wohletz and Sheridan, 1983; Fisher et al., 1983). Tuff cones are typically composed of three major deposit types which, in order of emplacement, are: 1) explosion breccias composed of underlying country rocks, 2) cross- to plane-stratified, thin-bedded surge deposits, and 3) thick-bedded to massive ash-rich deposits and bedded fall material (Wohletz and Sheridan, 1983).

Within the study area mafic debris-flow deposits, commonly ash-rich and massive, are similar to thick-bedded deposits which form the bulk of tuff-cone crater rims. Mafic debris-flow deposits also contain large lapilli or blocks which form recognizable layering within finer mafic ash and scoria (Fig. 11). These stratifications

are analogous to bedded fall material within thick-bedded tuff-cone deposits. The clast-rich (>50%) portions of the deposit are products of water-saturated surges emplaced on the flanks of a steep-sided, submerged mafic vent. Thin pillow lavas and subordinate hyaloclastite may be a result of deeper-water, non-explosive extrusions along the perimeter of the growing tuff cone.

Thin-bedded surge deposits are lacking or have not been recognized within the Darkwater Lake section. Their emplacement may have been prohibited by excessive water/magma ratios (i.e. subaqueous versus subaerial extrusion), or possibly their identifying structures (i.e. cross-bedding) have been obliterated by later alteration processes.

The felsic block-and-ash deposit which underlies the mafic debris-flow deposits most likely represents explosion breccia at the base of the "tuff-cone" succession. The large, angular felsic lava flow blocks and accessory juvenile fragments form a chaotic, ash-supported deposit which was emplaced by "vent breaching" of the underlying felsic lava flow horizon (Plate 1).

The locus of the phreatomagmatic activity within the Darkwater Lake portion of the study area appears to have been centered around a northeast extension of an 020° trending shear which is visible within portions of the volcanic footwall (Plate 1). Numerous porphyritic andesite dikes and sills in this region suggest that the area may have been an active vent late in the formation of the footwall succession.

The apparent juxtaposition of mafic debris-flow deposits against massive pumiceous pyroclastic flows may be a result of synvolcanic

faulting along the 020° shear. Faulting would have occurred after emplacement of the mafic debris flows but prior to the extrusion of quartz-porphyritic ash-flow tuff which forms a uniformly thick deposit across the upper portion of the footwall sequence (Plate 1). Such faulting could have led to large-scale slumping and collapse of the eastern tuff-cone rim into the cone crater (Wohletz and Sheridan, 1983). This in turn would have allowed the emplacement of pumiceous pyroclastic deposits against the newly formed mafic succession. The pumiceous deposits, also products of shallow-water phreatomagmatic eruptions, would have originated from a more easterly situated vent and traveled into the newly formed topographic low.

The above model is idealized, and it requires detailed sedimentological study of the mafic debris-flow deposits to ascertain their similarity to modern tuff-cone depositional sequences. The present knowledge of the stratigraphic succession within the Darkwater Lake region forms a strong argument for relatively shallow water mafic hydrovolcanism analogous to modern tuff-cone-forming proccesses.

STRATIGRAPHIC SUCCESSION AND GEOLOGIC HISTORY

The present footwall succession beneath the Mattabi deposit is a product of two large-scale volcanic processes: a) a mafic to felsic cycle of volcanism and b) the interfingering and intermixing of lavas and fragmental rocks originating from source areas both east and west of the study area.

Sustained subaqueous mafic volcanism produced a thick sequence of mafic lava flows and breccias. Laterally continuous flows of

relatively uniform thickness were deposited across the entire length of the study area indicating that eruptions were both lengthy and voluminous. Minor amounts of intercalated felsic pyroclastic material were supplied by a distant felsic source developing east of the present Mattabi orebody.

These events were followed by localized felsic volcanism. Vents both east and west of Mattabi produced thin felsic lava-flow horizons capping the extensive mafic base. Felsic lava flows east of Mattabi were also intercalated with well-bedded pyroclastic flows from a possibly more distant source.

The gradual shallowing upward of the submerged vents resulted in the commencement of phreatomagmatic eruptions. West of Mattabi, the thin felsic lava-flow horizon was breached by an explosive eruption, and debris flows laden with mafic juvenile material were emplaced above the brecciated felsic lava flows. At the same time or shortly after, felsic phreatomagmatic eruptions commenced further east and supplied extensive felsic pyroclastic material which intercalated and intermixed with the basaltic debris. Explosive volcanism east of the present Mattabi deposit continued and eventually overrode and truncated mafic debris-flow deposits. This series of explosive eruptions produced a succession of primary pyroclastic material over 600 meters thick.

During this period of felsic volcanism the Beidelman Bay intrusion was emplaced within the lower mafic lithologies. REE data and U-Th dates have confirmed that the intrusion is a subvolcanic

equivalent to the felsic footwall immediately beneath Mattabi (Franklin, pers. comm., 1983).

As felsic volcanism waned, hydrothermal activity within the volcanic pile increased, and several discharge areas were established on the sea floor. Base and precious metals were precipitated in considerable quantities at several of the vent areas forming what are now the Mattabi, Sturgeon Lake, and F-Zone massive sulfide deposits. This event was rapid, and it was eventually terminated by abating felsic pyroclastic activity. Mafic volcanism again commenced and began a new differentiated cycle of volcanism marked by the emplacement of mafic agglomerate and pillowed mafic lava flows (Franklin et al., 1977).

ALTERATION AND METAMORPHISM

INTRODUCTION

The volcanic rocks beneath the Mattabi massive sulfide deposit have been subjected to hydrothermal alteration associated with a major ore-forming event. Subsequently, both altered and unaltered rock types have undergone regional greenschist facies metamorphism and locally hornblende hornfels facies contact metamorphism near the margins of large intrusions (Trowell, 1974).

It is the purpose of this study to examine the progressive mineralogical and chemical changes within the footwall succession and to relegate such changes to either synvolcanic hydrothermal alteration or post-mineralization metamorphism. Particularly, hydrothermal alteration must be examined in terms of least-altered and most-altered sample types from individual lithologies. After grouping and delimiting various styles and intensities of alteration within the study area, semiquantitative comparisons can then be made.

ALTERATION ASSEMBLAGES

Field observations and petrographic studies permit the establishment of alteration assemblages throughout the Mattabi footwall succession. Such assemblages are a function of anomalous mineral abundances (notably ankerite, chlorite, sericite, and chloritoid) which cannot be accounted for by regional metamorphism alone. Chloritoid, although metamorphic in origin, is indicative of iron-rich, alkali- and CaO- depleted, aluminous rocks (Latour et al., 1980). Such chemical conditions have been documented beneath the Mattabi deposit (Franklin et al., 1975), and therefore the mineral

constitutes part of an important alteration assemblage.

The alteration assemblages established within the study area include a) a least-altered assemblage, b) an iron carbonate-chlorite-rich assemblage, c) a sericite-rich assemblage and d) a chloritoid-rich assemblage. The assemblages vary in terms of mineral abundances and accessory minerals, and in many cases thin-section study establishes the replacement of one assemblage by another. Nevertheless, the assemblages are readily recognizable in the field, and individual lithostratigraphic units can be traced from least-altered areas through several alteration zones. The alteration zones are not necessarily conformable to stratigraphy, although in many areas a direct correlation does exist. Plate 3 shows the distribution of each assemblage throughout the study area and highlights both crosscutting and semiconformable alteration geometries.

The following descriptions are a summary of megascopic and microscopic features and mineral abundances for each alteration assemblage. More complete modal mineral abundances for individual rock types are tabulated in Appendix A.

Least-Altered Assemblage (albite + quartz ± chlorite, sericite, carbonate, epidote, stilpnomelane, actinolite)

Least-altered rocks are those rocks, both mafic and felsic, which display typical greenschist facies mineral assemblages and modes most consistent with primary igneous compositions. The rocks, however, cannot be classified as unaltered; certain samples within the assemblage do indeed show questionable textures or mineral abundances

which are most likely attributable to hydrothermal alteration. When compared to more-altered lithologic equivalents, however, they are the least-altered rock types within the study area.

Least-altered rocks are situated primarily within the lower mafic portion of the footwall strata (Plate 3). Much of the mafic debris-flow horizon is also composed of least-altered assemblages, and felsic lava-flow interiors southeast of Mattabi (Plate 2) are included in this group.

Least-altered mafic rocks contain albite, quartz, chlorite, actinolite, epidote and carbonate. Plagioclase phenocrysts are generally euhedral and display only minor carbonate, epidote, and sericite alteration. Amygdules are well preserved and filled with dolomite/calcite, quartz, or chlorite. Mafic debris-flow fragments commonly exhibit felty to pilotaxitic feldspar groundmasses.

Least-altered felsic rocks are composed of fine-grained (0.1 mm) quartz and feldspar mosaics with disseminated chlorite, sericite, and stilpnomelane. Where present, plagioclase microphenocrysts and amygdules are well preserved.

Iron Carbonate-Chlorite Assemblage (ankerite + chlorite ± sericite, quartz, chloritoid)

Iron carbonate-chlorite assemblage rocks form an elongate zone which extends from the north shore of Darkwater Lake upward to the immediate mine footwall strata (Plate 3). Smaller zones of iron carbonate-bearing rocks are also present above felsic lavas near Darkwater Lake and within rocks situated on the shore of Tailings Lake.

X-ray diffraction studies of ten samples from carbonate-rich rocks reveal that ferroan dolomite/ankerite is the predominant carbonate species, whereas calcite/dolomite is present within least-altered samples (Table 12, Appendix C). Franklin et al. (1975) note that siderite is present in a "pipe-like" zone beneath the Mattabi ore body and that the boundary between siderite and ferruginous dolomite (ankerite) outlines the proximal alteration described in their work. Siderite, however, was not identified in the XRD analyses. This may be a function of the lack of outcrop immediately due south of the ore deposit. Pitwall samples which appeared to contain siderite did not have sufficient amounts of carbonate for qualitative XRD analysis.

Ankeritic rocks are easily identified in the field by thick iron oxide rinds imparted on exposed surfaces. The rocks typically display a multicolored mottling, and fragments are outlined by iron oxide rims. Pits (1-2 cm in diameter) are common on outcrop surfaces.

In thin section it is generally not possible to differentiate ankerite from dolomite, although deeply weathered samples may show limonite-hematite along carbonate cleavage planes. Carbonate grains are typically subhedral and average 0.1-0.2 mm in size. Rounded carbonate-chlorite domains (2-10 mm in diameter) are a common microscopic feature within ankeritic rocks (Fig. 29). Plagioclase phenocrysts and pumiceous fragments are particularly susceptible to carbonate replacement.

A technique for staining ferroan dolomite/ankerite with potassium ferricyanide was employed on selected carbonate-rich samples. A

solution was prepared according to Evamy (1963), and selected thin sections were stained. The potassium ferricyanide reacts with ferrous iron in the carbonate and imparts a blue stain. Siderite does not stain unless heated. Staining reaffirmed that much of the carbonate within the carbonate-chlorite altertion assemblage is iron-bearing carbonate, i.e. ferroan dolomite and/or ankerite.

Ferroan dolomite/ankerite (10-40%) and chlorite (5-30%) are essential constituents of this alteration assemblage. Anastomosing veinlets of sericite (0-35%) commonly envelope ankerite-chlorite domains. Chloritoid (0-8%) may be present as ragged porphyroblasts or irregular veinlets.

Sericite Assemblage (sericite + quartz ± chlorite, carbonate, chloritoid)

Sericite-assemblage rocks occur as: a) broad zones within the upper pyroclastic horizon, b) vein-controlled alteration which crosscuts ankerite-assemblage rocks and c) as massive alteration within mafic breccias and felsic lavas near Darkwater Lake (Plate 3). The rocks are typically light green-brown in color and well-foliated. Felsic fragments commonly show 2-5 mm light green sericitized rims.

In thin section sericite occurs as either very fine-grained (<0.1 mm) shreds replacing feldspar or as anastomosing veinlets of massive sericite. Ilmenite grains are commonly concentrated in the centers of massive sericitic veining. Plagioclase phenocrysts are pseudomorphed or totally obliterated by sericite. Felsic fragments, where altered, exhibit sericitized rims and groundmasses, whereas pumiceous fragments generally retain their carbonate-rich character.

Sericite comprises 12 to 60% of the rocks, and quartz (15-70%) is ubiquitous. Chlorite (0-32%) and carbonate (0-28%) are typically present, and chloritoid (0-6%) occurs within several sericite-assemblage rocks as irregular patches or subhedral laths.

Chloritoid Assemblage (chloritoid + ankerite + sericite + quartz, ± chlorite, andalusite)

Chloritoid-assemblage rocks are located primarily within the upper pyroclastic horizon and increase in abundance towards the Mattabi deposit. The mineral is also present in significant amounts within felsic lavas north of Darkwater Lake (Plate 3). Where well-developed, chloritoid porphyroblasts are generally visible in the field as black, stubby 1 mm grains within a gray siliceous groundmass.

In thin section chloritoid occurs as: a) veins of 0.2-1 mm anhedral grains, b) ragged subhedral laths 0.5-1 mm in size and c) 1 mm subradial "bow tie" porphyroblasts (Fig. 30). Chloritoid is typically developed within sericite-rich portions of the rock, although less commonly it is present within iron carbonate-chlorite domains. Pumiceous fragments more rarely display Type (a) chloritoid around amygdules, whereas quartz- and feldspar-rich fragments generally exhibit sericite-assemblage alteration. Chloritoid varies in abundance from 5-35%.

Andalusite is present within several chloritoid-assemblage rocks as 2-10 mm ragged poikiloblasts. It occurs only within chloritoid-bearing rocks, and where present amounts to 1-8% of the rock.

Sericite (4-36%) and quartz (15-60%) are essential constituents

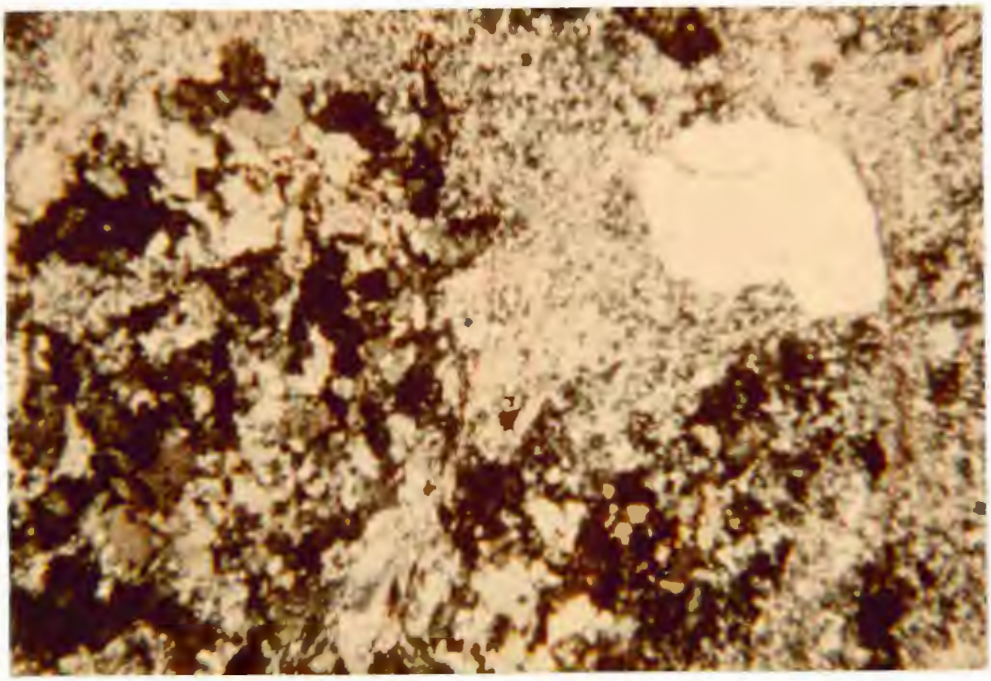

Figure 29. Photomicrograph of iron carbonate-chlorite alteration within quartz-porphyritic ash-flow tuff. Coarser-grained carbonate (bright) and chlorite (green) form sub-spherical domains within sericitized quartzofeldspathic groundmass. Crossed polars, field of view: 2 x 3 mm.

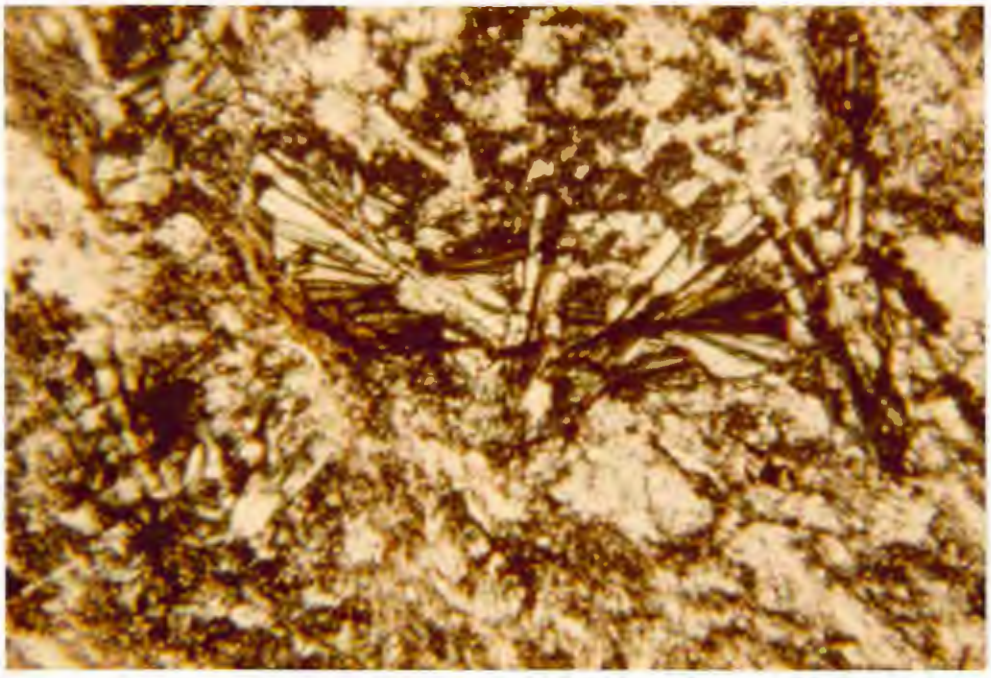

Figure 30. Photomicrograph of well-developed chloritoid porphyroblasts within sericitized quartz-porphyritic ash-flow tuff 3 km west of the Mattabi deposit. Crossed polars, field of view: 2.5 x 4 mm.

of chloritoid-assemblage rocks. Ankerite (0-42%) is also present in all but one sample. Chlorite (0-18%) occurs in 13 of 18 samples containing greater than 5% chloritoid.

Factors Governing Distribution of Alteration

The distribution of the four alteration assemblages within the study area (Plate 3) suggests that there is a considerable degree of stratigraphic conformity. Franklin et al. (1975) describe a "pipe-like" geometry to the alteration immediately beneath Mattabi. However, such an alteration pattern was not found within the rocks of the study area. Instead, broad subconcordant zones of alteration are present, and the intensity of the alteration increases upward toward the massive sulfide deposit.

Iron carbonate-chlorite alteration appears to have been controlled to a large degree by the primary permeability of the rocks. The alteration assemblage is confined largely to pumiceous pyroclastic and block-and-ash deposits. Sericitized felsic lavas north of Darkwater Lake (Plate 3) form a sharp boundary against the ankeritic fragmental units.

Sericitic alteration is less conformable to stratigraphy, and it crosscuts several lithologies within the southeast corner of the study area (Plate 3). Portions of the iron carbonate-chlorite alteration zone are also enveloped by anastomosing sericitic alteration. In the uppermost footwall rocks beneath Mattabi, however, sericitic alteration forms elongate, semi-conformable zones within quartz-porphyritic ash-flow tuffs and massive felsic pyroclastic-flow deposits (Plate 3).

The crosscutting alteration within the lower footwall rocks was most likely controlled by synvolcanic faults and fractures which provided channelways for hydrothermal solutions through relatively impermeable lava flows. Conformable alteration zones higher in the succession were preferentially developed in permeable felsic pyroclastic rocks, and, as the solutions migrated through these units, early iron carbonate-chlorite domains were enveloped by sericite.

Chloritoid-assemblage alteration forms discontinuous zones within ankeritic and sericitic rocks. The distribution of this metamorphic mineral is controlled largely by bulk chemical composition established prior to metamorphism. Its presence is discussed further in following sections.

Regional Metamorphism

The rocks within the South Sturgeon Lake region have undergone regional greenschist facies metamorphism (Trowell, 1970). Mafic rocks (debris-flow deposits and lava flows) are typically composed of albite, quartz, chlorite, epidote, actinolite and carbonate with or without stilpnomelane and/or sericite. These minerals are products of metamorphic reactions within basaltic rocks which originally contained calcic plagioclase, clinopyroxene, and possibly orthopyroxene and/or olivine (Winkler, 1976). Nearer to the Beidelman Bay intrusion, mafic volcanic rocks contain fine-grained, fibrous amphibole clusters with albite, quartz, epidote, chlorite, biotite and sphene. Winkler (1976) labels similar assemblages "low-grade amphibolites", whereas Turner (1981) indicates that such an assemblage represents the greenschist-

amphibolite transition. The presence of almandine porphyroblasts in mafic rocks east of the Bell River (Plate 2) is also indicative of similar metamorphic grades. Trowell (1974) notes that almandine-amphibolite assemblages are common near the margin of the Beidelman Bay intrusion and that the regional metamorphic grade increases eastward across the South Sturgeon Lake area.

For several hundred meters away from the outer margin of the Beidelman Bay intrusion (Plate 1), mafic flows and breccias more rarely contain circular aggregates of epidote (4-20 mm in diameter) with albite, quartz and carbonate. Kuniyoshi and Liou (1976) describe similar epidote "spherules" within massive basaltic lava flows adjacent to Coast Range intrusions in British Columbia. They indicate that the albite-epidote-actinolite-chlorite assemblage within these rocks is representative of albite-epidote hornfels facies metamorphism. Turner (1981) notes that this facies is mineralogically identical to regional greenschist facies assemblages, and it is a low pressure variant of the two. The circular epidote clusters in the rocks of the study area are possibly textural relicts of an early albite-epidote facies aureole which survived later regional greenschist facies metamorphism.

The development of chloritoid and andalusite is assumed to have been brought about by regional metamorphism; porphyroblastic and poikiloblastic textures support this assumption. Chloritoid is present in both ankerite and sericite-assemblage rocks, but its development is most pronounced within well-foliated, sericitized rocks near the Mattabi deposit. The development of chloritoid within

similar ankerite- and sericite-bearing volcanic rocks has been described by Gustafson (1946) at the Hollinger Mine in Ontario and more recently by Goodwin (1962) and Nebel (1982) at the Michipicoten iron range near Wawa, Ontario. Nebel (1982) attributes the formation of chloritoid at the Helen Mine to a premetamorphic assemblage of chlorite and pyrophyllite which was unstable at greenschist facies conditions. Franklin (pers. comm., 1982) proposes that iron carbonate was involved in the production of chloritoid within the immediate mine footwall rocks. Its formation within the ankeritic and sericitic rocks of the study area will be examined in greater detail within the following Geochemistry chapter.

ALTERATION GEOCHEMISTRY

INTRODUCTION

The Geological Survey of Canada's analytical chemistry section performed whole rock major oxide and trace element analyses on 103 selected samples from the study area. Sample locations are shown on Plates 2 and 3 (outcrop numbers), and results have been compiled in tables 7 and 8 of Appendix B. "In-house" standard results and analytical statistics are also given in Appendix B.

Major oxides were analyzed by fused pellet X-ray fluorescence (XRF) except FeO, H_2O^T, CO_2 and S which were done by rapid chemical analysis. Loss on ignition (volatile content), after analysis for H_2O and CO_2, was determined to be free (elemental) carbon. Cu, Zn, Co, Cr and Ni values were obtained with standard atomic absorption techniques, while Rb, Sr, Y and Zr were analyzed with energy dispersive XRF.

Inspection of whole rock analyses reveals that the rocks within the study area vary from basalt to rhyolite in terms of SiO_2 content (44.8 to 78.9 wt.%). Mafic volcanic rocks range from 44 to 55% SiO_2, whereas felsic lavas vary from 52 to 78%. Altered felsic pyroclastic rocks have relatively low SiO_2 values (57% average), and mafic debris-flow deposits have SiO_2 values similar to mafic volcanic rocks.

Average TiO_2 values are relatively high in each of the footwall lithologies, particularly within altered pumiceous pyroclastic rocks. The average for mafic volcanic rocks is 1.11% TiO_2, for mafic debris-flow deposits 1.18%, and for felsic pyroclastic rocks 0.92%. Felsic lavas, in addition to having high SiO_2 values, are readily

distinguished by low (average 0.60%) TiO_2 values.

The analyses also show that the entire study area is anomalously rich in CO_2. Excluding rocks with greater than 70% SiO_2, extrusive footwall lithologies have a minimum of 3% CO_2. The mean for all samples is 4.1% CO_2. Altered pumiceous pyroclastic rocks exhibit the highest CO_2 values; these rocks average 8.0% CO_2. Samples from east of the Bell River have relatively low CO_2 contents.

Elemental carbon values vary from 0.3 to 2.3%. It is most prevalent within carbonate-rich, pumiceous pyroclastic rocks and is presumed to exist in a cryptocrystalline, amorphous form.

The degree of alteration in the rocks from the study area prohibits the use of standard petrochemical plots and indexes for rock classification, magmatic affinity, etc. Instead, alteration trends have been examined and mass-balance computations utilized to identify the different alteration features.

ALTERATION TRENDS

Figure 31 is an alkali ratio diagram from Hughes (1973); it is subdivided into regions corresponding to unaltered calc-alkaline and tholeiitic volcanic rocks ("igneous spectrum") and spilitic rocks. Those rocks which have undergone hydrothermal alteration tend to plot outside of the igneous field (Meyers and MacLean, 1983).

Analyses of mafic lava flows ("basalts" in Fig 31), felsic lavas and intrusive rocks from the study area reveal several features when plotted on the diagram. First, mafic as well as felsic lava flows display sodium depletion and/or potassium enrichment relative to the

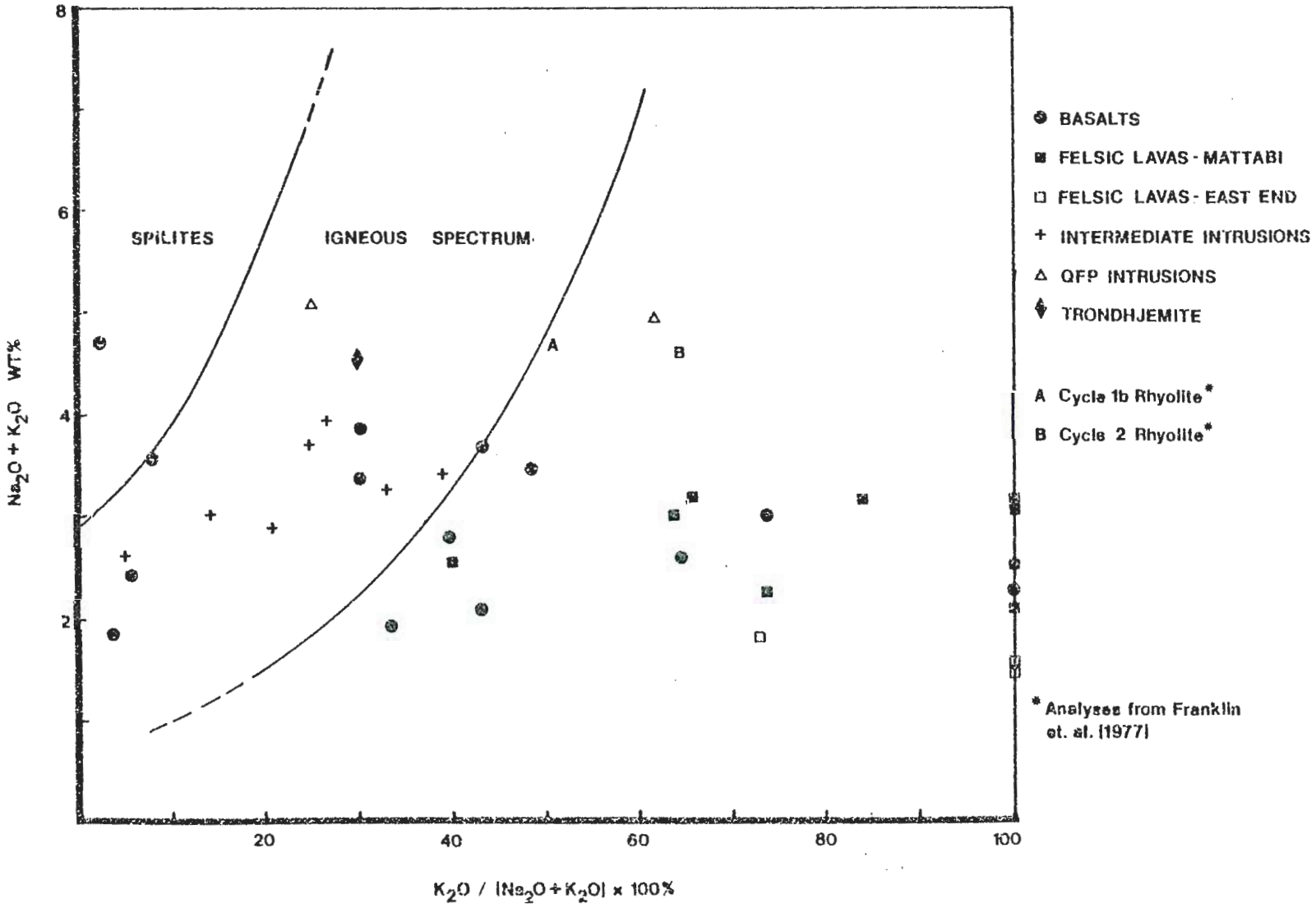

Figure 31. Alkali ratio diagram (from Hughes, 1973) with selected footwall units plotted. Points A and B are from stratigraphically higher cycles of volcanism in the Sturgeon Lake area.

igneous spectrum. None of the felsic lava samples plot within the igneous field suggesting that alteration of these rocks is widespread. Secondly, least-altered basalts show little evidence of an early spilitization event. Hydrothermal alteration, however, may have shifted spilitized rocks back into the igneous field by mutually depleting K_2O and Na_2O. Thirdly, feldspar-porphyry intrusions and subconcordant sills plot within the igneous field; this supports their post-alteration nature.

Sodium Depletion

Franklin et al. (1977) note that there is a wide zone of Na_2O-depleted rocks within the Mattabi footwall strata relative to the hanging wall. Their analyses of rhyolitic rocks from higher cycles of volcanism in the South Sturgeon Lake area list Na_2O values of 1.5 to 2.2%, whereas "rhyolitic" rocks immediately beneath the Mattabi deposit contain 0.20% Na_2O. Severin (1982) also documents Na_2O depletion within footwall felsic volcanic rocks at the Sturgeon Lake mine 6 km east of Mattabi (Fig 3). His altered rocks have an average Na_2O content of 0.35% versus "unaltered" equivalents containing 1.29% Na_2O.

The alkali ratio diagram (Fig. 31) highlights the marked depletion of sodium and/or addition of potassium within felsic lava samples from the study area relative to similar unaltered rock types within the Sturgeon Lake area ([Fig 31], points A and B). The geochemical results in Table 7 further indicate that a zone of sodium depletion (which includes felsic lavas and felsic pyroclastic rocks) extends 2.5 km southwest of Mattabi. Further west, marked sodium

depletion is limited to felsic lavas; pyroclastic rocks tend to have Na_2O values greater than 1% (0.4 to 4.4%). In the Bell River area east of Mattabi (Plate 3), felsic lavas and tuff-breccias are also sodium-depleted. These data support Severin's (1982) observations of extensive sodium depletion within footwall felsic volcanic rocks for considerable distances west of the Sturgeon Lake mine.

It is apparent from chemical analyses that all felsic lava-flow samples from the study area are depleted in sodium relative to unaltered rhyolitic rocks, and the feature is most likely ubiquitous in felsic lava flows and flow-breccias throughout the length of the lowermost volcanic cycle. However, within several kilometers of the Mattabi deposit the selective depletion also includes felsic pyroclastic rocks, and it is more intense within this area. The total absence of Na_2O (within detection limits) in some of these samples represents a complete breakdown of feldspar and, in turn, helps to explain the presence of aluminosilicate phases (e.g. andalusite) within the immediate footwall strata beneath Mattabi (Franklin et al., 1977).

Carbonate and Iron Enrichment

The analyses in Table 7 disclose that the footwall succession beneath Mattabi is anomalously enriched in CO_2. Franklin et al. (1975) suggest that the entire South Sturgeon Lake volcanic pile may be enriched in CO_2 relative to other Archean volcanic terranes. Indeed, samples from the hanging wall strata above Mattabi show that

high CO_2 values are not unique to the Mattabi footwall rocks (Tables 1 and 9 of Franklin et al., 1977).

Field observations and staining techniques have shown that much of the carbonate within substantially altered footwall rocks is either ferroan dolomite or ankerite, whereas least-altered rock types generally contain dolomite and/or calcite. A convenient way of graphically estimating carbonate species within a large number of samples has been implemented by Davies et al. (1982) for carbonatized metabasalts within the Timmins, Ontario area. The method employs CO_2/CaO molar ratios as a rapid estimation of carbonate species. This parameter differentiates rocks that have essentially calcite and Ca-bearing silicate minerals ($CO_2/CaO \leq 1$) from those rocks which contain dolomite and/or ankerite ($CO_2/CaO > 1$). Molar ratios greater than 2 arise when dolomite or ankerite with siderite or magnesite are present. Davies et al. (1982) demonstrate that mafic rocks containing actinolite, chlorite, and epidote form calcite before dolomite or ankerite. With this assumption and supportive X-ray diffraction data, one can estimate the carbonate species in mafic rocks from the study area.

In addition to the mafic volcanic rocks, pyroclastic and felsic lava-flow samples have been plotted in Figure 32. Felsic volcanic rocks would not be subject to identical carbonate-forming reactions as mafic rocks, yet few of the samples have Ca-bearing silicate minerals other than plagioclase or stilpnomelane. Staining shows that plagioclase is essentially pure albite, and stilpnomelane, which incorporates minimal amounts of CaO, rarely exceeds 10% in the felsic

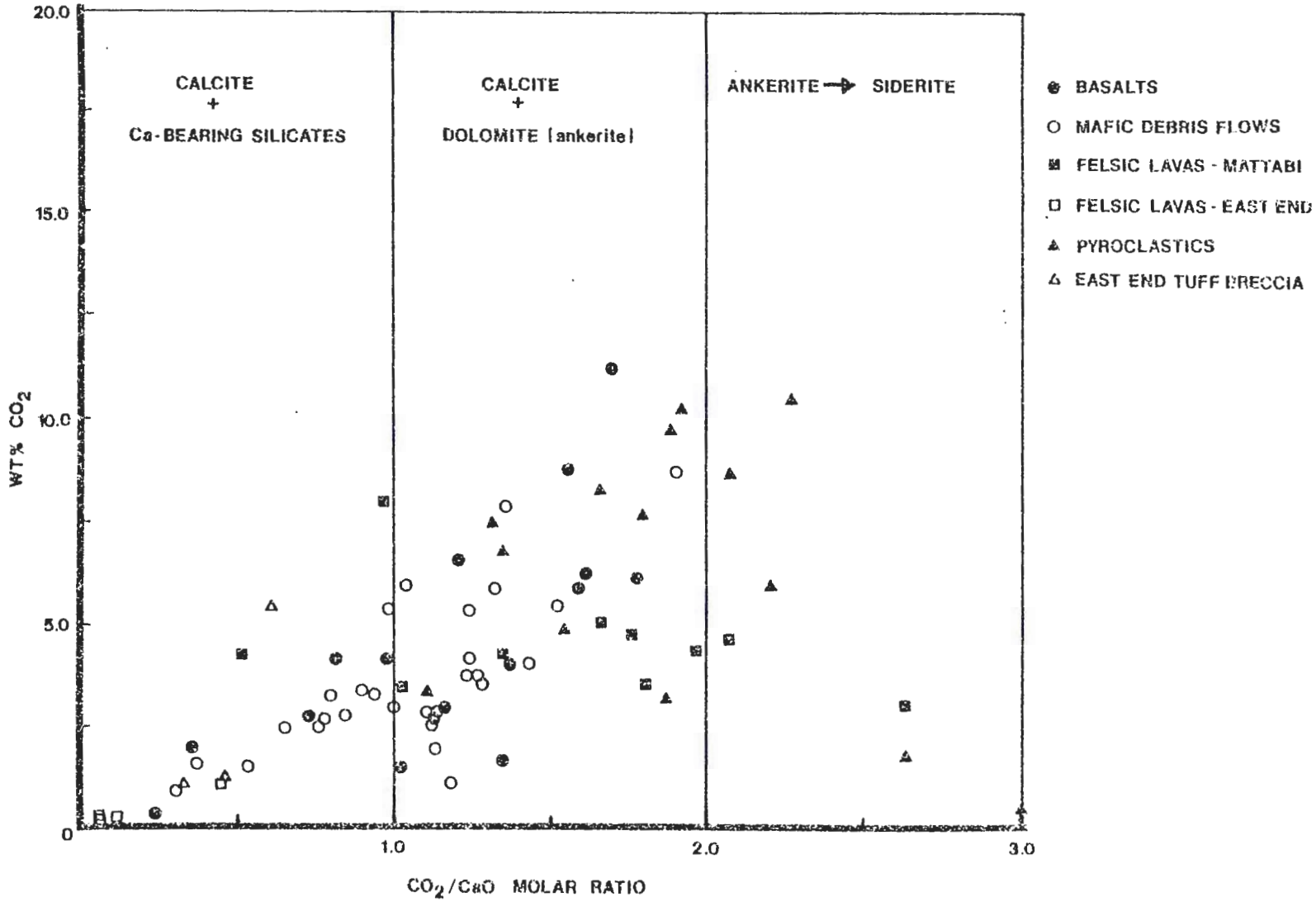

Figure 32. CO_2/CaO molar ratio plot (from Davies et al., 1982) with selected Mattabi-footwall samples plotted. Samples of lower-horizon pyroclastics, quartz-porphyritic ash-flow tuff and intrusive rocks have been omitted.

rocks. CaO must be confined largely to carbonate, and therefore the CO_2/CaO molar plot is applicable to these rock types as well.

Figure 32 shows that calcite is restricted largely to mafic volcanic rocks. Felsic lavas southwest of Mattabi display progressive iron enrichment of the carbonate species towards the mine, whereas felsic lavas east of the Bell River (Plate 2) have only minor amounts of carbonate which is largely calcite. Felsic pyroclastic samples exhibit high CO_2 values which plot within the dolomite/ankerite regions.

The high CO_2 values within mafic debris-flow and felsic pyroclastic flow deposits suggest that much of the carbonate formed during early diagenesis within an originally porous and permeable succession of rocks. However, crosscutting ankeritic veinlets within mafic lava flows and carbonate-chlorite alteration within felsic lavas indicates that considerable remobilization of CO_2 occurred during hydrothermal alteration. Iron enrichment of the carbonate is clearly restricted to the felsic pyroclastic rocks and intercalated lava flows. This enrichment can be traced upward though these rocks until it intersects the siderite-defined alteration "pipe" outlined by Franklin et al. (1975).

MASS BALANCE COMPUTATIONS

In addition to the alteration trends previously discussed, more subtle ion exchange and /or volume change has no doubt taken place within altered rocks of the study area. Simple one-to-one comparisons of chemical analyses alone cannot show these changes; it is necessary to incorporate the specific gravity of the analyzed samples in order

to discern any volume changes that may have occurred.

Specific gravities of samples were determined on a modified beam balance, and an aluminum standard (S.G.=2.71) was used to calibrate the apparatus. Specific gravities are included in Table 7 of Appendix B.

Gresens (1967) derives an equation for bulk rock comparison of unaltered rocks and their metasomatized equivalents using weight fractions of elements or oxides and specific gravities of the rocks. The general form of the equation is:

$$100[f_v(g_B/g_A)c_n^B - c_n^A] = X_n \qquad (1)$$

where f_v= the volume factor, i.e. the ratio between the final and initial volumes of the rock mass,

g_A, g_B= the specific gravities of the unaltered or least-altered rock (A) and its altered equivalent (B),

c_n^A, c_n^B= the weight fractions of component n in rock A and B,

X_n= gain or loss of component n from rock A to rock B.

The equation can be used on rocks from the study area to compare progressive alteration within distinct lithologies. Given the chemical analyses and specific gravities, equation (1) can be used to solve for either f_v or X_n. It is necessary that one of the two variables be eliminated before solving for the other. Several assumptions can be made:

1. The changes from one alteration assemblage to another have been volume for volume, i.e. f_v=1. This assumption is often made where delicate primary textures are preserved.
2. One or several components have behaved isochemically during the alteration, i.e. X_n=0 for these components. The f_v value for the rock is then determined and used to calculate gains and losses for the remaining components.
3. Several arbitrary f_v values can be used to obtain X_n values and generate a composition-volume (C-V) graph (see Fig. 35). Elemental trends from rock A to rock B are expressed as sloping lines on the C-V diagram. If a group of components intersect the X_n=0 line at a certain f_v value, this value can then be assumed to represent the actual volume change. Conversely, once an appropriate volume factor is deduced, elemental gains and losses (in grams per 100 grams) can be read from the graph.

The geochemical data and specific gravities listed in Tables 7 and 8 were used to produce a) volume-factor (f_v) histograms, b) mass exchange data (gains and losses) using the mean f_v value from the histograms and c) composition-volume diagrams.

The volume-factor histograms (e.g. Fig. 33) are generated by comparing several less-altered samples against a single, more intensely-altered equivalent (e.g. five least-altered samples versus a single carbonate-chlorite sample from the same unit, three carbonate-chlorite samples vs. a sericite-carbonate-chlorite sample, etc.). Volume factors are computed for each element by setting X_n=0 in

equation (1), and these values are then plotted on a $\log_{10}$ scale in histogram form.

Several alteration features can be obtained from these diagrams. First, the f_v value with the greatest frequency can be used as an assumed volume factor for gain-loss calculations. A strong peak with a symmetrical "shouldering" of f_v values generally occurs at this value on the histogram. Secondly, those elements which consistently plot away from this peak have either been gained or lost. Elements which plot as negative $\log_{10} f_v$ values (a volume decrease) have been gained, whereas those which plot as positive $\log_{10} f_v$ values (a volume increase) have been lost from the parent rock. Elements which plot in the "peak" can be assumed to have been immobile during the alteration.

ALTERATION ASSEMBLAGES

CO_2 Enrichment Within Least-Altered Rocks

In an effort to assess the effect of CO_2 enrichment within least-altered rocks, mafic lava flows containing lowest CO_2 values have been compared with their carbonatized equivalents. Thin sections indicate that much of the carbonate is pseudomorphous after plagioclase, a feature which supports constant-volume replacement. The carbonate-rich rocks are also moderately sericitized.

Figures 33 and 34 are two volume-factor histograms which illustrate the chemical trends inherent with carbonatization. In both figures, five least-altered samples with 2-4% CO_2 have been compared with a single CO_2-rich (6-9%) equivalent. Sample 145 in Figure 34, however, has a higher CO_2 content than sample 137 in Figure 33. Both

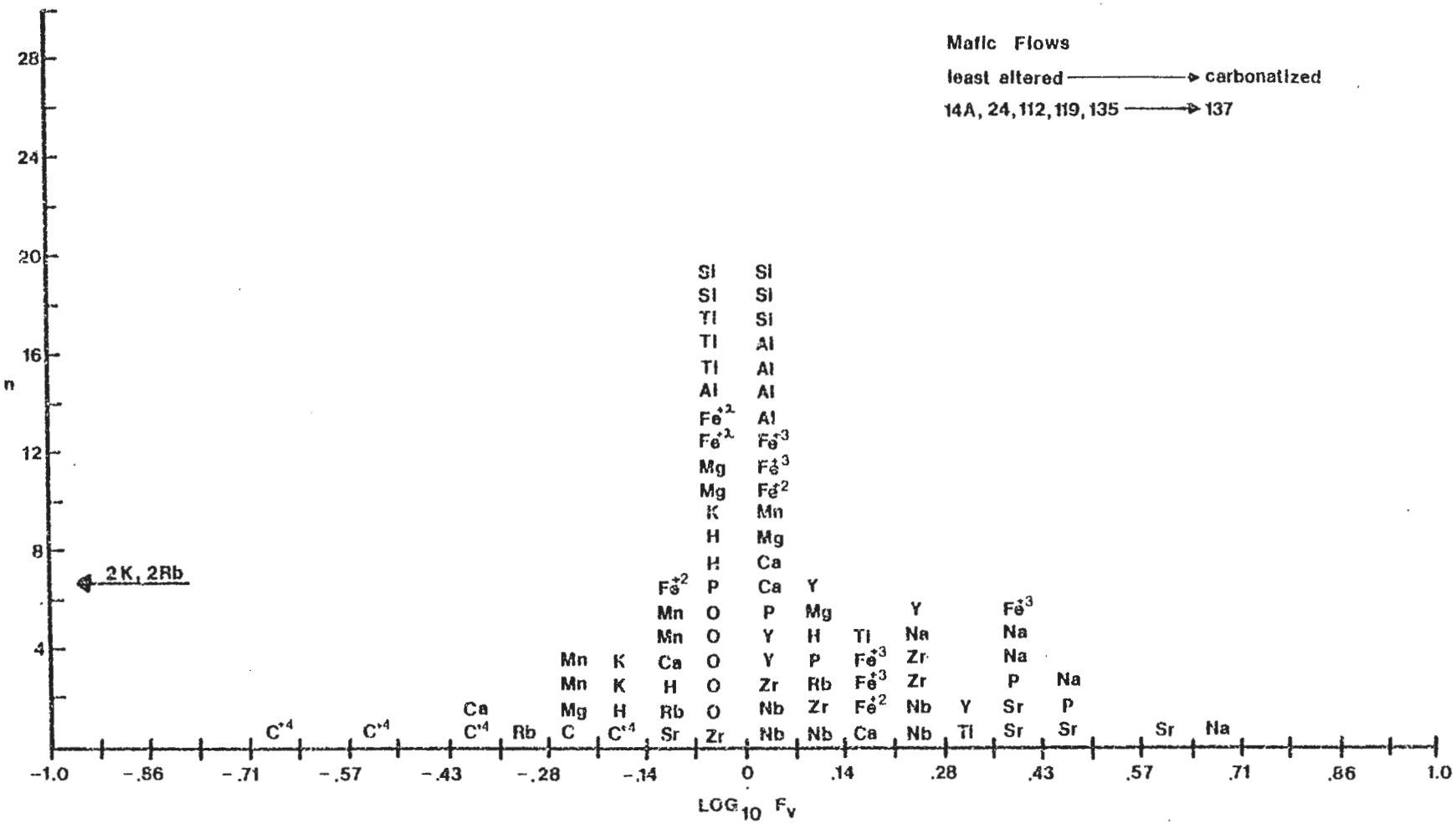

Figure 33. Volume-factor histogram for mafic lava flows: least-altered to carbonatized.

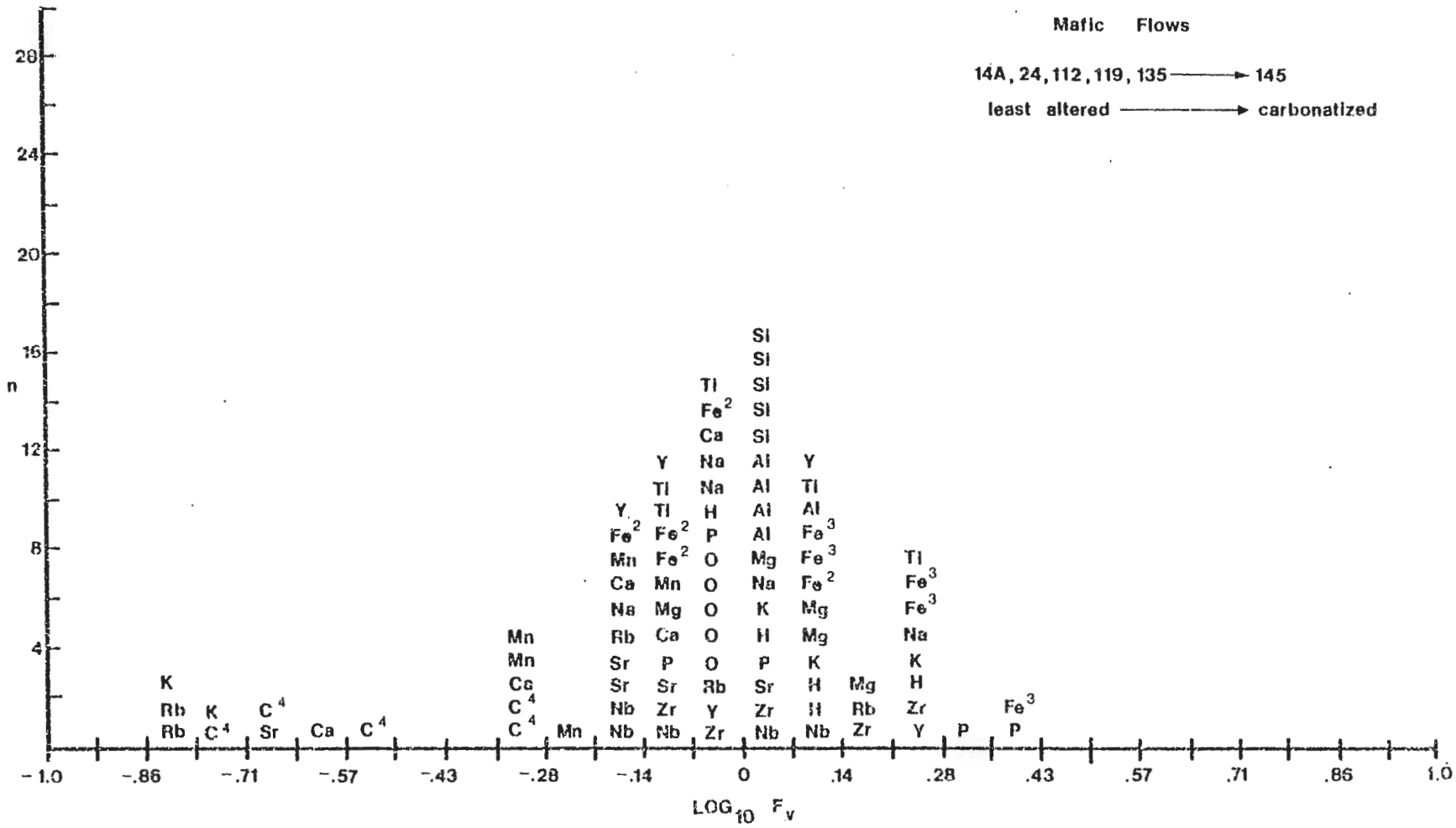

Figure 34. Volume-factor histogram for mafic lava flows: least-altered to carbonatized.

figures display a symmetrical peak of values centered closely around a volume factor of 1 ($\log_{10}=0$). With increasing carbonatization (Fig. 34), the peak becomes broader and less well-defined. As expected, C^{+4} (CO_2) plots as a substantial volume decrease, or in the case of constant volume, a significant mass gain. Mn also displays smaller yet consistent mass gains, and K and Rb show considerable gains in several comparisons. Figure 33 indicates losses of Fe^{+3}, Na and Sr, whereas in Figure 34 only ferric iron has apparently been lost.

Figure 35 is a composition-volume (C-V) diagram which further supports the histogram trends. In this particular comparison, a clustering of elemental slope intersections at the $X_n=0$ (zero compositional change) line occurs between f_v values of 0.92 to 1.02. If constant volume is implied, C^{+4} shows marked gains (roughly 1gm/100gms), and Fe^{+2}, Fe^{+3}, Ti and Na plot as lost components.

In summary, carbonatization within mafic lava flows is essentially a constant-volume process involving the addition of CO_2 and Mn, and the apparent loss of ferric iron. The constant-volume determination is in close agreement with the aforementioned petrographic textures, and the elemental gains and losses suggest that carbonate and/or dolomite has formed largely from the breakdown of calcic plagioclase. The K and Rb gains (Rb readily substitutes for K in muscovite) in several comparisons are a function of moderate sericitization (see modal analyses in Table 1) which has occurred during or after the influx of CO_2. Assuming that the original plagioclase component in the mafic rocks was labradorite to andesine in composition (Condie, 1981), a reaction can be written which

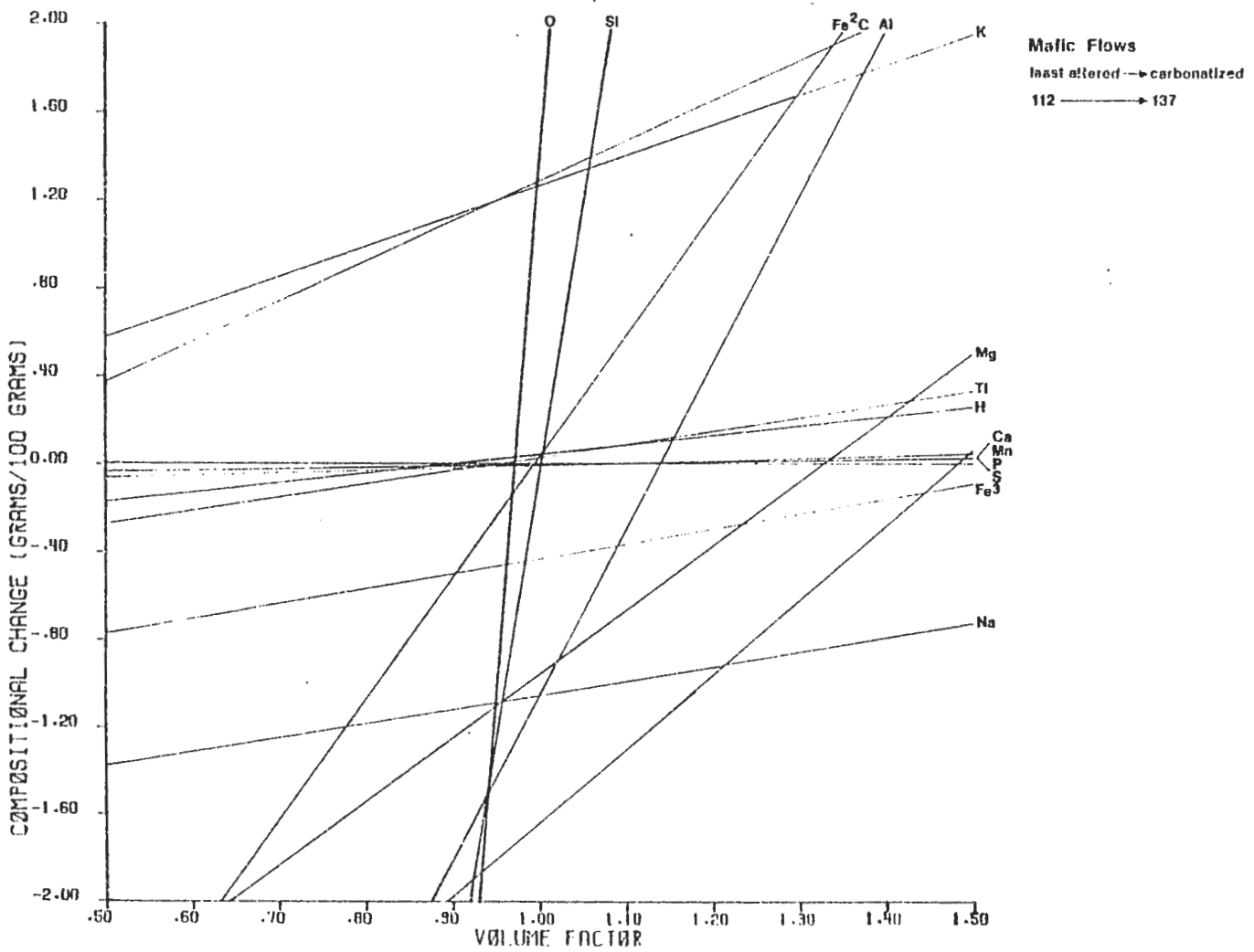

Figure 35. Composition-volume diagram for mafic lava flows: least-altered to carbonatized.

illustrates the above alteration features:

$$\underset{\text{labradorite}}{2Ca_{0.5}Na_{0.5}Al_{1.5}Si_{2.5}O_8} + HCO_3^- + 0.67K^+ + 0.33H^+ \longrightarrow$$

$$\underset{\text{albite}}{NaAlSi_3O_8} + \underset{\text{sericite}}{0.67KAl_3Si_3O_{10}(OH)_2} + \underset{\text{calcite}}{CaCO_3} \qquad (2)$$

In this case labradorite (An_{51}) is used to produce albite, sericite and calcite. The reaction as written represents an 12% volume increase on the product side; a slightly more sodic plagioclase would limit the production of sericite and calcite and eliminate the volume gain. Table 13 in Appendix C lists mineral formulas and molar volumes used to determine volume changes.

It appears that carbonatization in least-altered mafic lava flows is largely a product of CO_2 influx and minimal cation mobility. Na loss is most pronounced in those rocks which show increased K and Rb and is associated with accompanying sericitization.

Iron Carbonate-Chlorite Assemblage

Although iron carbonate-chlorite alteration is most abundant in felsic pyroclastic deposits, the lack of less-altered equivalents prevents mass-balance comparisons of the assemblage within these rocks. Felsic lavas, however, do allow for comparisons.

Volume-factor histograms for felsic lavas indicate that carbonate-chlorite assemblage rocks have undergone recognizable volume decreases. Si exhibits slight but consistent losses, whereas C^{+4}, Mn and Mg show limited gains. Mean volume factors from each histogram range from 0.62 to 0.69 (log-0.21 to -0.16); average Al volume factors vary from 0.74 to 0.87 (log-0.13 to -0.06). The volume-factor peak in Figure 36 is highlighted by a tight clustering of Al values around an

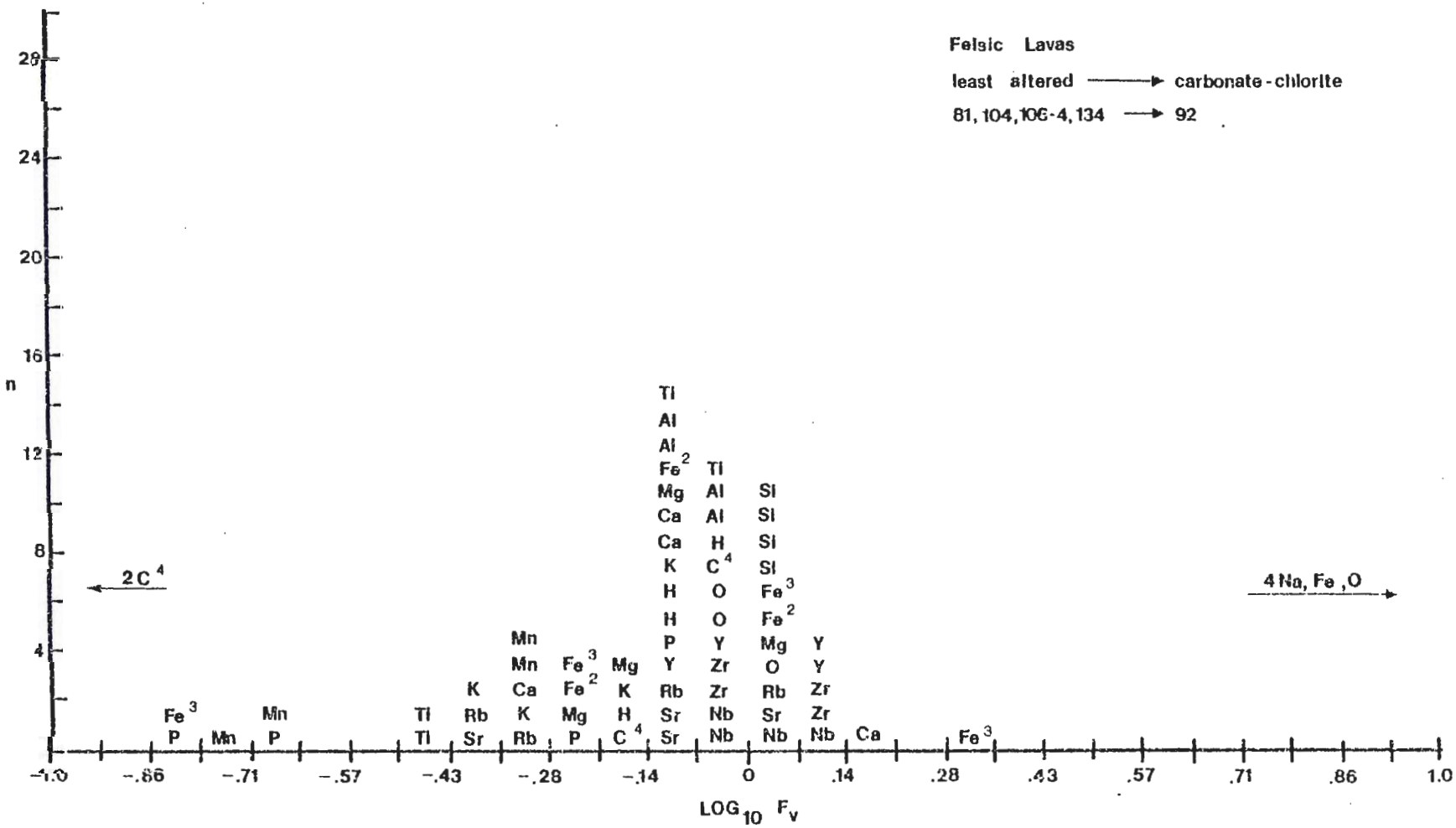

Figure 36. Volume-factor histogram for felsic lava flows: least-altered to iron carbonate-chlorite assemblage.

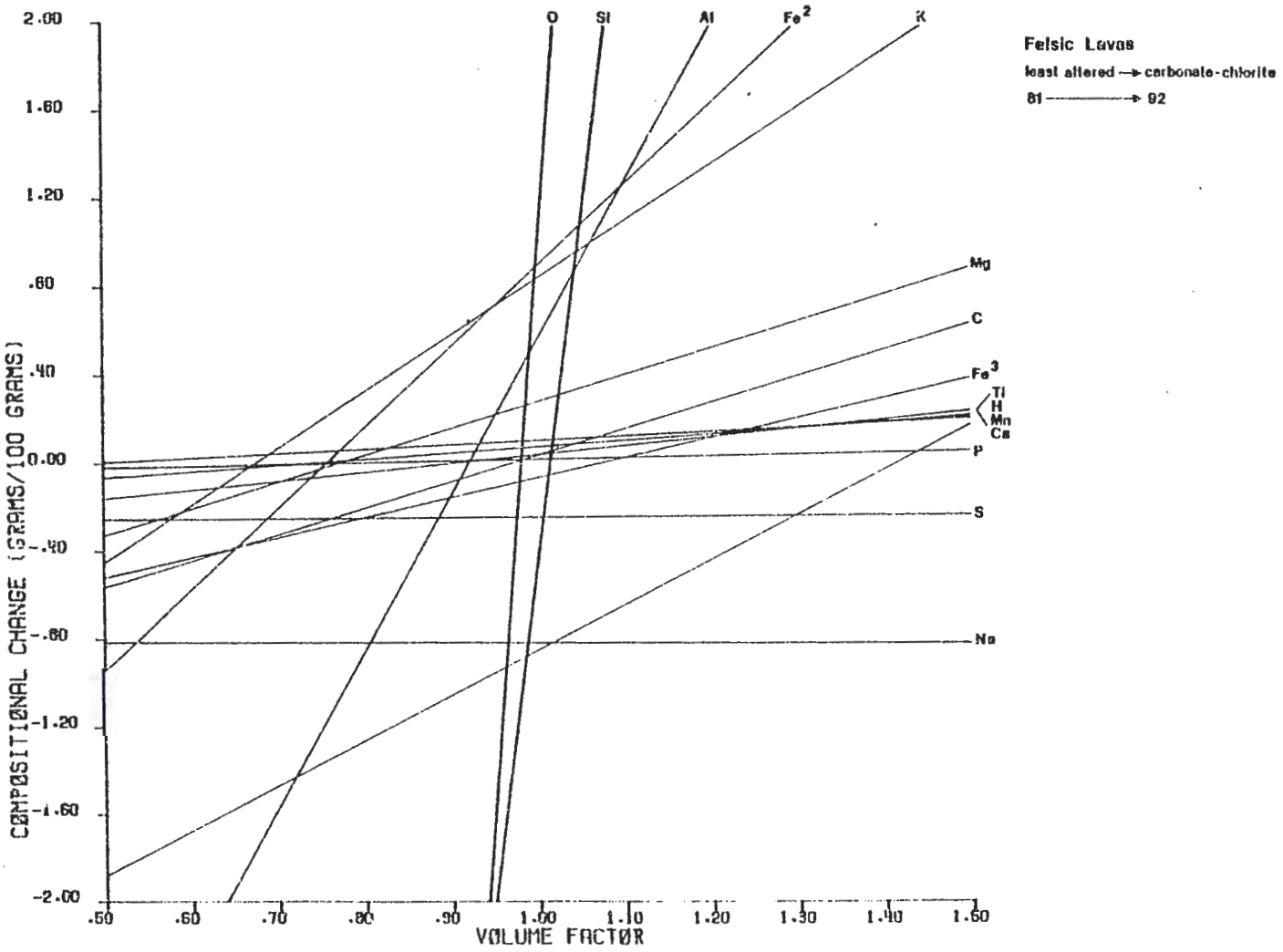

Figure 37. Composition-volume diagram for felsic lava flows: least-altered to iron carbonate-chlorite assemblage.

f_v value of 0.85 (log-0.07). Si forms a tight cluster at higher f_v values which represent compositional losses if Al and the volume factor peak represent the true volume change.

The majority of elemental trends can be readily accounted for by the alteration mineralogy within the felsic lavas. C^{+4} (CO_2), Mg and Mn gains are present as ferroan dolomite/ankerite-chlorite alteration. Ferrous and ferric iron, however, display inconsistent trends on the volume factor histograms. This is in part a result of relatively high FeO and Fe_2O_3 contents in two of the least-altered felsic lava samples. These rocks may have undergone iron enrichment during alteration and are not truly "least-altered" rocks, or they may be tholeiitic felsic lavas with originally high iron contents (see average "dacite" analysis in Condie, 1981). C-V diagrams do indicate gains of ferrous iron if Al and Ti are considered to be immobile. Figure 37 shows Al and Ti intersecting the X_n=0 (zero gains/losses) line at a volume factor of 0.92. Fe^{+2}, Mg and K have been gained, while Ca and Na show substantial losses.

If Al and Ti are immobile elements in this phase of alteration, carbonate-chlorite assemblage rocks have undergone a 10 to 20% volume decrease while gaining CO_2, Mg, Fe and Mn and losing silica. The antithetic trends of K versus Na in several of the comparisons is a function of sericitic veining which envelopes carbonate-chlorite mineralization.

The conformable nature of carbonate-chlorite alteration within felsic pyroclastic rocks suggests that this horizon was both porous and permeable during consolidation of the volcanic pile. Much of the

present carbonate mineralogy may also be a product of early diagenesis within glassy, fragmental volcanic rocks. Zen (1959) outlines clay mineral-carbonate relations within recent marine sediments containing glassy volcanic fragments of variable composition. He notes that calcite and kaolinite coexist in these rocks along with dolomite, chlorite and quartz. These phases are related by the reaction (Zen, 1959):

calcite + chlorite + CO_2 = dolomite + kaolinite + quartz + H_2O (3)

in which the Fe:Mg ratio in calcite, dolomite and chlorite plays a large role in determining the final assemblage.

Assuming that similar assemblages existed within the pyroclastic rocks beneath the Mattabi ore deposit, increasing a_{CO2} would drive equation (3) to the right (Zen, 1959). Later base-fixing activity within the evolving hydrothermal fluids would increase the iron content of the dolomite and form chlorite from kaolinite, thereby producing the present day carbonate-chlorite domains. Excess kaolinite (or another aluminosilicate phase such as pyrophyilite) which was not consumed during base-fixing reactions could later react with an iron-rich chlorite to form chloritoid during regional metamorphism.

Sericite Assemblage

Comparisons of sericitized mafic volcanic rocks, felsic lavas, and felsic pyroclastic rocks were made with least-altered and carbonate-chlorite assemblage rocks. Mass balance computations of least-altered versus sericitized mafic volcanic rocks indicate that

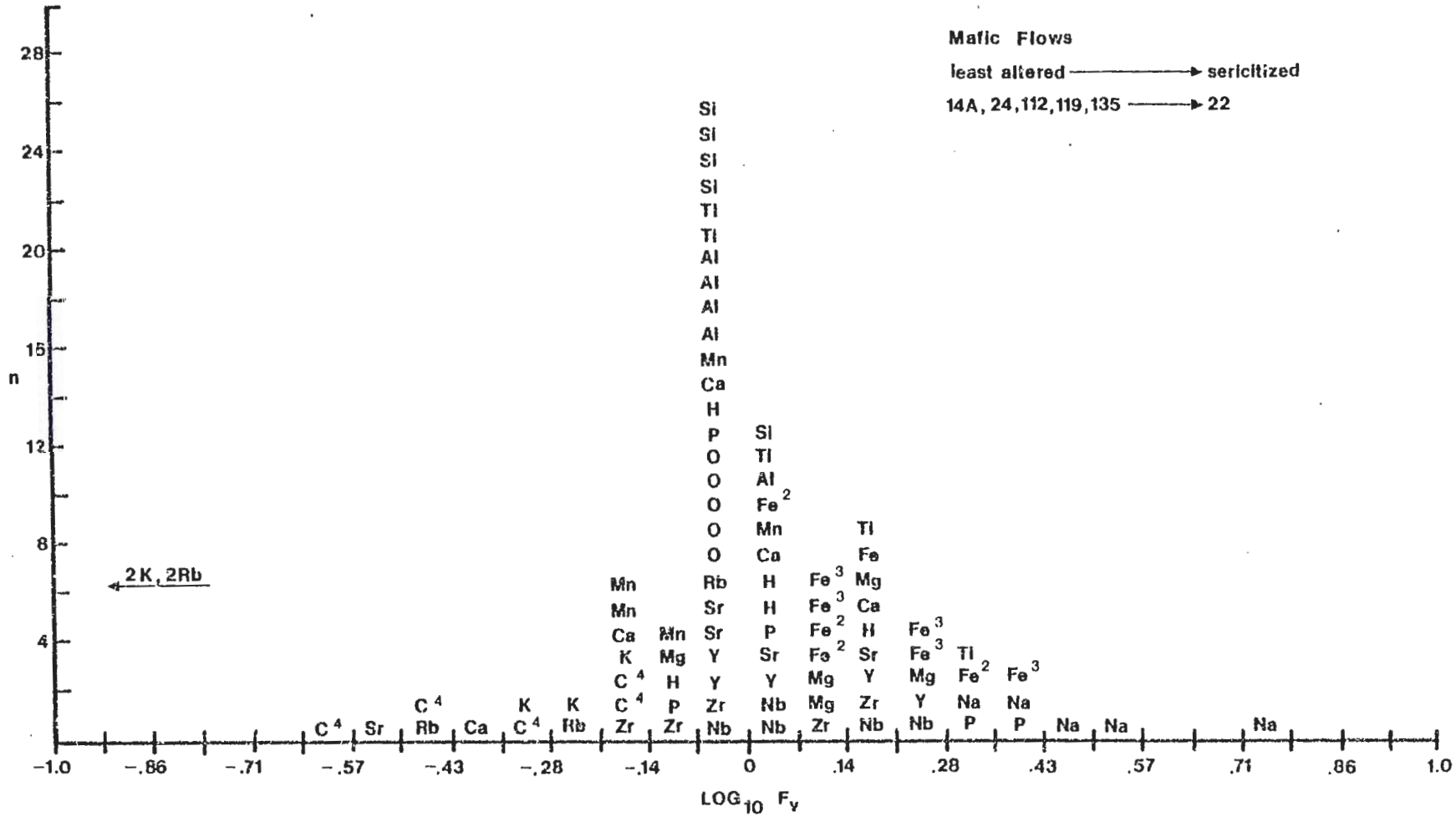

Figure 38. Volume-factor histogram for mafic lava flows: least-altered to sericite assemblage.

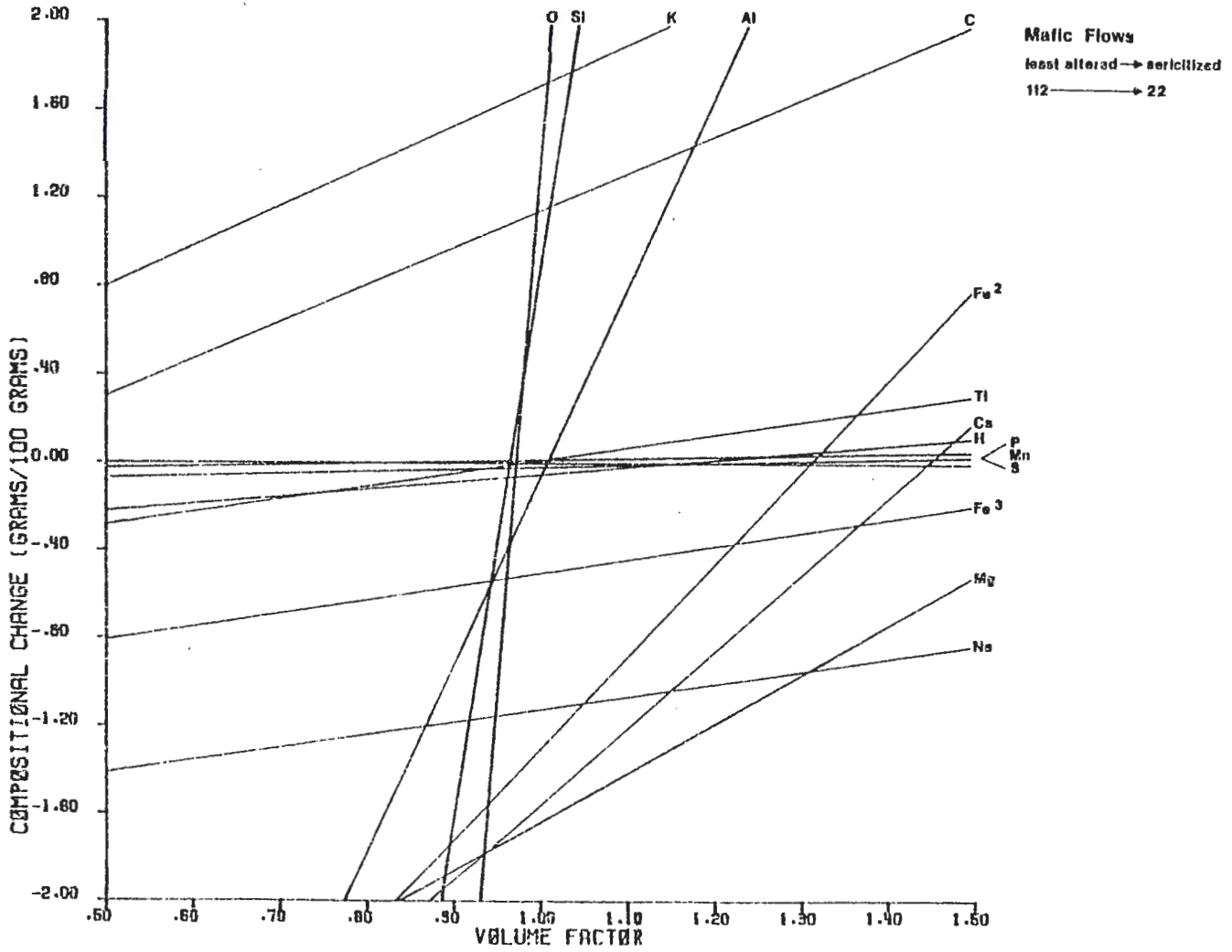

Figure 39. Composition-volume diagram for mafic lava flows: least-altered to sericite assemblage.

considerable base leaching is associated with the alteration. The volume factor histogram in Figure 38 shows that Fe^{+2}, Fe^{+3}, and Mg plot consistently to the right of a sharp volume factor peak at $f_v=1$. C-V diagrams (e.g. Figure 39) exhibit similar trends: Si, Al and Ti are generally immobile; K and C^{+4} have been added, and Na, Ca, Mg, Fe^{+2} and Fe^{+3} have been lost.

Felsic pyroclastic rocks and felsic lavas typically display sericitic alteration which envelopes carbonate-chlorite alteration domains. Mass-balance comparisons within these rocks produce elemental trends which are consistent with relative modal amounts of sericite and carbonate within the samples. K and Rb vary with sericite content in the compared samples, and C^{+4}, Mn and Ca trends are a function of relative carbonate contents.

The formation of sericite is restricted largely to a) the alteration of feldspar, and b) the sericitization of chlorite (Riverin and Hodgson, 1980; Parry and Hutchison, 1981). The alteration of plagioclase within felsic volcanic rocks can be written:

$$\underset{\text{oligoclase}}{2Ca_{0.3}Na_{1.7}Al_{2.3}Si_{5.7}O_{16}} + 0.2H_2O + 1.5K^+ + 3H^+ \longrightarrow \underset{\text{sericite}}{1.5KAl_3Si_3O_{10}(OH)_2} + \underset{\text{quartz}}{6.9SiO_2} + 0.1Al(OH_4)^- + 0.6Ca^{+2} + 3.4Na^+ \quad (4)$$

where Si is immobile, the plagioclase is oligoclase in composition, and the reaction proceeds at nearly constant volume (a 7% decrease). The production of sericite from chlorite in which Al and Si are also immobile:

$$\underset{\text{chlorite}}{1.5Fe_2Mg_3Al_2Si_3O_{10}(OH)_8} + K^+ + 14H^+ \longrightarrow$$

$$\underset{\text{sericite}}{KAl_3Si_3O_{10}(OH)_2} + \underset{\text{quartz}}{1.5SiO_2} + 12H_2O + 3Fe^{+2} + 4.5Mg^{+2} \quad (5)$$

involves a 45% volume decrease - far from the mass balance indications of constant volume. The formation of sericite from chlorite and an aluminosilicate phase (kaolinite or pyrophyllite), however, proceeds at constant volume according to the reaction (Nebel, 1982):

$$\underset{\text{chlorite}}{0.2(Fe,Mg)_5Al_2Si_3O_{10}(OH)_8} + \underset{\text{pyrophyllite}}{1.3Al_2Si_4O_{10}(OH)_2} + K^+ + H^+ \longrightarrow$$

$$\underset{\text{sericite}}{KAl_3Si_3O_{10}(OH)_2} + \underset{\text{quartz}}{2.8SiO_2} + (Fe,Mg)^{+2} \quad (6)$$

The above equations are base-leaching reactions which involve the input of K and H in exchange for Ca, Na, Fe and Mg. In addition, Riverin and Hodgson (1980) show that similar base-leaching solutions result in the chloritization of primary ferromagnesian minerals, thereby releasing excess Fe, Mg and Ca to the solution. The constant volume reaction is represented by the reaction (Riverin and Hodgson, 1980):

$$\underset{\text{diopside}}{2Ca(Mg,Fe)Si_2O_6} + 0.58Al(OH_4)^- + 5.68H^+ \longrightarrow$$

$$\underset{\text{chlorite}}{0.29(Mg,Fe)_5Al_2Si_3O_{10}(OH)_8} + \underset{\text{quartz}}{3.13SiO_2} + 2.84H_2O$$

$$+ 2Ca^{+2} + 0.55(Mg,Fe)^{+2} \quad (7)$$

Although mass balance computations do not support large-scale addition of alumina during this phase of alteration, contemporaneous alteration of feldspar (e.g. equation 4) could have supplied a portion of the necessary alumina to maintain constant volume. Such reactions would account for the chemical trends evident within the altered mafic

volcanic rocks. Microscopic textures and mass balance computations, however, do not support the formation of sericite at the expense of chlorite within felsic volcanic rocks, particularly carbonate-chlorite assemblage rocks which have also been sericitized. The sericite has most likely formed from the alteration of sodic plagioclase or, possibly, from an aluminosilicate phase formed during earlier carbonate-chlorite alteration.

Chloritoid Assemblage

Comparisons were made between chloritoid-assemblage rocks and similar carbonate-chlorite or sericite-assemblage rocks which lack chloritoid. Figure 40 is a representative volume-factor histogram. Carbonate-chlorite assemblage rocks exhibit negligible volume changes, some K and Rb gains, and generally minor Mn, Mg and/or Na losses. Sericite-assemblage rocks display no volume changes, minor CO_2 and Ca additions, and no consistent elemental losses.

The K, Rb, C^{+4} and Ca elemental trends reflect varying proportions of sericite and carbonate in the samples; they do not appear to indicate gains or losses necessary for the development of chloritoid. Its presence or absence in otherwise similar rock types is most likely a function of subtle alkali:alumina and Fe:Mg ratios (Halferdahl, 1961; Latour et. al.,1980).

Petrographic studies show that sericite is ubiquitous in chloritoid-assemblage rocks, ferroan dolomite/ankerite is present in all but one sample, and chlorite occurs in roughly two-thirds of the chloritoid-bearing samples. Whether at the expense of chlorite or

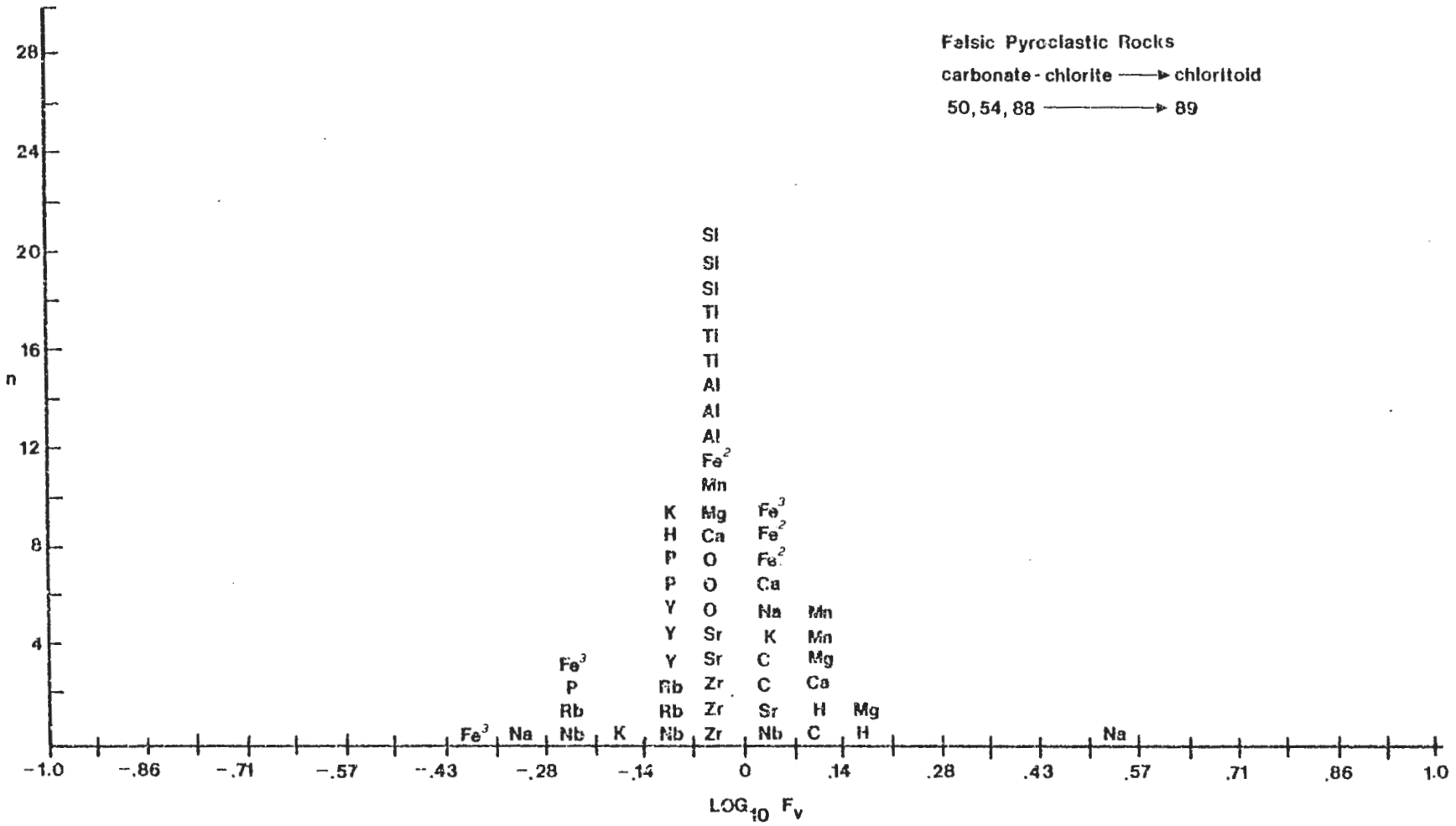

Figure 40. Volume-factor histogram for felsic pyroclastic rocks: iron carbonate-chlorite to chloritoid assemblage.

iron carbonate, the development of chloritoid also requires an aluminosilicate mineral such as kaolinite or pyrophyllite. Reactions first proposed by Zen (1960) involving chlorite include:

$$\underset{\text{kaolinite}}{4Al_2Si_2O_5(OH)_4} + \underset{\text{chlorite}}{(Mg,Fe)_5Al_2Si_3O_{10}(OH)_8} \longrightarrow$$

$$\underset{\text{chloritoid}}{5H_2(Fe,Mg)Al_2SiO_7} + \underset{\text{quartz}}{6SiO_2} + 7H_2O \qquad (8)$$

A similar reaction can be written using pyrophyllite in lieu of kaolinite (Zen, 1960).

Replacement of Fe^{+2} by Mg^{+2} in chloritoid rarely exceeds 30 atomic per cent (Deer et al., 1966). For the empirical formulas given in equation (8), the chlorite would have to be an iron-rich ripidolite (Hey, 1954). X-ray diffraction data from selected samples, however, determined the chlorite species in carbonate-chlorite assemblage rocks to be either ferroan clinochlore or magnesian ripidolite (Hey, 1954). These chlorites are too Mg-rich to produce chloritoid according to the above equation.

Chloritoid could also form from siderite and kaolinite according to the hypothetical reaction (Franklin, pers. comm.):

$$\underset{\text{siderite}}{(Fe,Mg,Mn)CO_3} + \underset{\text{kaolinite}}{Al_2Si_2O_5(OH)_4} \longrightarrow$$

$$\underset{\text{chloritoid}}{H_2(Fe,Mg,Mn)Al_2SiO_7} + \underset{\text{quartz}}{SiO_2} + CO_2 + H_2O \qquad (9)$$

Ankerite rather than siderite would yield calcite on the right hand side of the above equation.

While siderite could supply sufficient Fe and also account for the Mn in chloritoid (Franklin et al., 1977), microscopic textures do not support the production of chloritoid from either siderite or

ankerite. Siderite is abundant within the immediate footwall rocks containing chloritoid, but chlorite is scarce or altogether absent (Franklin et al., 1975). Staining for ferrous iron in the carbonate does not reveal any considerable depletion of modal ferroan dolomite/ankerite adjacent to chloritoid porphyroblasts. Indeed, most of the stained thin sections exhibit chloritoid growths with textures suggestive of chlorite rather than iron carbonate consumption.

Nebel (1982), in assessing the alteration beneath the Helen iron mine in the Michipicoten district of Ontario, suggests that chloritoid within altered felsic volcanic rocks formed according to equation (8). He notes that under similar conditions of formation within quartz-rich rocks any excess kaolinite or pyrophyllite would form andalusite (Winkler, 1974; Morton, pers. comm.). This implies that the andalusite within the footwall strata beneath the Mattabi deposit should exist in chloritoid- and quartz-bearing rocks exclusive of chlorite. These conditions are indeed met for the three andalusite-bearing samples found in the study area.

The present information on the formation of chloritoid within the Mattabi footwall rocks is inconclusive. Detailed microprobe analysis of chlorite, carbonate and chloritoid species would no doubt provide adequate restrictions on its formation. Petrographic textures and present mineral assemblages tend to support the growth of chloritoid at the expense of chlorite. Iron oxides may have also played an important role, although modal compositions (Appendix A) show no

consistent trends. These observations, however, do not preclude the development of chloritoid from siderite within the immediate alteration pipe outlined by Franklin et al. (1975).

ALTERATION MODEL

The widespread, semiconformable alteration zones present within the footwall strata beneath Mattabi differ considerably from the well-documented alteration zones beneath small, high-grade massive sulfide deposits in the Noranda district (e.g. Riverin and Hodgson, 1980; Parry and Hutchinson, 1981; Meyers and Maclean, 1983; Gibson et al., 1983). There, mafic to felsic lava flow/dome complexes are transected by high-angle, fault or fracture-controlled alteration pipes typified by chlorite-rich cores and sericitic fringes (Franklin et al., 1981). This focused alteration is superimposed upon earlier widespread, semiconformable quartz-epidote alteration and silicification within largely mafic lithologies (MacGeehan, 1978; Gibson et al., 1983).

At Mattabi, the stratigraphic succession is representative of evolved phreatomagmatic volcanism rather than lava flow extrusion and doming typical of Noranda stratigraphy. Mafic volcanic rocks are overlain by a thick sequence of pyroclastic and debris-flow deposits. Alteration within these rocks is largely subconcordant to stratigraphy (Plate 3) and consists of Fe, Mg-rich carbonate-chlorite alteration, widespread sericitization within the immediate footwall rocks, and restricted chloritoid development. The distribution of the alteration assemblages and the chemical trends evident throughout the footwall strata indicate that the hydrothermal solutions were constrained by 600 m of porous, carbonate-rich pyroclastic rocks lying above a hydrothermal reservoir situated within mafic lava flows and breccias (Fig. 41). The alteration assemblages, however, are much more diffuse and widespread within the permeable fragmental lithologies than

alteration zones at Noranda which have been confined by relatively impermeable lava flows.

The Beidelman Bay subvolcanic trondhjemite sill has been identified as a likely heat source for the Mattabi hydrothermal system (Franklin, 1976; Franklin et al., 1981). The sill has intruded a 2 to 3 km thick succession of mafic volcanic rocks topped by the rocks of the study area. The mafic rocks are amygdaloidal and brecciated, and therefore would have served as an adequate reservoir rock for connate seawater. The following alteration model is proposed to account for the chemical trends and present day mineralogy within the Mattabi footwall.

Heating of connate seawater during the solidification of the Beidelman Bay intrusion resulted in the leaching of Fe, Mn, Ca, Na, and K from the mafic rocks and the formation of hydrous alteration minerals (Seyfried and Bischoff, 1981; Lydon, 1981). The felsic lavas above the mafic succession served as a cap rock, thereby constructing a closed, heated reservoir (Fig. 41).

High-angle synvolcanic faulting allowed the sudden release of the hydrothermal fluids from the pressurized reservoir. The massive, pumiceous pyroclastic deposits within the study area in part provided a permeable channelway for the focused hydrothermal discharge. Upwelling solutions underwent base-fixing reactions with the surrounding pyroclastic rocks. Existing diagenetic assemblages of calcite/dolomite and aluminous clay reacted to form ferroan dolomite/ankerite and chlorite. Additional CO_2 was

precipitated from the hydrothermal solution as ankeritic veinlets and amygdule fillings in mafic lavas, and possibly as spherical carbonate domains within felsic lavas.

As the solutions approached the seawater/seafloor interface, boiling commenced due to limited hydrostatic pressure from shallow water depths (Hodgson and Lydon, 1977). Boiling began in near surface rocks, and a steep thermal gradient was established in the hydrothermal conduit (Riverin and Hodgson, 1980). Near saturation levels of CO_2 in the fluids (Seyfried and Bischoff, 1981) resulted in siderite precipitation as veins in the discharge zone (Franklin et al., 1977). Iron and Cu, Zn sulfides then rapidly accumulated on the seafloor.

As reservoir pressures decreased, the rapid fluid discharge gave way to a recharged seawater convection cell (Fig. 42). Closed reservoir reactions had occurred at low water/rock ratios and produced only limited K exchange with Mg from seawater; high water/rock ratios, typical of open cell convection, resulted in complete K removal (Seyfried and Bischoff,1981). Thus, hydrothermal fluid emanating from the discharge zone evolved from Fe-Mn-Ca-CO_2-rich solucions to K^+-rich fluids. The increased K^+ activity and lower temperatures at the discharge zone caused widespread sericitization within the immediate footwall rocks (Riverin and Hodgson, 1980) . Reactions between these fluids and plagioclase or an aluminosilicate phase produced enveloping sericitic alteration around carbonate-chlorite domains. Partial or complete sealing of the discharge area forced the fluids outward along

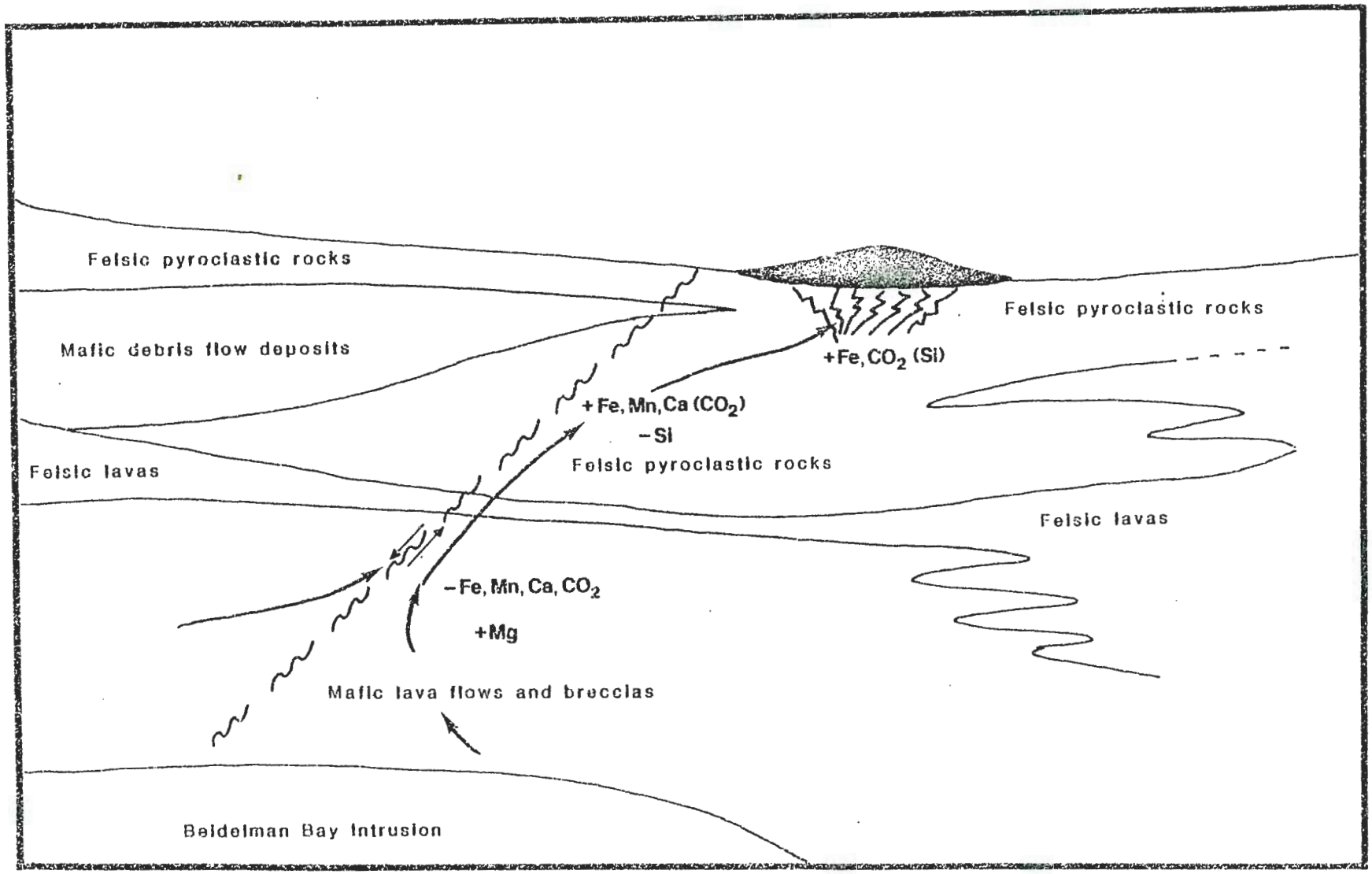

Figure 41. Schematic of chemical trends associated with rapid hydrothermal-fluid discharge from a closed, pressurized reservoir. Movement and extent of faulting have been inferred; parentheses denote minor chemical changes.

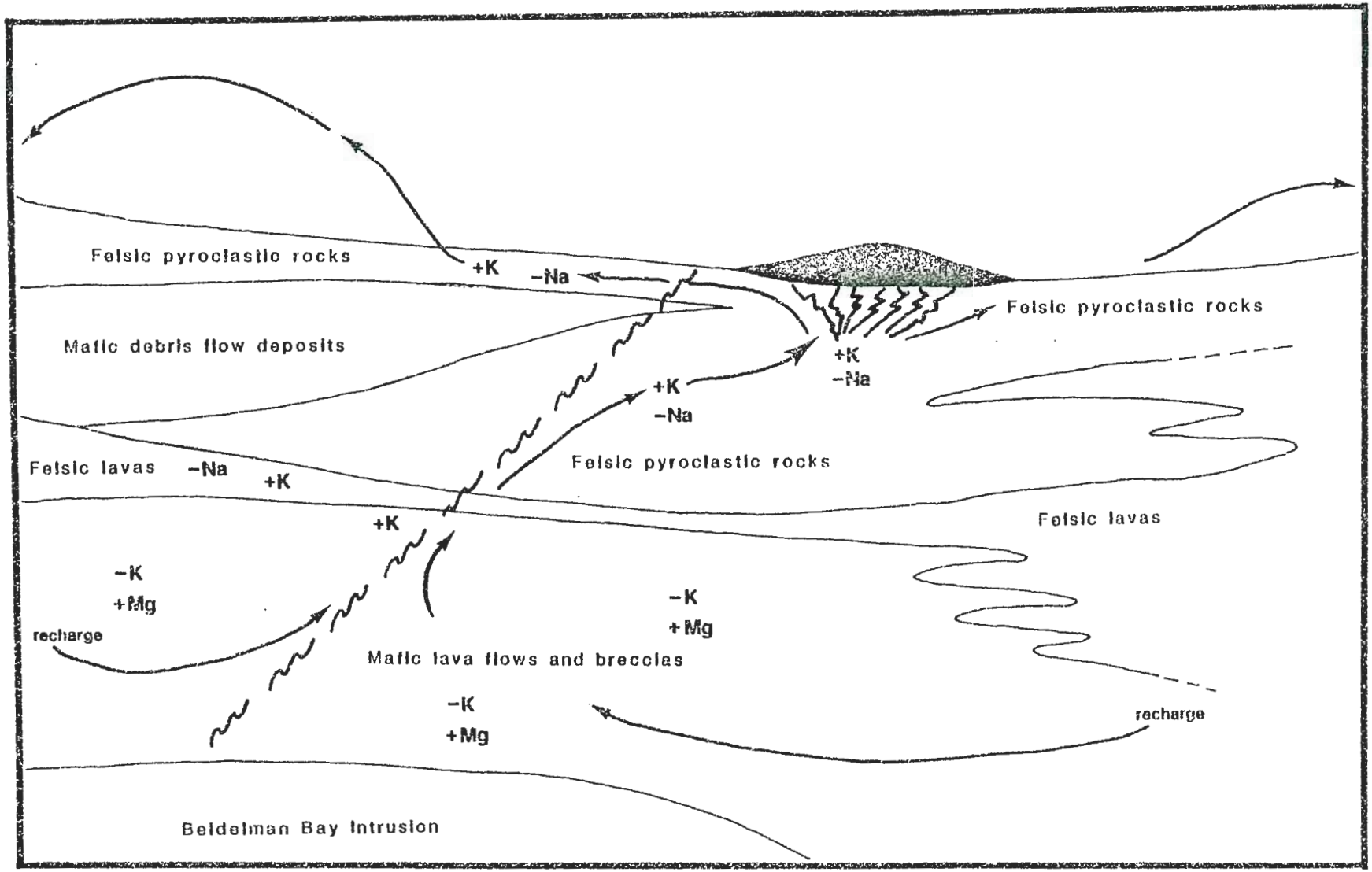

Figure 42. Schematic of major chemical changes associated with the development of a late-stage, seawater convection cell. Partial or complete self-sealing of discharge zone forces fluids to migrate laterally within uppermost footwall rocks.

permeable horizons thereby creating widespread sericitization and Na depletion beneath the Mattabi ore horizon.

This proposed hydrothermal model is a variation of the "seismic pumping" model discussed by Sibson et al. (1975). Lydon (1981) notes that such a model, activated by deep-seated tectonism, accounts for the presence of several massive sulfide occurrences at a precise stratigraphic interval. This is particularly the case in the Sturgeon Lake region where three massive sulfide deposits are known to exist at the same stratigraphic level (Franklin et al., 1977).

SUMMARY AND CONCLUSIONS

STRATIGRAPHY AND VOLCANOLOGY

The Mattabi footwall sequence within the study area is a complex succession of altered, subaqueous volcanic rocks intruded by the Beidelman Bay trondhjemite sill. Detailed geologic mapping and petrographic studies have shown that the previously undifferentiated footwall rocks can be divided into several distinct lithologies.

The lowermost portion of the footwall strata is composed of mafic lava flows and flow breccias with lesser amounts of intercalated debris-flow and pyroclastic deposits. Mafic lava flows are typically microporphyritic, amygdaloidal, and massive. They are believed to represent relatively shallow-water, proximal deposits from voluminous lava outpourings.

Above the mafic volcanic base, thin felsic lava flows increase in abundance towards both the western and eastern margins of the study area. Individual flows are generally less than 40 m thick, exhibit narrow amygdaloidal margins, and are enveloped in felsic tuff-breccia. The distribution of the lavas and associated breccias indicates that several localized felsic vents were operative at this stratigraphic level. The enveloping tuff-breccias are block-and-ash-flow deposits formed from felsic dome/lava skin disintegration during extrusion. Directly south of Mattabi, thin felsic lavas are overlain by bedded lapilli-and-ash tuffs which are distal equivalents to block-and-ash deposits further east.

Above the mafic and felsic lava flows, mafic debris flows and felsic pyroclastic deposits comprise the upper 600 m of the footwall

succession. The two deposit types intermix and intercalate west of the Mattabi deposit.

Mafic debris flows form a wedge-shaped unit which pinches out among massive pyroclastic flows 3 km west of Mattabi. The poorly bedded and graded deposits are composed of scoriaceous to amygdaloidal mafic clasts within a chloritic matrix. Accessory felsic lithic and pumiceous clasts form poorly stratified layers near the top of the deposit and at the eastern terminus. The deposits are believed to be both in-situ and slumped products of mafic hydrovolcanism which was situated within the study area.

Explosive, subaqueous felsic volcanism, along with periodic lava flow extrusion, emplaced thick successions of massive pyroclastic deposits directly under and east of the Mattabi deposit. These pyroclastic flows also overrode and truncated mafic debris flow deposits.

Within the study area, pyroclastic deposits are subdivided into a) massive pyroclastic beds and overlying bedded ash tuff, b) graded, lapilli-rich beds, and c) massive, pumice-rich deposits. In addition, distinctive quartz-porphyritic ash-flow tuffs are interbedded with massive pyroclastic beds and form uniformly thick deposits across the length of the study area. The immediate footwall rocks within the Mattabi open pit are largely poorly sorted, non-graded, massive pumiceous pyroclastic deposits with sparse sulfide-rich fragments.

It is envisioned that an expansive submarine shield volcano gave rise to localized felsic vents upon a thick sequence of mafic flows.

A shallowing-upward progression, or an increasing water/magma ratio brought about a change from lava extrusion to phreatomagmatic volcanism. Hydrothermal circulation commenced as the explosive volcanism waned, and focused discharge of metal-rich fluids occurred at several locations, including the site of the present Mattabi deposit.

ALTERATION

The footwall volcanic rocks beneath the Mattabi deposit and within the study area have been subjected to hydrothermal alteration asssociated with the formation of several volcanogenic massive sulfide deposits. They have subsequently undergone regional greenschist facies metamorphism. Field mapping and petrographic studies allow the establishment of four major alteration assemblages within the footwall strata. In order of apparent alteration intensity, the assemblages are:

1. Least altered (albite + quartz ± chlorite, sericite, carbonate, epidote, actinolite, stilpnomelane). Least-altered assemblage rocks are largely mafic flows located in the southwest corner of the study area and mafic debris flow deposits north of Darkwater Lake.
2. Iron carbonate-chlorite (ferroan dolomite/ankerite + chlorite ± sericite, quartz, chloritoid). This alteration assemblage is confined largely to felsic pyroclastic deposits and felsic lavas.

3. Sericite (sericite + quartz ± chlorite, carbonate, chloritoid). Sericite alteration is widespread within felsic pyroclastic deposits in the immediate footwall beneath the Mattabi deposit, and it also envelopes carbonate-chlorite alteration.
4. Chloritoid (chloritoid + ankerite + sericite + quartz ± chlorite, andalusite). Chloritoid-bearing rocks are most prominent within sericitized rocks immediately beneath the Mattabi deposit, but the mineral also occurs in carbonate-chlorite assemblage rocks at distances greater than 2.5 km from Mattabi.

Mass balance computations which utilize chemical analyses and specific gravities of footwall samples indicate that the majority of chemical changes have taken place at constant volume. The volume changes and elemental trends associated with progressive alteration comparisons are summarized in Table 1. In general, alteration within the study area increases upward through the footwall strata towards the Mattabi deposit and involves enrichment of Fe, Mn, and CO_2 in the upper pyroclastic succession of rocks.

It is envisioned that connate seawater trapped within a thick succession of amygdaloidal mafic lava flows and breccias was heated by the penecontemporaneous Beidelman Bay intrusion. Thin, impermeable felsic lava flows capped the mafic succession and produced a closed reservoir. Relatively low water/rock ratios within the reservoir resulted in nearly complete leaching of Ca, Fe, and Mn from the rocks.

TABLE 1: Summary of Volume Changes and Chemical Trends Within Progressively Altered Lithologies

PROGRESSION	LITHOLOGY	VOLUME CHANGE	GAINS[1]	LOSSES
Least-altered to carbonatized	Mafic lava flows	None	CO_2, (K, Rb)	Fe^{+3}
Least-altered to carbonate-chlorite	Felsic lavas	- 10 to -20%	CO_2, Mn, Mg, (Fe^{+3})	Si
Least-altered to sericite	Mafic volcanic rocks	None	K, Rb.	Na, Fe^{+2}, Fe^{+3}, Mg, (Ca)
Carbonate-chlorite to sericite	Felsic volcanic rocks (pyroclastics and lavas)	None	K, Rb	(CO_2, Mn, Ca)
Carbonate-chlorite to chloritoid	Felsic volcanic rocks	None	(K, Rb)	(Mn, Mg, Na)
Sericite to chloritoid	Felsic volcanic rocks	None	(CO_2, Ca)	____

1. Parentheses denote minor elemental trends.

Deep-seated tectonism within the volcanic pile produced high-angle faulting which allowed the sudden release of hydrothermal fluids from the reservoir. Migration of the fluids through permeable felsic pyroclastic rocks resulted in base-fixing reactions in the surrounding rocks and created a large, semiconformable alteration zone. Boiling took place at the seafloor, and a large thermal gradient was established along the hydrothermal conduit. Siderite was deposited throughout the rocks beneath the discharge area, and iron sulfides accumulated on the seafloor.

After depletion of connate waters from the resrvoir, a seawater convection cell propelled large volumes of water through the footwall rocks. These fluids evolved into acidic, K-rich solutions which produced widespread sericitization throughout the uppermost felsic volcanic rocks.

REFERENCES CITED

Berry, L.G., ed., 1974. Selected Powder Diffraction Data For Minerals. Joint Committee on Powder Diffraction Standards.

Campbell, I.H., Franklin, J.M., Gorton, M.P., Hart, T.R. and Scott, S.D., 1981. The role of subvolcanic sills in the generation of massive sulfide deposits. Econ. Geology, 76: 2248-2253.

Condie, K.C., 1981. Archean Greenstone Belts. Elsevier Scientific Publishing Co., 434pp.

Covello,L., 1971. The structure,stratigraphy and petrology of the north end of Abitibi Block 7, Sturgeon Lake. Unpubl. B.Sc. thesis, Lakehead University, Thunder Bay, Ontario. 60 pp.

Davies, J.F., Whitehead, R.E.S., Cameron, R.A. and Duff, P., 1982. Regional and local patterns of CO_2-K-Rb-As alteration: a guide to gold in the Timmins area, in Hodder, R.W., ed., Geology of Canadian Gold Deposits, Proceedings of the CIM Gold Symposium, Sept. 1980, CIM Special Volume 24, 286 pp.

Deer, W.A., Howie, R.A. and Zussman, J., 1966. An Introduction to the Rock Forming Minerals. Longman Group Ltd., London. 528 pp.

De Rosen-Spence, A.F., Provost, G., Dimroth, E., Gochnauer, and Owen,V., 1980. Archean subaqueous felsic flows, Rouyn-Noranda, Quebec, Canada, and their Quaternary equivalents. PreCambrian Res., 12: 43-77.

Dimroth, E., Cousineau, P., Leduc, M., Sanschagrin, Y. and Provost, G., 1979. Flow mechanisms of Archean subaqueous basalt and rhyolite flows. Geol. Survey Can. Paper 79-1A: 207-211.

Evamy, B.D., 1963. The application of a chemical staining technique to a study of dedolomitization. Sedimentology, 2: 164-170.

Fisher, R.V., Schmincke, H.-U., and Bogaard, P.v.d., 1983. Origin and emplacement of a pyroclastic flow and surge unit at Laacher See, Germany. Jour. Volcanol. and Geotherm. Res., 17: 375-392.

Fiske, R.S., 1963. Subaqueous pyroclastic flows in the Chanapecosh Formation, Washington. Geo. Soc. Am. Bull., 74: 391-406.

_____, and Matsuda,T.,1964. Submarine equivalents of ash flows in the Tokiwa Formation, Japan. Am. Jour. Sci., 262: 76-106.

Franklin, J.M., Kasarda, J. and Poulsen, K.H., 1975. Petrology and chemistry of the alteration zone of the Mattabi massive sulfide deposit. Econ. Geology, 70: 63-79.

_____, 1976. Role of laharic breccia in the genesis of volcanogenic massive sulfide deposits. Geol. Survey Can. Paper 76-1A, pp. 293-300.

_____, Gibb, W., Poulsen, K.H. and Severin, P., 1977. Archean Metallogeny and Stratigraphy of the South Sturgeon Lake Area; Mattabi Trip, 23rd Annual Meeting, Institute on Lake Superior Geology, 73pp.

_____, Sangster, D.M. and Lydon, J.W., 1981. Volcanic-associated massive sulfide deposits, in Skinner, B.J., ed., Economic Geology 75th Anniversary Volume. Economic Publishing Co., 964pp.

Friske, P., 1974. The Beidelman Bay copper-porphyry deposit. Unpubl. B.Sc. thesis, Lakehead University, Thunder Bay, Ontario. 108pp.

Goodwin, A.M., 1962. Structure, stratigraphy, and origin of iron formations, Michipicoten area, Algoma District, Ontario, Canada. Geol. Soc. Am. Bull., 73: 561-586.

Gresens, R.L., 1967. Composition-volume relationships of metasomatism. Chem. Geol., 2: 47-65.

Gustafson, J.K., 1946. Two occurrences of chloritoid as a hydrothermal mineral in igneous rocks. Amer. Min., 31: 313-316.

Halferdahl, L.B., 1961. Chloritoid: its composition, x-ray and optical properties, stability, and occurrence. Jour. Petrology, 2: 49-135.

Harvey, J.D. and Hinzer, J.B., 1981. Geology of the Lyon Lake ore deposits, Noranda Mines Limited, Sturgeon Lake area, Ontario. CIM Bull., 74(#833): 77-84.

Hey, M.H., 1954. A new review of the chlorites. Min. Magazine, 30: 277-292.

Horwood, H.C., 1937. Geology of the Darkwater Mine. Ont. Div. Mines, 46: 26-35.

Hughes, C.J., 1973. Spilites, keratophyres, and the igneous rock spectrum. Geological Mag., 109: 513-527.

Hurlbut, C.S., Jr., 1971. Dana's Manual of Mineralogy, 18th Edition. John Wiley and Sons, Inc. 579pp.

Irvine, T.N. and Barager, W.R.A., 1971. A guide to the chemical classification of the common volcanic rocks. Can. Jour. Earth Sci., 8: 523-548.

Kasarda, J., 1973. Wall rock alteration and trace element geochemistry of the footwall rocks of the Mattabi deposit, Sturgeon Lake area, Ontario. Unpubl. B.Sc. thesis, Lakehead University, Thunder Bay, Ontario.

Kerr, P.F., 1977. Optical Mineralogy. McGraw-Hill, Inc. 492pp.

Kuniyoshi, S. and Liou, J.G., 1976. Contact metamorphism of the Karmutsen volcanics, Vancouver Island, British Columbia. Jour. Petrology, 17: 73-99.

LaTour, T.E., Kerrich, R., Hodder, R.W. and Barnett, R.L., 1980. Chloritoid stability in very iron-rich pillow lavas. Contrib. Mineral. Petrol., 74: 165-173.

Lydon. J.W., 1981. A discussion, in Goldie, R. and Bottrill, T.J., Seminar on seafloor hydrothermal systems. Geoscience Can., 8: 101-103.

MacGeehan, P.J.,1978. The geochemistry of altered volcanic rocks at Matagami, Quebec: a geothermal model for massive sulfide genesis. Can. Jour. Earth Sci., 15: 551-570.

Meyers, R.E. and MacLean, W.H., 1983. The geology of the New Insco copper deposit, Noranda district, Quebec. Can. Jour. Earth Sci., 20: 1291-1304.

Morton, R.L. and Nebel, M., 1983. Physical character of Archean felsic volcanism in the vicinity of the Helen Iron Mine, Wawa, Ontario, Canada. PreCambrian Res., 20: 39-62.

Nebel, M., 1982. Stratigraphy, depositional environment and alteration of Archean felsic volcanics, Wawa, Ontario. Unpubl. M.Sc. thesis, Univ. Minnesota-Duluth, Duluth, MN, 114pp.

Parry, S. and Hutchinson, R.W., 1981. Origin of a complex alteration assemblage, Four Corners Cu-Zn prospect, Quebec, Canada. Econ. Geol., 76: 1186-1201.

Post, J.L. and Plummer, C.C., 1972. The chlorite series of Flagstaff Hill area, California: a preliminary investigation. Clays and Clay Mineral., 20: 271-283.

Poulsen, K.H. and Franklin, J.M., 1981. Copper and gold mineralization in an Archean trondhjemitic intrusion, Sturgeon Lake, Ontario. Geol. Survey Can. Paper 81-1A, pp. 9-14.

Riverin, G. and Hodgson, C.J., 1980. Wall-rock alteration at the Millenbach Cu-Zn mine, Noranda, Quebec. Econ. Geol., 75: 424-444.

Robie, R.A., Bethke, P.M., and Berdsley, K.M., 1967. Selected X-ray crystallographic data, molar volumes and densities of minerals and related substances. U.S. Geol. Survey Bull. 1248, 87pp.

Severin, P.W.A., 1982. Geology of the Sturgeon Lake Cu-Zn-Pb-Ag-Au deposit. CIM Bull., 75(#846): 107-123.

Seyfried, W.E. Jr. and Bischoff, J.L., 1981. Experimental seawater-basalt interaction at 300° C, 500 bars: chemical exchange, secondary mineral formation and implications for the transport of heavy metals. Geochim. Cosmochim. Acta., 45: 135-147.

Sheridan, M.F. and Wohletz, K.H., 1981. Hydrovolcanic explosions: The systematics of water-pyroclast equilibration, Science, 212: 1387-1389.

_____, and Wohletz, K.H., 1983. Hydrovolcanism: basic considerations and review. Jour. Volcanol. and Geotherm. Res., 17: 1-30.

Sibson, R.H., Moore, J. McM., and Ranking, A.H., 1975. Seismic pumping - a hydrothermal fluid transport mechanism. Geol. Soc. London Jour., 131: 653-659.

Staargaard, C.F., 1981. Lithogeochemical features associated with volcanogenic massive sulfide mineralization in the Sturgeon Lake area of Ontario, Canada. Unpubl. M.Sc. thesis, Queen's University, Kingston, Ontario. 199pp.

Trowell, N.F., 1974. Geology of the Bell Lake-Sturgeon Lake area, Districts of Kenora and Thunder Bay. Ont. Div. Mines, GR 120. 31pp.

_____, Blackburn, C.E. and Edwards, G.R., 1980. Preliminary synthesis of the Savant Lake-Crow Lake Metavolcanic-metasedimentary belt, northwestern Ontario, and its bearing upon mineral exploration. Ont. Geol. Survey, Misc. Paper 89, 30pp.

Turner, F.J., 1981. Metamorphic Petrology. Second Edition. McGraw-Hill Co., 524pp.

Winkler, H.G.F., 1976. Petrogenesis of Metamorphic Rocks. Fourth Edition, Springer-Verlag New York Inc., 334 pp.

Wohletz, K.H. and Sheridan, M.F., 1983. Hydrovolcanic explosions II. Evolution of basaltic tuff rings and tuff cones. Amer. Jour. Sci., 283: 385-413.

Wright, J.V., Smith, A.L. and Self, S., 1980. A working terminology of pyroclastic deposits. Jour. Volcanol. Geotherm. Res., 8: 315-336.

Zen, E-an, 1959. Clay mineral-carbonate relations in sedimentary rocks. Amer. Jour. Sci., 257:29-43.

_____, 1960. Metamorphism of lower Paleozoic rocks in the vicinity of the Taconic Range in west-central Vermont. Amer. Miner., 45:129-175.

APPENDIX A: Modal Compositions

Mineral abbreviations used:

QTZ	quartz
FELD	feldspar
CHL	chlorite
CARB	carbonate
EP	epidote
ACT	actinolite
SER	sericite
STILP	stilpnomelane
BIOT	biotite
HB	hornblende
GNT	garnet
AND	andalusite
CHLTD	chloritoid
TOUR	tourmaline

Fragments

L	lithic
P	pumice

Phenocrysts

QTZ	quartz
PLAG	plagioclase (albite)

Values are in percent.

TABLE 2: Modal Composition of Mafic Volcanic Rocks

T.S. #	TEXTURES[1]	QTZ,FELD	CHL	CARB	EP	ACT	SER	STILP	OPAQUES	OTHER
14	MP	61	30	7					2	
22		27	12	20			35		6	
24	A,MP	50	20	13			11		4	
26	P	41	35	5			14		4	
28	MP	51	22	7	16				4	
79		25		3	20		30	20	1	
80	P	64	20	5			7		3	
87	P	85		7					4	3BIOT
111	B	70	11		8	7				2SPHENE
112	P	62	8	4	5	16				3SPHENE
119		58	17	9				14	2	
129	A,MP	57	10	5					10	15HB
135	P,B	63	20	7			8		3	
137	A	65	12	16			15		2	
138	MP,B	52	31	10			3		3	
139	B	37	27	12		15	6		3	
142	B	47	28	19					6	
144	A,MP	40	5	27			18		4	
145		45	20	22	5				6	

1. P= porphyritic
   MP= microporphyritic
   A= amygdaloidal
   B= brecciated

TABLE 3: Modal Composition of Mafic Debris Flow Deposits

T.S. #	CLASTS[1]	QTZ,FELD	CHL	CARB	EP	STILP	ACT	SER	OPAQUES	OTHER
1	10S,10F	41	38	11				13	4	
2	45,7F	62	28	4				5	1	
3	38,8F	38	30	15			12		3	
5	60	47	29	18				5	2	
8	40	46	24	9				7		14BIOT
9	30	32	41	7	5	12			2	
10	45	41	12	10	14	20			2	
11	55	36	7	11	9	17	18		2	
12	65	60	14	6				14	6	
13	10	42	25	30					3	
16	20	37,15	33	7				5	3	
18	30	62	4	4	5		20		5	
19	45S	56	12	4	10	15			1	
23	35(S)	48	27	1				8	2	
30	20(MT)	48	12	14	6	13			7	
33	5	34	32	16	3	9			6	
34	15S	42	17	16	13	12			TR	
35	25(S)	49	13	8	12	17			2	
36	25(S)	48	14	10	6	19			3	
37	60S	49	18	25		4			2	
44	45	52	5	9	10	19			2	
45	75(S)	33,5	15	6	9	7	20		4	
46	20(F)	37,10	13	7	5	22			6	
47	25S	54	25	9	3	7			3	
48	25S	47	29		6	1		12	3	
57	20	31	23	19				21	6	

TABLE 3 (Continued)

T.S. #	CLASTS[1]	QTZ,FELD	CHL	CARB	EP	STILP	ACT	SER	OPAQUES	OTHER
59	25S	59	9	8	5	16			3	
60	15(F)	65	11	14	6	2			2	
63	85	40	40	15	2				3	
107	15	15	28	37				18	2	
114	10	49	24	12		5			3	3GNT,1HB
115	10	50	22	16		1			1	

1. Percentage of total rock. Basaltic clasts unless otherwise indicated. S=scoria, MT=magnetite-rich, F=felsic. Parentheses denote accessory fragment component (less than 5%).

TABLE 4: Modal Composition of Felsic Pyroclastic Rocks

T.S. #	FRAGMENTS L	FRAGMENTS P	PHENOCRYSTS QTZ	PHENOCRYSTS PLAG	QTZ,FELD	SER	CHL	CARB	CHLTD	OPQS	OTHER
7	25				40	34	3	20		3	
38	60				30	16	22	30		2	3BIOT
40				1	55	15	10	14		4	
41					34	26	24			4	
43	55				46	22	17	11		3	
47	20	5			60		12	10		3	14EP
49		15			37	20	21	14		3	14STILP
50	25			1	48		14	32		2	
52	15				28	24	26	17	2	3	
53	50				49	8	7	34	4	2	
54	10	15			43	16	13	27		2	
56	7				45	18	26	9		2	
64		30			26	22	10	25	12	4	
65		15			31	16	19	28		6	
66	5	25			25	40	15	15		5	
68		50			55	11	11	19	1	3	
69	10	15			56	15	8	18		2	
70		35			42	21	12	12	9	4	
71	10	5			23	26	18	29		4	
73	4	4			20	18	15	30	13	4	
74	5				20	20	8	32	15	5	
75	35				53	5	4	29	6	3	
76					37	20	10	20	7	6	
77	35				23	6		37	21	8	5AND
88		5			30		17	35	8	3	2EP
89		10			35	13	9	30	10	3	
90	35				45	25	14	12		3	
93	5				63	22	1	12	1	1	

TABLE 4 (Continued)

T.S. #	FRAGMENTS L	FRAGMENTS P	PHENOCRYSTS QTZ	PHENOCRYSTS PLAG	QTZ,FELD	SER	CHL	CARB	CHLTD	OPQS	OTHER
96					45	2		42	8	2	1AND
97		5	3		57	27	5	6		1	
98	5				40	5	15	35		3	
108	65				68		18	7		1	6HB
110			1	8	60	10	5	13		1	
120	85				35	35	12	16		2	
121			5		46	22	18		8	1	
125			3		70	12		5	6	2	
131	35				31	7	27	33		1	
158	35	5			51	23	4	12	8	2	1BIOT

TABLE 5: Modal Composition of Felsic Lavas

T.S. #	TEXTURES[1]	QTZ,FELD	SER	CHL	CARB	STILP	CHLTD	OPAQUES	OTHER
21		12	59	16	12			1	
61	P,F	71	25		5			1	
81	MP	79	10	10				1	
91		43	25	8	10		10	1	
92	A	48	21	8	15		4	3	
94	F	39	30	15	14			2	
95	A,MP	15,32	28	15	7			2	
98-2		40	5	15	35			3	
100	P	52	28	4	6		9	1	
101	A,F	17	34		27		17	4	
104	A	75	12	1				1	1BIOT
105	A	85						1	14BIOT
106-2	F	77	7	8				1	7BIOT
106-3	A	49,24	15	7				1	4BIOT
106-4		85	10	5				TR	
132	P,F	45	40	5	8			1	
133	A,MP	30	25	6	23		10	4	
134	MP	70	20	5	3			2	
136	P	64	20	7	8			1	
154		35	24	5	19		5	2	8AND[2]

1. P= porphyritic
   MP= microporphyritic
   A= amygdaloidal
   F= flow breccia

2. Veins.

TABLE 6: Modal Composition of Intrusive Rocks

T.S. #	PHENOCRYSTS QTZ	PHENOCRYSTS PLAG	QTZ,FELD	CHL	SER	CARB	EP	STILP	OPAQUES	OTHER
20		30	30	8	15	6	7		2	
27			74	10	8	7			1	
29			48	18	17	10	14		2	
30-4	TR	14	53	5	22			5	1	
31		4	33	13	27	8	4	7	2	2SPHENE
39			37	20	16	12		7	8	
55			21,42	15	8	11			1	1APATITE
58		1	16,52	6	15	9			2	
62			55	8	30				5	
82			70	5	15	4			3	1TOUR
83			68	12		10		8	2	
84		45	10,10				15			15HB,5SPHENE
85		10	65				10			8HB,3BIOT,2SPHENE
86			30,45	7	10	5			2	
102			42	32	25				1	
106-1	TR		25	28		33			1	12BIOT
117	1	4	80	4	2			6	TR	
122			8,37	10	24	15			4	1SPHENE
126			33	7	27	28			4	1SPHENE,APATITE
128		12	62			3	5		1	15HB,1SPHENE

APPENDIX B: Chemical Analyses

The following tables are a compilation of major and trace element chemical analyses performed by the Geological Survey of Canada. Unless otherwise noted, blank values represent quantities below detection limits (i.e. not found). Sample numbers correspond to outcrop locations on Plates 1 and 2.

TABLE 7: Whole Rock Chemical Analyses of Major Oxides*

SAMPLE#	SiO_2	TiO_2	Al_2O_3	Fe_2O_3	FeO	MnO	MgO	CaO	Na_2O	K_2O	H_2O	CO_2	P_2O_5	S	C	Ba	Zn	TOTAL	S.G.
1	51.3	1.08	15.6	1.8	6.8	.13	6.05	4.34	3.1	1.12	4.2	4.2	.23	.05		.029	.011	100.1	2.77
2	57.7	.95	13.9	1.3	6.4	.13	5.16	3.59	1.7	1.79	4.1	3.6	.21	.04		.047	.009	100.7	2.77
3	56.2	1.04	14.4	1.1	6.8	.14	4.78	3.95	3.2	1.03	3.5	3.8	.22	.06		.031	.010	100.3	2.77
5	53.8	.85	13.7	1.5	6.3	.13	5.65	4.56	1.6	2.34	3.0	6.3	.20	.02	0.6	.023	.012	100.7	
6	54.7	.99	15.0	1.5	6.5	.14	6.00	3.09	1.6	1.90	4.5	2.2	.24	.02	0.3	.062	.011	98.9	
9-1	48.1	1.06	13.2	1.4	7.5	.19	8.09	7.02	2.0	.37	5.4	5.4	.34			.010	.011	100.2	
9-2	55.0	1.03	14.7	1.5	7.3	.15	5.42	4.24	3.2	1.16	3.3	2.8	.22			.023	.010	100.0	2.79
10-2	54.8	1.03	15.1	2.1	6.0	.12	3.78	4.51	5.2	1.44	2.0	3.3	.23			.032	.009	99.8	2.79
11	57.6	.93	14.3	1.6	5.8	.13	4.12	4.44	5.0	.89	1.8	2.7	.21			.021	.009	99.6	2.81
12	61.8	1.04	12.8	2.3	4.8	.12	2.59	3.84	4.5	.55	1.9	3.8	.20			.024	.006	100.3	2.78
13	47.9	1.19	13.6	1.4	8.7	.18	4.84	5.84	3.3	.94	2.5	8.7	.23		0.5	.019	.014	99.9	2.81
14A	53.9	1.07	15.4	1.2	7.3	.12	5.61	3.66	4.4	.17	3.7	4.1	.22			.006	.011	100.9	2.71
18	56.2	1.05	15.1	1.9	6.8	.13	5.07	3.59	5.2	.22	2.7	1.5	.22	.08		.007	.010	99.9	2.78
19	53.8	1.07	15.8	1.7	7.1	.14	5.08	3.82	4.6	1.08	3.0	3.0	.25	.08		.035	.011	100.7	2.76
20	62.4	.83	15.5	2.0	5.2	.08	2.07	3.42	2.1	1.34	2.7	2.3	.21			.103	.006	100.3	2.79
22	55.3	1.01	16.5	.9	5.5	.14	3.79	4.98	.8	2.24	3.1	6.3	.20			.034	.007	100.8	2.80
23	58.2	1.02	16.0	1.0	6.2	.10	2.88	4.86	2.0	1.27	3.0	3.4	.22			.024	.009	100.3	2.77
24	56.1	.97	15.7	2.4	5.8	.09	3.00	5.46	2.7	1.17	2.6	4.2	.19			.016	.010	100.5	2.79
25	48.5	.89	13.9	1.3	10.0	.21	4.99	6.97	1.3	.66	4.8	6.6	.18			.013	.014	100.5	2.81
26	58.8	.93	15.5	2.1	7.5	.18	4.88	1.61	0.0	2.29	4.4	1.7	.17			.093	.029	100.3	2.81
30-4	71.0	.61	13.8	1.3	3.9	.03	2.28	.39	1.9	3.06	2.2	0.0	.16			.047	.011	100.9	2.75
33	49.6	1.41	14.6	1.8	9.3	.22	5.51	4.62	3.5	1.10	3.2	5.5	.27			.022	.014	100.7	2.73
34	55.1	1.23	14.5	1.6	7.5	.16	4.58	4.23	3.4	1.84	2.7	2.5	.23			.030	.009	99.7	2.78
36	58.5	1.20	13.4	.7	8.4	.13	5.20	2.97	3.3	1.51	2.7	2.6	.21			.027	.010	100.8	2.79
40	62.1	.70	13.3	2.3	4.4	.13	2.48	4.37	.4	2.03	2.3	5.7	.19			.045	.014	100.4	2.80
41	53.5	1.03	16.1	1.2	7.3	.19	4.75	4.15	1.1	1.50	4.7	4.9	.21			.044	.032	100.8	2.81
42	56.2	1.04	16.3	.9	7.1	.17	4.90	3.69	.7	1.35	4.3	3.9	.24			.031	.022	100.9	
44	55.3	1.17	13.1	2.2	6.8	.17	4.00	5.30	3.7	1.59	2.4	3.3	.20	.11		.042	.011	99.4	2.79
45	55.1	1.28	15.0	2.1	8.0	.17	4.83	3.82	4.3	1.01	2.6	.9	.23	.01		.019	.012	99.3	2.78
46-1	53.1	1.29	15.3	2.1	8.2	.17	5.51	3.17	3.8	1.82	3.2	2.8	.24			.051	.012	100.9	
47-2	51.1	.78	16.5	1.1	6.1	.12	4.48	5.54	2.7	2.31	3.8	5.4	.10			.103	.009	100.3	2.76
47-4	54.6	1.33	14.2	3.6	6.6	.14	3.46	5.53	2.9	1.96	2.3	1.6	.21	.13		.072	.011	98.7	
48	53.5	1.34	14.9	1.7	9.0	.14	7.95	1.19	1.5	.92	5.0	1.1	.24			.027	.013	98.6	2.78

TABLE 7 (Continued)

SAMPLE#	SiO_2	TiO_2	Al_2O_3	Fe_2O_3	FeO	MnO	MgO	CaO	Na_2O	K_2O	H_2O	CO_2	P_2O_5	S	C	Ba	Zn	TOTAL	S.G.
50	49.0	1.10	13.0	1.3	7.3	.21	3.94	6.61	4.4	.63	1.6	9.8	.14		0.6	.010	.008	99.6	2.72
53	73.8	.31	10.8	1.1	2.9	.06	1.44	2.18	1.7	.94	1.7	3.2	.12	.01		.023	.007	100.4	2.76
54	51.3	1.24	14.0	.9	8.4	.15	4.71	5.35	1.5	1.03	3.2	8.7	.20			.014	.009	100.8	( )[1]
55	49.9	.76	14.0	3.7	5.2	.16	4.68	7.14	2.3	.60	3.5	8.1	.35	.19		.018	.013	100.6	2.75
56	50.3	1.04	14.1	2.0	7.6	.16	5.00	5.72	2.2	1.08	3.8	6.6	.29	.54		.028	.015	100.3	2.78
57	52.9	1.31	14.0	1.1	8.7	.13	4.59	5.72	.8	.94	4.0	5.9	.21	.06		.019	.014	100.4	2.83
59	56.2	1.34	14.5	1.6	8.2	.15	4.27	3.36	3.6	1.72	2.6	2.9	.21	.01		.035	.013	100.9	
60	57.5	1.33	14.2	3.1	7.1	.16	3.47	3.25	4.6	.53	2.3	2.9	.21	.15		.015	.012	100.8	2.79
61	75.8	.21	8.5	.4	2.6	.10	1.56	3.90	0.0	1.46	1.8	3.4	.05			.016	.011	99.9	2.68
63	54.5	1.44	15.2	1.9	9.1	.14	5.85	2.26	3.1	1.00	3.8	2.0	.21	.02		.019	.013	100.6	2.81
66	50.2	1.31	14.5	12.1		.10	5.12	3.47	.2	.84	5.0	6.0	.17	1.36		.013	.012	99.9[2]	2.83
70	47.2	1.19	13.8	.8	9.1	.15	6.09	5.88	.9	1.33	3.7	10.5	.16			.017	.014	100.9	2.88
71	47.7	1.21	14.4	.8	8.8	.15	5.42	4.04	2.3	2.29	2.1	4.9	.22		2.3	.030	.012	96.7	2.87
73	48.1	1.29	14.3	.7	9.4	.14	4.91	6.84	.3	.26	2.7	10.3	.19		0.6	.010	.010	100.0	2.94
74	47.4	1.23	14.2	1.0	8.6	.17	4.77	7.26	.5	1.63	2.7	7.5	.22		1.4	.036	.013	98.7	2.90
75	50.7	1.01	11.8	1.0	7.4	.15	6.25	7.34	.1	.36	2.4	7.9	.19		1.5	.006	.008	98.2	2.87
76	51.7	1.18	13.5	1.0	7.6	.14	4.73	6.36	1.2	1.09	2.7	8.3	.21		0.5	.013	.012	100.4	2.83
79	47.4	1.03	20.6	2.5	7.4	.16	7.01	1.61	1.0	6.07	4.2	.3	.31			.183	.021	99.9	2.89
80-1	45.8	.81	15.0	1.4	6.1	.20	4.46	8.51	1.8	1.69	2.5	11.3	.54	.43		.074	.006	100.5	2.81
80-2	61.2	.78	14.0	1.3	7.0	.16	4.13	3.28	1.2	.91	3.2	3.0	.19	.01		.045	.007	100.4	2.77
81	66.9	.61	12.4	1.4	3.6	.13	1.57	4.08	1.1	2.1	1.9	4.3	.15	.27		.036	.012	100.6	2.74
82-1	69.5	.60	12.8	.7	2.3	.05	2.99	2.61	0.0	3.17	2.8	2.6	.18			.049	.005	100.5	2.71
82-2	61.7	.69	14.8	.7	4.2	.07	4.59	4.18	3.3	.28	2.6	2.3	.13			.006	.007	99.6	2.70
83	57.4	.69	14.3	1.5	7.1	.11	4.94	4.25	2.8	.92	3.1	3.0	.15	.07		.020	.004	100.4	2.77
84	58.5	.71	15.9	2.1	5.0	.10	4.10	7.65	2.5	.13	2.0	.6	.19			.007	.005	99.5	2.84
85	56.7	.76	17.2	1.1	6.2	.10	4.17	6.82	2.6	.43	2.3	1.8	.18			.010	.007	100.4	2.83
86	74.0	.24	11.3	.9	1.9	.05	.30	2.68	3.2	1.34	.9	2.4	.05	.08		.045	.003	99.5	2.68
88	48.2	1.11	13.2	2.3	7.2	.20	5.65	7.42	.6	.71	2.6	7.9	.18		1.6	.013	.010	98.9	2.81
89	53.2	1.23	14.3	2.2	7.0	.16	3.82	5.45	1.3	.89	2.0	7.7	.23		0.8	.011	.010	100.2	2.86
91-1	62.4	1.07	14.4	1.6	4.7	.11	1.49	3.92	1.1	1.94	1.9	5.1	.35			.049	.009	100.3	2.86
91-2	65.6	.65	11.9	1.6	5.1	.11	1.93	3.48	.6	1.69	2.0	4.8	.22	.47		.035	.013	100.0	2.78
92	65.1	.68	13.3	1.3	4.7	.27	2.02	2.86	0.0	3.09	2.6	4.4	.20	.03		.087	.026	100.8	2.78

TABLE 7 (Continued)

SAMPLE#	SiO_2	TiO_2	Al_2O_3	Fe_2O_3	FeO	MnO	MgO	CaO	Na_2O	K_2O	H_2O	CO_2	P_2O_5	S	C	Ba	Zn	TOTAL	S.G.
94	69.3	.51	9.9	1.4	4.9	.20	2.14	2.54	0.0	2.12	2.3	3.6	.18			.041	.016	99.3	2.79
95	54.9	.98	15.2	1.5	8.7	.37	4.35	2.90	0.0	2.53	4.5	4.7	.18			.044	.034	100.9	2.78
96	49.1	1.10	12.9	1.7	6.7	.15	4.43	6.42	1.1	1.23	1.7	6.8	.23		2.2	.021	.008	95.8	2.88
97-1	78.9	.20	10.8	.8	1.8	.02	2.15	.08	.5	2.28	2.2	.3	.03	.06		.019	.010	100.2	2.69
97-2	76.3	.2	11.0	.3	2.1	.06	1.89	.87	0.0	2.70	2.0	1.8	.04			.025	.010	99.5	2.74
98	54.3	.71	15.8	1.0	5.8	.15	5.12	5.76	1.4	1.01	4.0	5.4	.20	.01		.032	.018	100.7	2.77
102	58.8	.80	14.8	1.7	9.5	.21	5.69	.44	0.0	1.62	5.3	0.0	.20	.13		.038	.024	99.4	2.82
103-1	53.1	.89	16.0	2.3	6.0	.14	3.33	8.04	1.5	1.64	1.3	5.3	.15			.074	.009	99.9	2.81
103-2	69.7	.62	12.5	.5	3.8	.13	2.07	3.90	0.0	2.85	1.4	1.0	.14	.10		.068	.006	98.9	2.76
104	71.0	.56	12.5	.8	4.8	.14	2.31	2.43	.5	1.34	2.3	.1	.11	.02		.047	.011	99.1	2.74
106-1	44.8	.61	13.5	1.0	7.6	.26	6.63	11.4	.4	2.55	3.1	5.4	.21	.23	1.0	.066	.008	98.9	2.83
106-2	73.6	.44	10.2	.6	4.1	.13	2.32	3.30	.2	1.67	1.8	1.2	.10			.041	.007	99.7	2.75
106-4	77.8	.24	11.3	2.6		.05	1.34	2.29	.2	1.48	1.7	.2	.03			.052	.004	99.3	2.72
107	52.2	1.07	15.8	1.9	12.1	.33	6.03	2.13	1.2	.51	5.3	.1	.17			.011	.077	99.0	
108-1	67.2	.51	12.0	.7	3.8	.18	2.64	3.55	.4	2.09	2.3	4.9	.18			.066	.006	100.6	2.78
108-2	54.6	.96	14.3	1.4	9.1	.29	5.64	4.73	1.1	.58	3.6	2.9	.17			.016	.038	99.5	2.83
110	67.1	.50	11.2	.3	3.4	.18	2.53	5.69	.7	1.04	2.0	4.9	.14			.038	.007	99.8	2.72
112	52.7	.97	16.4	1.6	7.1	.16	6.45	7.09	2.3	.14	3.5	2.0	.16			.006	.010	100.7	2.83
114	50.8	1.50	14.3	2.3	12.4	.41	5.62	4.93	0.0	.72	4.6	2.5	.34	.04		.018	.024	100.6	2.86
115	52.8	1.34	13.1	1.9	8.5	.28	4.03	7.40	1.1	.87	2.1	6.0	.33	.01		.019	.011	99.9	2.84
117	73.5	.37	13.2	.6	2.5	.07	.96	1.97	3.8	1.27	.9	.6	.08			.048	.007	99.9	2.68
119	54.0	2.04	14.0	1.5	8.3	.12	4.70	4.90	2.1	1.60	2.9	2.8	.42			.034	.006	99.5	2.82
121	64.0	.45	15.9	2.0	8.1	.17	2.29	.44	.1	1.39	4.0	.4	.17	.09		.010	.014	99.7	2.90
122	49.2	.96	17.5	2.0	7.1	.10	3.41	6.02	2.9	1.05	3.6	5.7	.20	.01		.016	.009	99.8	2.82
128	69.7	.65	14.2	.4	2.0	.05	1.79	4.31	4.6	.1	.6	.2	.17			.009	.003	98.9	2.71
129	49.5	1.72	12.2	6.2	10.0	.25	4.37	6.54	1.8	.07	2.4	4.2	.19	.13		.004	.013	99.7	2.94
131	48.8	.71	15.0	1.6	6.6	.21	4.41	10.7	1.5	.53	3.2	4.3	.08	.04	1.0	.025	.009	98.8	
132	48.3	.71	14.7	1.7	6.6	.21	4.28	10.6	1.2	.51	3.2	8.0	.06	.05		.026	.010	100.2	
134	74.6	.23	11.0	.2	2.7	.06	1.23	1.47	.5	2.63	2.1	3.1	.04	.07		.034	.016	100.1	2.76
135	55.0	1.62	15.0	1.1	1.3	.09	4.89	1.85	1.7	1.08	4.8	1.5	.47	.05		.015	.030	100.5	2.81
137	52.9	1.04	14.5	1.0	7.2	.16	4.91	4.83	.9	1.69	4.0	6.8	.17	.01		.027	.042	100.3	2.82
139	52.7	1.01	14.5	1.6	6.8	.18	5.48	4.81	2.0	1.60	3.6	6.1	.19	.09		.039	.035	100.9	2.81

TABLE 7 (Continued)

SAMPLE#	SiO_2	TiO_2	Al_2O_3	Fe_2O_3	FeO	MnO	MgO	CaO	Na_2O	K_2O	H_2O	CO_2	P_2O_5	S	C	Ba	Zn	TOTAL	S.G.
140	55.6	.91	13.9	1.1	8.7	.12	4.20	3.90	.6	1.52	3.7	6.1	.19	.16		.035	.017	100.9	2.84
144	50.6	1.10	15.6	.7	7.1	.15	3.78	6.83	1.8	1.33	2.8	8.2	.17	.02		.020	.012	100.3	2.84
145	48.9	1.21	14.0	.9	8.5	.19	4.02	7.22	2.4	.98	2.8	8.9	.19	.04		.021	.012	100.3	2.81

* Done at the Geological Survey of Canada, Ottawa, Ontario.
All analyses by fused pellet XRF except FeO, H_2O^T, CO_2 and S (rapid chemical).

1. Specific gravities, matrix = 2.84, lithic fragments = 2.77.
2. Total is minus the oxygen equivalent for elemental sulfur (.51).

TABLE 8: Trace Element Values For Accompanying Whole Rock Analyses*

SAMPLE #	Cu	Zn	Ni	Co	Cr	V	Rb	Sr	Y	Zr
1	47	105	51	36	62	277	26	152	27	182
2	9	95	46	31	55	243	40	126	20	151
3	45	97	41	31	55	230	23	152	23	154
5	24	111	30	29	16	196	88	218	23	164
6	46	104	36	30	17	294	49	71	28	183
9-1	8	119	220	38	354	260	8	189	22	189
9-2	44	101	49	33	50	260	21	188	25	154
10-2	39	91	48	30	55	254	28	133	31	167
11	31	82	49	28	58	215	20	331	25	146
12	28	61	25	29	14	262	8	102	27	138
13	29	149	37	37	20	293	22	122	33	159
14A	48	107	48	37	60	252	5	126	24	160
18	50	100	44	38	60	269	8	134	31	170
19	37	105	47	40	56		23	141	33	169
20		64	9	20	9		32	107	37	284
22		75	18	26	6		60	110	25	188
23	9	90	15	28	8		36	120	23	196
24		79	17	28	10		32	103	29	184
25	6	140	36	42	12	21	22	73	31	178
26	5	271	35	28	17	230	59	46	24	177
30-4	5	117		13	9	37	68	87	47	486
33	52	160	36	40	23	264	21	162	33	175
34	64	106	33	33	20	260	32	231	26	159
36	44	95	31	35	20	252	29	160	26	157
40	14	139	14	20	9	112	51	58	41	282
41		312	23	29	7	186	38	101	27	196
42	35	229	26	31		206	33	74	32	202
44	126	104	30	36	17	206	31	221	28	158
45	39	117	30	36	20	258	22	213	32	169

TABLE 8 (Continued)

SAMPLE #	Cu	Zn	Ni	Co	Cr	V	Rb	Sr	Y	Zr
46-1	42	115	31	37	21	267	42	120	29	166
47-2	71	93	73	36	28	196	38	20	16	98
47-4	63	112	16	38	7	292	37	325	37	199
48	32	136	33	32	16	256	27	54	31	169
50	36	86	24	28	13	184	15	133	31	162
53	144	46	26	20		156	22	114	53	347
54	6	106	30	32	15	237	19	134	30	165
55	7	118	29	35	39	193	19	147	31	159
56	33	161	21	35	23	230	40	106	36	191
57	19	135	10	22	6	258	16	67	36	184
59	49	112	10	28	7	276	35	279	33	185
60	25	124	9	20		280	17	195	32	185
61	10	106					34	83	50	342
63	58	127	10	33	9	313	34	94	35	201
66	259	115	45	113	21	227	19	151	29	174
70	9	127	27	31	25	230	34	216	32	163
71	34	125	24	27	21	217	53	199	30	150
73	9	107	28	28	21	214	10	93	31	169
74	50	121	28	30	21	228	39	202	28	167
75	22	82	22	21	19	182	10	85	24	121
76	29	118	29	27	20	223	25	161	24	155
79		201	79	27	71	191	118	109	21	243
80-1	12	54	19	48	12	186	44	209	27	249
80-2		78	7	20	9	99	23	122	35	256
81	17	122		41	6	33	51	79	43	343
82-1	5	35	13		7	21	59	23	24	332
82-2		52	43	8	64	124	9	161	43	268
83	47	38	47	20	96	147	37	201	26	173
84	6	38	59	15	78	139	5	250	21	182
85	6	68	63	16	88	163	14	252	25	196
86	12	25			5		34	87	62	430
88	9	107	24	19	22	215	19	156	28	152

TABLE 8 (Continued)

SAMPLE #	Cu	Zn	Ni	Co	Cr	V	Rb	Sr	Y	Zr
89	31	94	29	25	21	227	25	149	37	162
91-1	6	93				39	57	142	39	260
91-2	74	115		19		21	56	114	43	301
92	11	191				17	65	70	48	347
94	7	158				18	50	40	44	285
95	32	324	15	23	7	176	73	64	28	183
96	17	76	21	24	23	197	30	110	30	160
97-1	7	96					54	24	49	412
97-2	8	92					66	26	57	444
98	7	159	66	26	75	137	28	123	19	156
102	87	239	20	14	24	125	41	90	18	150
103-1	7	84	60	25	118	182	44	24	19	130
103-2	65	73			28	26	71	63	49	336
104	5	117			6	19	26	56	41	347
106-1	8	77	106	24	520	217	87	45	18	126
106-2	9	70			7	16	48	23	43	312
106-4		28					31	30	64	431
107	7	748	25	32	85	252	18	46	28	137
108-1	14	59	17		17	26	57	47	50	358
108-2	5	365	19	26	83	223	19	71	22	125
110		46		23	7	19	27	107	45	311
112	6	54	57	30	143	198	5	155	24	128
114	20	235		33	11	291	24	56	27	179
115	8	17		22	14	263	25	91	27	159
117	7	46					26	85	54	428
119	6	41		29	9	186	5	107	36	251
121	27	130	54	12	6	23	34	65	51	332
122	169	100	84	32	73	196	29	192	22	119
128	8	31	8		12	36	4	173	36	351
129	66	123	16	38	36	358	6	92	62	169
131	82	97	30	40	16	296	15	154	17	60
132	82	97	30	41	17	286	19	170	22	65

TABLE 8 (Continued)

SAMPLE #	Cu	Zn	Ni	Co	Cr	V	Rb	Sr	Y	Zr
134[1]							72	51	63	457
135[1]							22	31	49	278
137[1]							43	41	23	145
139[1]							53	179	34	196
140[1]							41	69	36	212
144[1]							33	104	32	206
145[1]							34	150	29	155
±ppm							10	10	10	10

* Comments:

Cu, Zn, Co, Cr, and V by atomic absorption.
Rb, Sr, Y and Zr by energy dispersive XRF.
Sample #99 reported 19 ppm Pb.

1. Cu, Pb, Zn, Ni, Co, Cr, and V values not reported.

TABLE 9: Precision of XRF Method*

ELEMENT	CALIBRATION RANGE %	TOTAL MAX. ERROR ABSOLUTE +	RELATIVE%	DETERMINATION LIMIT	STANDARD DEVIATION
SiO_2	0 - 100	0.50	1	0.50	0.61
TiO_2	0 - 3	0.02	1	0.02	0.03
Al_2O_3	0 - 60	0.50	1	0.50	0.50
Fe_2O_3	0 - 90	0.10	1	0.10	0.25
FeO	0 - 30	0.03	2	0.03	
MnO	0 - 1	0.01	2	0.01	0.01
MgO	0 - 50	0.15	1	0.15	0.15
CaO	0 - 35	0.10	1	0.10	0.10
Na_2O	0 - 10	0.50	3	0.50	0.50
K_2O	0 - 15	0.05	1	0.05	0.07
H_2O	0 - 5	0.05	5	0.05	
CO_2	0 - 20	0.02	3	0.02	
P_2O_5	0 - 1	0.02	2	0.02	0.02
S	0 - 3	0.02	5	0.02	
Ba	0 - 0.3000	0.002	1	0.002	0.003
Zn	0 - 0.0200	0.002	10	0.002	0.002

* Comments:

As reported by the Geological Survey of Canada

Determination on fused disc: 1gm sample + 5gm $Li_2B_4O_7$ + 0.3gm LiF.
Single reading of 20 min./disc.
Matrix effects corrected by alpha coefficients.

TABLE 10: GSC Standard Results*

	4 Sample Mean	Standard Deviation
SiO_2	52.2	0.2
TiO_2	0.75	0.01
Al_2O_3	15.9	0.3
Fe_2O_3	2.1	0.5
FeO	5.4	0.5
MnO	0.17	0.01
MgO	3.83	0.12
CaO	9.05	0.05
Na_2O	1.7	0.2
K_2O	0.55	0.03
H_2O	2.9	0.1
CO_2	5.6	0.1
P_2O_5	0.09	0.02
S	0.03	0.03
Ba	0.027	0.001
Zn	0.009	0.001
TOTAL	100.31	

* Geological Survey of Canada standard 'LUI' (Mattabi hanging wall andesite, see Franklin et al., 1977).

APPENDIX C: Normative Mineral Compositions

The following tables are a summary of normative mineral compositions which were calculated from the chemical analyses listed in Table 7. The calculations have been performed by the Geological Survey of Canada, and the following conditions prevail:

1. CO_2 and H_2O have been removed and remaining analyses normalized to 100%.
2. Ferric iron has not been converted to ferrous iron.
3. A rock name has been applied according to Irvine and Barager's (1971) classification scheme.

Abbreviations

T. - tholeiitic
C.A. - calc-alkaline
BSLT - basalt
AND - andesite
RHY - Rhyolite
(KR) - K (potassium)-rich series
(KP) - K-poor series

MINERAL ABBREVIATIONS

Q	Quartz
C	Corundum
OR	Orthoclase
AB	Albite
AN	Anorthite
DI	Diopside
HE	Hedenbergite
EN	Enstatite
FS	Ferrosilite
MT	Magnetite
IL	Imenite
AP	Apatite
PY	Pyrite

Values are in weight per cent.

TABLE 11: Normative Mineral Compositions

SAMPLE#	Q	C	OR	AB	AN	DI	HE	EN	FS	MT	IL	AP	PY	ROCK NAME
1	7.70	2.13	7.23	28.63	21.86			16.45	10.21	2.85	2.24	0.58	0.11	C.A. BSLT
2	23.62	3.38	11.40	15.49	17.70			13.84	9.98	2.03	1.94	0.53	0.09	T. BSLT (KR)
4	14.39		3.60	15.62	38.22	4.66	3.46	8.36	7.11	2.68	1.53	0.28	0.11	C.A. BSLT (KR)
5	15.16	0.80	15.27	14.93	23.51			15.52	10.07	2.40	1.78	0.51	0.05	T. BSLT (KR)
6	20.73	5.75	12.26	14.77	15.01			16.30	10.12	2.37	2.05	0.61	0.05	C.A. BSLT (KR)
9-1	15.20	1.47	6.56	29.14	19.54			12.81	10.76	1.72	2.13	0.55	0.13	C.A. BSLT
9-2	5.87		2.45	18.96	29.07	4.07	1.98	20.68	11.53	2.27	2.26	0.88		T. BSLT
10-2	11.19	1.06	7.31	28.83	20.86			14.37	11.44	2.32	2.08	0.54		C.A. BSLT
11	8.25		5.54	44.52	14.68	3.44	2.35	9.20	7.21	2.44	1.86	0.51		C.A. AND (KP)
12	21.72		3.44	40.27	13.86	2.33	1.71	5.74	4.83	3.53	2.09	0.49		C.A. AND (KP)
13	1.97		6.31	31.68	22.15	3.83	3.65	11.90	13.02	2.30	2.57	0.61		C.A. BSLT
14A	7.66	1.99	1.08	40.01	17.97			15.01	11.68	1.87	2.18	0.55		C.A. AND (KP)
18	6.56	0.32	1.36	46.04	17.13			13.21	9.69	2.88	2.09	0.53	0.17	C.A. AND (KP)
19	3.53	0.76	6.76	41.18	18.32			13.39	10.54	2.61	2.15	0.61	0.17	C.A. AND (KP)
20	33.83	5.13	8.33	18.67	16.39			5.42	7.02	3.05	1.66	0.51		C.A. AND (KP)
22	24.84	4.58	14.50	7.41	25.61			10.33	8.70	1.43	2.10	0.51		T. BSLT (KR)
23	25.06	3.23	8.01	18.05	24.18			7.65	9.67	1.55	2.07	0.54		C.A. BSLT (KR)
24	18.15	0.56	7.40	24.41	27.62			7.98	7.73	3.72	1.97	0.47		C.A. BSLT (KR)
25	11.10		4.39	12.37	33.91	1.43	1.63	13.31	17.37	2.12	1.90	0.47		T. BSLT (KR)
26	37.09	11.17	14.42		7.32			12.93	11.53	3.24	1.88	0.42		T. BSLT (KR)
28	67.60	4.88	4.79	1.76	3.46			6.25	10.13		0.85	0.29		T. BSLT (KR)
30-4	42.78	7.15	18.39	16.33	0.90			5.77	5.22	1.92	1.18	0.38		C.A. RHY
33	1.65		7.08	32.21	22.71	0.13	0.12	14.87	14.81	2.84	2.91	0.68		C.A. BSLT
34	8.78		11.53	30.48	19.99	0.30	0.24	11.95	11.23	2.46	2.48	0.57		C.A. AND
36	14.69	1.51	9.35	29.23	13.99			13.56	13.72	1.06	2.39	0.51		C.A. AND
40	40.12	3.20	13.00	3.66	22.12			6.68	5.70	3.61	1.44	0.47		T. BSLT (KR)
41	23.00	6.18	9.75	10.22	21.11			13.00	12.16	1.91	2.15	0.54		C.A. BSLT (KR)
42	29.66	8.16	8.63	6.40	18.07			13.18	11.77	1.41	2.13	0.60		T. BSLT (KR)

TABLE 11: Normative Mineral Compositions

SAMPLE#	Q	C	OR	AB	AN	DI	HE	EN	FS	MT	IL	AP	PY	ROCK NAME
44	9.82		10.04	33.43	15.42	5.24	4.05	8.21	7.28	3.41	2.37	0.50	0.24	C.A. AND
45	6.69	0.46	6.23	37.96	18.20			12.55	11.62	3.18	2.54	0.56	0.02	C.A. AND (KP)
46-1	4.71	2.00	11.37	33.95	14.95			14.49	12.15	3.2	2.59	0.59		C.A. AND
47-2	4.69		15.04	25.15	28.71	0.40	0.26	12.10	10.01	1.76	1.63	0.26		C.A. BSLT (KR)
47-4	12.65		12.25	25.92	21.06	3.12	2.19	7.66	6.17	5.51	2.67	0.52	0.28	T. BSLT (KR)
48	23.31	10.66	5.89	13.74	4.69			21.43	14.26	2.67	2.76	0.60		T. AND
50	0.32		4.25	42.48	15.82	8.67	8.40	7.18	7.98	2.15	2.38	0.37		C.A. AND (KP)
53	54.54	3.47	5.83	15.08	10.52			3.76	4.19	1.67	0.62	0.29	0.02	C.A. AND
54	16.70	1.32	6.86	14.30	28.42			13.21	14.55	1.47	2.65	0.52		T. BSLT (KR)
55	13.62	3.99	21.87	29.34	4.60	1.77	10.97	4.84	6.03	1.62	0.91	0.44		T. BSLT
56	11.40		7.10	20.68	28.23	0.58	0.40	13.57	10.65	3.22	2.20	0.75	1.23	T. BSLT (KR)
57	22.34	1.96	6.15	7.48	29.85			12.64	14.40	1.76	2.75	0.54	0.14	T. BSLT (KR)
59	10.86	1.17	10.69	32.01	16.07			11.17	12.38	2.44	2.67	0.51	0.02	C.A. AND
60	14.03	0.69	3.28	40.71	15.43			9.04	8.65	4.70	2.64	0.51	0.32	C.A. AND (KP)
61	61.05		9.13		19.96	0.06	0.06	4.08	4.50	0.61	0.42	0.12		T. BSLT
63	14.53	5.71	6.25	27.69	10.39			15.38	13.71	2.91	2.89	0.51	0.04	C.A. AND (KP)
66[1]	35.45	8.35	5.64	1.92	18.28			14.47				0.45	0.21	T. BSLT (KR)
70	10.51	0.66	9.08	8.79	32.48			17.51	16.59	1.34	2.61	0.43		T. BSLT (KR)
71	3.62	1.51	15.51	22.28	21.30			15.46	15.78	1.33	2.63	0.58		C.A. BSLT (KR)
73	19.87	1.79	1.78	2.94	37.82			14.15	17.14	1.17	2.84	0.51		T. BSLT (KR)
74	12.41		11.08	4.86	36.43	1.40	1.36	13.01	14.51	1.67	2.69	0.59		T. BSLT (KR)
75	23.20		2.47	0.98	35.56	2.60	1.66	16.83	12.30	1.68	2.22	0.51		T. BSLT (KR)
76	17.66		27.27	11.45	31.82	0.98	0.83	12.82	12.46	1.63	2.53	0.55		T. BSLT (KR)
79	0.73	10.72	37.76	8.90	6.27			18.36	10.64	3.81	2.06	0.76		C.A. BSLT (KR)
80-1	4.74		11.53	17.56	32.12	6.23	4.01	9.92	7.32	2.34	1.77	1.45	1.02	C.A. BSLT (KR)
80-2	35.24	5.88	5.72	10.78	15.96			10.92	11.44	2.00	1.57	0.47	0.02	T. BSLT (KR)
81	42.29	1.32	13.23	9.87	20.42			4.15	4.38	2.15	1.23	0.37	0.59	T. BSLT (KR)
82-1	49.07	5.32	19.76		12.40			7.85	2.90	1.07	1.20	0.44		T. BSLT (KR)
82-2	24.53	1.88	1.75	29.50	21.01			12.07	6.47	1.07	1.39	0.32		C.A. AND (KP)
83	17.68	1.41	5.78	25.14	21.34			13.06	11.38	2.31	1.39	0.37	0.15	C.A. BSLT
84	20.25		0.79	21.83	32.81	2.67	1.47	9.30	5.88	3.14	1.39	0.46		T. BSLT (KP)
85	15.92	0.51	2.64	22.85	33.93			10.79	9.77	1.66	1.50	0.43		C.A. BSLT

TABLE 11: Normative Mineral Compositions

SAMPLE#	Q	C	OR	AB	AN	DI	HE	EN	FS	MT	IL	AP	PY	ROCK NAME
86	45.05		8.25	28.19	13.03	0.11	0.30	0.73	2.21	1.36	0.48	0.12	0.17	T. DACITE
88	16.87		4.84	5.85	35.99	2.58	1.58	15.02	10.53	3.84	2.43	0.48		T. BSLT (KR)
89	23.69	2.05	5.86	12.25	28.44			10.60	10.36	3.55	2.60	0.59		T. BSLT (KR)
91-1	39.02	4.51	12.33	10.00	18.43			3.99	6.17	2.49	2.18	0.87		T. BSLT (KR)
91-2	46.18	3.52	10.71	5.44	16.96			5.15	6.65	2.49	1.32	0.55	1.04	T. BSLT (KR)
92	44.42	5.59	19.54		13.77			5.38	7.35	2.02	1.38	0.50	0.07	T. BSLT (KR)
94	14.07		3.72	17.43	35.94	6.08	4.07	7.79	5.98	3.15	1.55	0.23		T. BSLT (KR)
95	29.18	8.32	16.34		14.42			11.82	15.07	2.37	2.03	0.46		T. BSLT (KR)
96	17.42		8.55	10.94	31.30	2.07	1.53	12.01	10.19	2.90	2.46	0.63		T. BSLT (KR)
97-1	64.49	7.62	13.82	4.33	0.20			5.49	2.28	1.19	0.39	0.07	0.13	C. A. RHY (KR)
97-2	62.69	6.90	16.73		4.25			4.93	3.52	0.46	0.44	0.10		T. BSLT (KR)
98-2	20.62	2.64	6.55	12.98	29.88			13.97	9.76	1.59	1.48	0.51	0.02	T. BSLT (KR)
102	39.38	13.55	10.21		0.93			15.09	15.81	2.63	1.62	0.49	0.29	T. BSLT (KR)
103-1	15.25		10.42	13.63	34.46	3.31	2.75	7.37	7.03	3.58	1.82	0.37		T. BSLT (KR)
103-2	46.93	2.76	17.50		19.14			5.35	5.79	0.75	1.22	0.34	0.21	T. BSLT (KR)
104	53.08	6.29	8.21	4.38	11.75			5.96	7.72	1.20	1.10	0.26	0.04	T. BSLT (KR)
106-1[2]			16.91	3.80	30.84	15.50	9.93	9.98	7.33	1.63	1.30	0.55	0.53	T. BSLT (KR)
106-2	54.63	2.38	10.22	1.75	16.26			5.98	6.78	0.90	0.87	0.24		T. BSLT (KR)
106-4[3]	65.91	5.42	8.99	1.74	11.47			3.43			0.11	0.07		T. BSLT (KR)
107	22.81	10.50	3.23	10.87	10.12			16.07	20.87	2.95	2.18	0.42		C.A. BSLT
108-1	46.27	3.28	13.26	3.63	17.63			7.05	6.32	1.09	1.04	0.45		T. BSLT (KR)
108-2	22.95	3.95	3.69	10.02	24.07			15.12	15.62	2.19	1.96	0.43		T. BSLT (KR)
110	44.85		6.63	6.38	26.24	1.50	1.14	6.10	5.33	0.47	1.02	0.35		T. BSLT (KR)
112	10.22		0.87	20.47	35.78	0.06	0.04	16.87	10.93	2.44	1.94	0.39		C.A. BSLT (KP)
114	22.90	5.75	4.56		23.81			14.99	20.43	3.57	3.05	0.85	0.09	T. BSLT (KR)
115	19.52		5.61	10.15	30.81	2.77	2.97	9.66	11.87	3.01	2.78	0.84	0.02	T. BSLT (KR)
117	40.14	2.22	7.64	32.70	9.41			2.43	3.68	0.89	0.72	0.19		C.A. DACITE (KP)
119	15.37	0.97	10.10	18.97	23.01			12.49	11.59	2.32	4.14	1.04		T. BSLT (KR)
121	50.97	14.55	8.65	0.89	1.13			6.00	13.26	3.05	0.90	0.42	0.20	C.A. BSLT (KR)
122	7.03	1.25	6.87	27.13	31.57			9.39	11.02	3.21	2.01	0.51	0.02	C.A. BSLT
128	31.19		0.66	39.72	18.14	1.41	0.65	3.90	2.06	0.59	1.26	0.40		C.A. DACITE (KP)
129	16.44		0.45	16.38	26.90	2.98	2.53	10.33	10.06	9.67	3.51	0.47	0.29	T. BSLT (KP)

TABLE 11: Normative Mineral Compositions

SAMPLE#	Q	C	OR	AB	AN	DI	HE	EN	FS	MT	IL	AP	PY	ROCK NAME
130	70.24	12.23	0.49		0.34			3.13	9.64	2.11	1.24	0.34	0.26	T. BSLT (KR)
131	9.48		3.48	14.07	36.19	10.19	8.04	7.45	6.74	2.57	1.50	0.21	0.09	T. BSLT (KR)
132	11.32		3.39	11.42	37.36	9.76	7.85	7.46	6.88	2.77	1.52	0.16	0.12	T. BSLT (KR)
134	57.80	5.02	16.42	4.47	7.42			3.23	4.62	0.31	0.46	0.10	0.15	T. AND (KR)
135	24.65	9.35	6.79	15.28	6.48			12.94	18.30	1.69	3.27	1.16	0.11	T. AND
137	21.29	3.15	11.19	8.53	25.58			13.69	12.27	1.62	2.21	0.44	0.02	T. BSLT (KR)
139	13.86	1.31	10.41	18.60	24.87			15.00	10.61	2.55	2.11	0.49	0.20	T. BSLT (KR)
140	28.69	5.10	9.89	5.59	19.92			11.51	14.81	1.76	1.90	0.49	0.36	T. BSLT (KR)
144	12.08		8.82	17.08	34.26	1.03	1.04	10.08	11.65	1.14	2.34	0.44	0.05	C.A. BSLT (KR)
145	7.28		6.55	22.93	27.71	4.42	5.05	9.26	12.15	1.47	2.60	0.50	0.09	T. BSLT (KR)

1. also 1.49% RUTILE, 13.74% HEMATITE.

2. also 0.95% FORSTERITE, 0.77% FAYALITE.

3. also 0.19% RUTILE, 2.67% HEMATITE.

TABLE 12: X-Ray Diffraction Results*

SAMPLE #	CARBONATE SPECIES	CHLORITE SPECIES
9B-2	Calcite & Dolomite	Ripidolite
44	Calcite	Clinochlore
53	Dolomite	
54	Dolomite[1]	
63		Clinochlore
70	Dolomite[1]	
71	Dolomite	
73	Dolomite[2]	Clinochlore
74	Dolomite	Clinochlore, Ferroan IIb
75	Dolomite[1]	
80-1	Dolomite	
88	Dolomite/Ankerite	Clinochlore, Ferroan IIb
89	Dolomite[3]	Clinochlore, Ferroan IIb
95	Dolomite	Ripidolite
96	Dolomite/Ankerite	
98-2	Calcite & Dolomite	Clinochlore, Ferroan IIb

* Comments:

Picker Diffractometer with CuK_{α} radiation.
6-60° 2θ scans @ 1° /min.
Unoriented slide mounts.
Identifications made with Berry (1974), and Post and Plummer (1972).

1. Determined to be ferroan dolomite from potassium ferricyanide staining.
2. Weakly stained ferroan dolomite and unstained carbonate.
3. Also unstained carbonate with hematite rims - siderite(?).

TABLE 13: Mineral Formulas and Molar Volumes Used in Determining Volume Changes for Alteration Reactions.

MINERAL	FORMULA[1]	MOL. WT.	DENSITY[2]	MOLAR VOLUME
Labradorite (An_{51})	$Ca_{0.5}Na_{0.5}Al_{1.5}Si_{2.5}O_8$	271	2.71	100
Oligoclase (An_{16})	$Ca_{0.3}Na_{1.7}Al_{2.3}Si_{5.7}O_{16}$	265	2.65	100
Pyrophyllite	$Al_2Si_4O_{10}(OH)_2$	360	2.85	126
Kaolinite	$Al_2Si_2O_5(OH)_4$	258	2.64	98
Sericite	$KAl_3Si_3O_{10}(OH)_2$	398	2.80	142
Chlorite	$Fe_{2.5}Mg_{2.5}Al_2Si_3O_{10}(OH)_8$	635	2.95	215
Calcite	$CaCO_3$	100	2.71	37
Quartz	SiO_2	61	2.65	23

1. Formulas from Deer et al. (1966) and Kerr (1977).

2. Densities from Hurlbut (1971), Deer et al. (1966), and Robie et al. (1967).